2015

The Cellular and Molecular Mechanisms of Myxomatous Mitral Valve Disease and Associated Mitral Valve Prolapse: The Role of Dchs1 and Filamin-A

Kimberly Melissa Sauls
Medical University of South Carolina

The Cellular and Molecular Mechanisms of Myxomatous Mitral Valve Disease and Associated Mitral Valve Prolapse: The Role of Dchs1 and Filamin-A

by

Kimberly Melissa Sauls

A dissertation submitted to the faculty of the Medical University of South Carolina in partial fulfillment of the requirements for the degree of Doctor of Philosophy in the College of Graduate Studies.

Department of Regenerative Medicine and Cell Biology

2015

Approved by:

Chairman, Advisory Committee

Roger Markwald

Russell Norris

Donald Menick

Arno Wessels

Robin Muise-Helmericks

DEDICATION

I would like to dedicate this work first to my family: my mom, dad, my brother Ben, my sister Sarah, brother-in-law Juan, my niece Mia, my dog Bentley, and all my other extended family, since none of this could have been accomplished without their love and support. Second, I would like to dedicate this work to the families and patients who participated in the studies described in this dissertation. Their participation and support for this research effort has helped myself, our lab, and collaborators make important progress in studying heart valve disease.

ACKNOWLEDGEMENTS

The writing and completion of the work in this dissertation has been one of my greatest academic accomplishments and could not have been fulfilled without the support and guidance from a number of people. First I would like to thank God for guiding me along this path. I would like to express my sincere gratitude to Russell "Chip" Norris who had faith in me enough to take me on as a laboratory technician and PhD student. Chip has given me so much knowledge, challenged me scientifically, promoted my development and provided many opportunities to collaborate with leading scientists in the field. Chip, your support and guidance has been invaluable to me; I cannot express the extent of my gratitude which goes beyond the amount of space I am given to write in this section. To my committee members who have guided me through this process and challenged me to become a better scientist. To my amazing lab members Katherine, Kate, Amanda, and Annemarieke, y'all have kept me level headed, entertained, given me encouragement, confidence, and friendships that I will treasure forever. Last, but certainly not least, I would like to thank my family who have been very supportive in my decision to pursue my PhD. I am so thankful to have a wonderful and loving family to encourage me to pursue my dreams. Your support has been an essential part of this process.

TABLE OF CONTENTS:

LIST OF FIGURES

LIST OF ABBREVIATIONS

MVP – Mitral valve prolapse
MVD – Myxomatous valvular dystrophy
AV – Atrioventricular
ECM – extracellular matrix
Endo-MT – Endothelial to mesenchymal transition
cKO – Conditional knockout
BMP – Bone morphogenic mrotein
Has2 – Hyaluronan-synthase2
FGF – Fibroblast growth factor
MEK –
EGF – Epidermal growth factor
VEGF – Vascular endothelial growth factor
NFATc1 – Nuclear factor of activated T cells cytoplasmic 1
TG2 – Transglutaminase-2
MMPs – Matrix metalloproteinases
ERK – Extracellular signal-regulated kinase
JNK – Jun N-terminal kinase
ARB – Angiotensin II type 1 receptor blocker
TGFβ – Transforming growth factor beta
Scx – Scleraxis
5-HT – 5-hydroxytrptamine / serotonin
SAVIC – Sheep aortic valve interstitial cells
ROS – Reactive oxygen species
SOD-1 – superoxide dismutase-1
ANP – Atrial natriuretic peptide
BNP – Brain natriuretic peptide
α-SMA – Alpha smooth muscle actin
VEC – valvular endothelial cells
VIC – Valvular interstitial cells
eGFP – Green fluorescent protein
Hsp – Heat shock protein
TNS1 – Tensin-1
LMCD1 – LIM and cysteine-rick domains 1
FLNA – Filamin-A
ABD – Actin-binding domain
E – Embryonic day
Dchs1 – Dachsous 1 (Mammalian*)*
Ds – Dachsous (*Drosophila*)
PCP – Planar cell polarity
IHC – Immunohistochemistry
Wt – Wildtype

HaBP – hyaluronan binding protein
LV- Left ventricle
RV – Right ventricle
MV- Mitral valve
TV – Tricuspid valve
AVSC – Atrioventricular septal cushions
RA – Right atrium
LA – Left Atrium
3D – 3-dimensional
AL – Anterior Leaflet
PL – Posterior Leaflet
XMVD – X-linked myxomatous valvular dystrophy
Tph-1 – Tryptophan hydroxylase-1
SERT – Serotonin transporter
ICC – Immunocytochemistry
SNV – Single nucleotide variants
AVC – Atrioventricular constriction
Hpf – Hours post-fertilization
MO – Morpholino
HEK – Human embryonic kidney
CHX – Cycloheximide
P – Postnatal day
IVS – Interventricular septum
d – Diastole
s – Systole
LVID – Left ventricular internal dimension
LVPW – Left ventricular posterior wall
EF – ejection fraction
FS – Fractional shortening
EPDC – Epicardial-derived cells
FBN1 – Fibrillin-1
YAP – Yes-associated protein
TAZ – Transcriptional coactivator with PDZ binding motif
MCP-1 Monocyte chemoattractant protein-1
MRI – Magnetic resonance imaging

KIMBERLY MELISSA SAULS, The Cellular and Molecular Mechanisms of Myxomatous Mitral Valve Disease and Mitral Valve Prolapse: The Role of Dchs1 and Filamin-A. (Under the Direction of **RUSSELL A. NORRIS**)

ABSTRACT

Mitral valve prolapse (MVP) affects 1 in 40 people worldwide and is the leading cause of mitral valve surgery. MVP is defined as the displacement of one or both leaflets during ventricular systole and commonly leads to mitral regurgitation as well as other secondary cardiac defects including arrhythmias, congestive heart failure, and sudden cardiac death. Structural changes observed in MVP patients include myxomatous degeneration of the mitral leaflets, which is characterized by collagen fragmentation and accumulation of proteoglycans. Additionally, hyperproliferation and activation of interstitial cells (to myofibroblasts) also contribute to valve enlargement and degeneration, respectively. **The molecular and genetic etiology of nonsyndromic MVP is unknown.** This is likely due to the lack of knowledge regarding specific genes that cause nonsyndromic MVP in the human population. Work presented here identifies the first genetic mutations in patients with nonsyndromic MVP. Using linkage analysis and deep sequencing, mutations in the cell-polarity gene, *DCHS1* were identified. These mutations were shown to be loss of function by *in vitro* assays and zebrafish knockdown. Consistent with this finding, we observe *Dchs1* heterozygote mice (*Dchs1*$^{+/-}$) exhibit structural (myxomatous degeneration), functional (MVP), and molecular (altered Erk1/2 signaling) defects that phenocopy MVP patients.

We traced the etiology of the disease in the *Dchs1*$^{+/-}$ mice to defects during valve development where valve morphogenetic defects in tissue shape coincident with aberrant myofibroblast differentiation and elevated pErk1/2 activation. We additionally confirm a developmental origin for the disease in another mouse model that conditionally deletes filamin-A from valve tissue resulting in myxomatous valvular dystrophy, which leads to MVP. The filamin-A mice exhibit developmental defects in valvular cytoskeletal organization and matrix remodeling, which lead to myxomatous mitral leaflets with elevated pErk1/2 activities and increased hematopoietic cell infiltration in the adult. Importantly, defects in both models of disease are observed prior to myxomatous degeneration suggesting processes that control valve shape and maturation are critical for maintaining the valve in a non-degenerative state. Thus, **we hypothesize** that the cell polarity gene *Dchs1* regulates adhesion, migration, and alignment of pre-valvular fibroblasts, and filamin-A regulates matrix remodeling during normal valve morphogenisis. All of which work together to build and shape mitral leaflets during the post-EndoMT stage of valve development. As a corollary hypothesis, we propose that infiltration of circulating progenitor cells contribute to disease through the Erk1/2 signaling pathway. The goal of this work is to define molecular and cellular mechanisms by which Dchs1 and filamin-A regulate valve morphogenesis and to identify common pathogenic mechanisms of myxomatous degeneration, with the potential benefit of targeting the MEK/Erk pathway and/or immune cell infiltration to abrogate MVP disease pathogenesis.

CHAPTER 1: INTRODUCTION

Atrioventricular Valve Development

The atrioventricular (AV) valves of the heart are located at the interface between the ventricles and atria, and consist of both the mitral valve, separating the left ventricle from the left atrium, and the tricuspid valve, separating the right ventricle from the right atrium. The primary function of these valves is to promote unidirectional, forward blood flow during the cardiac cycle by remaining open to allow blood to fill the ventricle during diastole, and remaining closed during ventricular systole to direct blood into the great arteries incumbent on differential pressure from each side. The AV valves are composed of a highly specialized support structure made up of organized extracellular matrix (ECM) components (e.g. Collagen I, elastin, proteoglycans) and dynamic cell populations derived from multiple cellular sources including endothelial cells, epicardial cells, and hematopoietic cells (de Lange, Moorman et al. 2004, Lincoln, Alfieri et al. 2004, Hajdu, Romeo et al. 2011, Wessels, van den Hoff et al. 2012). The mature AV leaflets are stratified by ECM components into three distinct layers oriented by blood flow, the atrialis (elastin), the spongiosa (proteoglycans), and the fibrosa (collagen) layers (Hinton, Lincoln et al. 2006). The AV valves are connected to the heart by the fibrulus annulus, a fibrous ring structure surrounding the atrioventricular orifices. On their free edge, the leaflets are attached to chordae tendineae, structures that exert tensile force

from the papillary muscle. Together these structures make up the subvalvular apparatus. This apparatus is responsible for preventing the valve leaflets from prolapsing back into the atria during ventricular systole.

During early heart formation, the heart exists as a linear tube with an outer myocardial layer and an inner endocardial layer (Markwald and Smith 1972, Markwald, Fitzharris et al. 1977, Runyan and Markwald 1983, Krug, Runyan et al. 1985). Just beneath the endocardial layer is the cardiac jelly, an a-cellular tissue consisting of proteoglycan glycosaminoglycans including hyaluronan and chondroitin sulfates as the major components (Funderburg and Markwald 1986, Person, Klewer et al. 2005). Once the heart begins to rightward loop, the cardiac jelly will swell into the lumen of the heart at localized regions of myocardium, being the AV junction and the outflow tract. These swellings of cardiac jelly at the AV junction, known as the cardiac cushions, will eventually give rise to the valvular leaflets of the mitral and tricuspid valves. The formation of the AV cushions is induced by myocardial produced signaling molecules that inhibit expression of chamber-specific genes and increased synthesis of ECM components (Lyons, Pelton et al. 1990, Harrelson, Kelly et al. 2004, Ma, Lu et al. 2005). The hydrophilic nature of proteolgycans in addition to the increased production of this matrix between the myocardium and the endocardial layers causes the cushions to protrude inwards towards the lumen of the heart (Markwald, Fitzharris et al. 1977, Camenisch, Spicer et al. 2000). In order to become cellularized tissues, these primordial structures will undergo an endothelial-to-mesenchymal transition (EndoMT) event, marking the

commencement of valve development (Markwald, Fitzharris et al. 1977, Markwald, Fitzharris et al. 1979). During EndoMT, the endocardial layer of cells, which lie adjacent to the cardiac cushions on either side of the atrioventricular canal, respond to signals produced by the underlying myocardium. These signals are required to induce the delamination of endothelial cells; their subsequent transition into a mesenchymal phenotype is followed by migration into the AV cushions (Markwald, Fitzharris et al. 1977, Mjaatvedt and Markwald 1989). Two AV cushions form in the AV canal, the inferior and superior cushions, which will eventually fuse to give rise to the septal leaflets of the mitral and tricuspid valves (Wessels and Sedmera 2003). The lateral leaflets of both these valves will arise from mesenchymal cushions that will form in the AVC after the fusion of the inferior and superior cushions (de Lange, Moorman et al. 2004). After this event, Epicardial-derived cells will migrate through the AV sulcus and preferentially populate the lateral AV cushions (Gittenberger-de Groot, Vrancken Peeters et al. 1998, Perez-Pomares, Phelps et al. 2002, Wessels, van den Hoff et al. 2012). The majority of cells within these leaflets are derived from the epicardium compared to the major cushions, which are largely derived from an endothelial origin (de Lange, Moorman et al. 2004, Lincoln, Alfieri et al. 2004, Wessels, van den Hoff et al. 2012). Contrary to previous reports stating a lack of neural crest derived cells in the AV valves (de Lange, Moorman et al. 2004), recent studies using two different lineage tracing Cre models, Wnt1-Cre/R26R and PO-Cre/R26R, have demonstrated neural crest contribution to the septal leaflet of the tricuspid valve and the aortic leaflet of the mitral valve, but not the mural leaflets (Nakamura,

Colbert et al. 2006). A fourth cell type has also been shown to contribute to the AV valves, whereby transplantation of eGFP-positive bone marrow cells into a wildtype irradiated mouse reveals eGFP-positive cells in the cardiac valves(Yang, Hills et al. 2008). These bone marrow-derived cells were also positive for collagen I demonstrating these cells are able to functionally mimic VICs in the cardiac valves (Visconti, Ebihara et al. 2006, Hajdu, Romeo et al. 2011). This population of cells was also observed to express CD45, a marker for hematopoietic stem cells, indicating these cells are derived from the blood. The temporal profile of the infiltration of these cells and their role in valve development and homeostasis has yet to be determined. Understanding the lineage of cells within the AV valves will likely give insight into differential penetrance of disease between leaflets in the same valve and also provide insights in valve development.

The process of EndoMT requires the coordinated activity of multiple molecular signaling pathways present in myocardium and endocardium. This process has been extensively studied in *in vitro* cell culture systems as well as *in vivo* animal models. The initial que, Bone Morphogenic Protein 2 (BMP2) which signals through Smad1/5/8, is produced by the myocardium in a regional specific manner where it is specifically expressed and serves as a direct stimulus to the endocardium to initiate EndoMT (Runyan and Markwald 1983, Nakajima, Yamagishi et al. 2000, Ma, Lu et al. 2005). This has been demonstrated in BMP2 conditional knockout mice (cKO) where the genetic removal of BMP2 from the myocardium results in failure of the AV cushions to form. Additionally, *Tbx2*

expression, required for chamber specification and cushion ECM secretion was lost in this cKO mouse, indicating BMP2 is an important early signal required to initiate valve formation (Ma, Lu et al. 2005, Rivera-Feliciano and Tabin 2006). BMP2 has also been shown to initiate TGFβ signaling in the AV cushions, another signal required for EndoMT progression (Ma and Martin 2005). TGFβ was one of the first signaling molecules shown to be required for the initiation of EndoMT (Brown, Boyer et al. 1996). The TGFβ ligands and receptors are expressed in AV cushions during mammalian EndoMT and signal through Smad2/3 to induce expression on the transcription factor slug, which promotes endothelial cell activation and invasion (Romano and Runyan 1999, Romano and Runyan 2000). In mouse embryos and AV explants, EndoMT fails to occur when β-catenin expression is lost in endocardial cells (Tie2-Cre). Additionally, TGFβ is unable to induce EndoMT in endocardial cells that lack β-catenin, indicating the TGFβ and the Wnt pathway exhibit crosstalk during AV cushion development and are both required for EndoMT induction (Liebner, Cattelino et al. 2004). Notch signaling through receptors Notch1-4 and ligand Delta4, are also required for EndoMT initiation, whereby loss of Notch1 results in AV cushion swellings devoid of mesenchymal cells. The endocardial cells of notch signaling mutants extend processes into the cardiac jelly but are unable to delaminate and migrate(Grego-Bessa, Diez et al. 2004, Timmerman, Grego-Bessa et al. 2004). This failure to delaminate and subsequently migrate, results from loss of expression of the pro-migratory transcription factor Snail1, which is induced by Notch signaling.

Snail1 represses VE-cadherin promoter activity thereby allowing endocardial cells to break free from one another (Karsan 2008). Additionally, Notch mutations in humans have been associated with defects in AVC cushions in addition to other cardiac abnormalities, further supporting a role for this pathway in EndoMT initiation (Garg, Muth et al. 2005). The physical environment of the cardiac cushions provides a scaffold for mesenchymal cell migration and an environment that promotes an invasive cell phenotype (Schroeder, Jackson et al. 2003). The ECM in the cardiac cushions is made up of adheron-like proteins including, ES1, fibronectin, transferrin, ES130, and hLAMP1 (Krug, Runyan et al. 1985, Mjaatvedt, Krug et al. 1991, Krug, Rezaee et al. 1995). The hydrophilic nature of the matrix within the cardiac cushions stems from the proteoglycan content of the cushions and is also required for EndoMT to occur. Loss of hyaluronan-synthase2 (has2) or versican gene expression results in loss of cushion formation and/or endocardial cell migration, indicating an important role for AV cushion matrix in the support and induction of EndoMT (Camenisch, Spicer et al. 2000).

Concurrent with an EndoMT event, the resulting mesenchymal cells will undergo proliferation to populate the AV cushions and continued ECM secretion (Armstrong and Bischoff 2004). These mesenchymal cells express multiple transcription factors including Tbx20 and Twist1, which have been shown through expression and genetic studies to be responsible for maintaining a proliferative phenotype to populate the cardiac cushions and preserve the secretion of primitive ECM components (Shelton and Yutzey 2007, Shelton and

Yutzey 2008, Chakraborty, Wirrig et al. 2010). BMPs are also important for maintaining proliferation, where *BMP4* mutant mice exhibit hypocellular AV cushions (Jiao, Kulessa et al. 2003). In contrast, genetic removal of *SMAD6,* the BMP inhibitory Smad, results in AVC hyperplasia, indicating balanced levels of both positive and negative signals are required to maintain mesenchymal cell proliferation (Galvin, Donovan et al. 2000). Fibroblast growth factors (FGF) are also responsible for promoting cushion mesenchyme proliferation. FGF receptors 1, 2, and 3 expression is restricted to the AV cushions, while FGF4 expression is observed throughout the AV complex in chick embryos. Treatments with FGF4 on chick endocardial cushion explants or injection with FGF4 coding sequence delivered by retrovirus directly into chick hearts results in increased mesenchymal cell proliferation and hyperplastic AV cushions respectively (Sugi, Ito et al. 2003). Cushion growth is also shown to be regulated by Erk1/2 signaling, whereby Noonan-causing gain-of-function mutations in the protein tyrosine phosphatase Shp2 result in increased outgrowth of AV cushion explants that was abolished by direct inhibition of MAPK/Erk kinase (MEK)-1 (Krenz, Yutzey et al. 2005). Epidermal growth factor (EGF) signaling inhibits cushion mesenchymal cell proliferation by antagonizing BMP-induced activation of SMAD1/5/8, and mutations reducing this signaling result in hypercellular cushions (Chen, Bronson et al. 2000).

Endothelial cell proliferation is essential to maintain the endocardium while the AV cushions undergo EndoMT (Markwald, Fitzharris et al. 1975). Vascular endothelial growth factor (VEGF) expression becomes restricted to the

AV cushion endocardium during EndoMT and is required to maintain endocardial cell proliferation and survival (Miquerol, Gertsenstein et al. 1999, Miquerol, Langille et al. 2000). VEGF also functions to inhibit EndoMT of endothelial cells by sustaining an endothelial cell phenotype, and therefore must be tightly regulated during valve development to allow for EndoMT to progress and also maintain a population of endothelial cells (Miquerol, Langille et al. 2000). The transcription factor, Nuclear factor of activated T cells cytoplasmic 1 (NFATc1), is a direct target of VEGF and is expressed by endocardial cushion cells during EndoMT and is later restricted to endocardial cells. Loss of NFATc1 in mice results in normal progression of endocardial cushion formation and EndoMT, with reduced cell proliferation and failure to undergo remodeling. This ultimately results in embryonic lethality by E14.5 due to congestive heart failure (de la Pompa, Timmerman et al. 1998, Ranger, Grusby et al. 1998). As a mechanism, NFATc1 induces expression of Cathepsin K, and in NFATc1 knockouts, this remodeling proteinase is also lost resulting in unremodeled valve primordia (Lange and Yutzey 2006). As EndoMT begins to shut down, VEGF expression decreases along with cushion cell proliferation, and NFATc1 becomes restricted to the endocardium.

The second major phase of valve development, which follows EndoMT, is the post-EndoMT phase; the cellular and molecular mechanisms of which are poorly understood. During this phase endothelial-derived mesenchymal cells differentiate into fibroblastic interstitial cells and remodel the surrounding ECM to form mature leaflets and their supporting apparatus (i.e. chordae tendinae)

(de Lange, Moorman et al. 2004, Norris, Potts et al. 2009). As they differentiate, these cells increase secretion of fibrillar matrices including collagens 1, 2, 3, 4 and 9 and decrease expression of mesenchymal transcription factors (snail, twist) (Lincoln, Alfieri et al. 2004, Peacock, Lu et al. 2008, Chakraborty, Wirrig et al. 2010, Tan, Junor et al. 2011). Previous reports have proposed that there are two signaling fields that exist in the cardiac cushions as mesenchymal cells begin to differentiate into fibroblasts: a proliferative field located beneath the distended endocardium, and a differentiation field located in the leaflet region nearest to the myocardium (Maria V. de la Cruz 1998, de Vlaming, Sauls et al. 2012). In support of this idea, regional specific expression of collagen has been observed in the valve primordia and may identify those cells that have differentiated into fibroblasts (Norris, Potts et al. 2009, Tan, Junor et al. 2011). Transglutaminase-2 (TG2) expression is also regionalized in the valve during development and defines a cushion boundary interface (de Vlaming, Sauls et al. 2012). Other signals that define these boundaries have yet to be defined, but work published investigating periostin suggest the ECM can influence cellular differentiation in the AV valves. Periostin, an ECM component expressed in post-EndoMT valve tissues, is an important autocrine signal that promotes cell autonomous differentiation. Periostin null mice exhibit aberrant differentiation of AV cushion mesenchyme and rescue experiments demonstrate periostin functions as a hierarchical switch, delineating mesenchymal cells into fibroblasts and represses their differentiation into other lineages such as myocytes (Norris, Moreno-Rodriguez et al. 2008, Norris, Potts et al. 2009).

Simultaneous attenuation and elongation of the leaflets is required for the cushions to undergo a transition into a tightly compacted and highly organized array of interstitial cells and ECM (de Vlaming, Sauls et al. 2012). How the valvular ECM in the mature leaflets becomes an organized and tightly compacted structure remains elusive in valve development, but likely involves biomechanical input from blood flow and cellular input from differentiated valvular fibroblasts (Yalcin, Shekhar et al. 2011). Recent studies have suggested valve fibroblasts play an important role in matrix remodeling since they acquire a contractile state upon stimulation (Butcher, McQuinn et al. 2007, Butcher and Nerem 2007). In order to provide a contractile force that is necessary for matrix condensation, input from the cytoskeletal actin-network and its interacting proteins, along with cell surface membrane receptors (integrins) which couple the actin cytoskeleton to the extracellular matrix are required (Butcher, McQuinn et al. 2007, Sandbo and Dulin 2011, Iwamoto and Calderwood 2015). Identification of valve cell contractility has been shown *in vitro,* where valve cells embedded into a collagen gel are able to make cell-to-cell contacts, establish polarized alignment, and contract the surrounding collagen into a thin and organized structure (de Vlaming, Sauls et al. 2012). Thus, mechanistic pathways that direct the post-EndMT phase likely involve the actin-cytoskeleton and integrin receptors. Studies have also suggested fibroblasts under tensile strain develop structures called fibropositors, which require input from the actin cytoskeleton and play a role in the alignment of collagen fibrils (Canty, Lu et al. 2004, Kadler 2004, Canty, Starborg et al. 2006, Kapacee, Richardson et al. 2008,

Ghatak, Misra et al. 2014). The presence of these structures have been described in the mitral valve during development, specifically during timepoints when the valve is synthesizing and organizing matrix (de Vlaming, Sauls et al. 2012). Work is still needed to elucidate mechanisms by which the AV valves undergo post-EndoMT remodeling, as defects in remodeling during this point during valvulogenisis may contribute to disease.

Increasing evidence supports a role for developmental processes in adult valve disease, whereby genetic mutations present at conception direct faulty valve development resulting in disease that is clinically detectable during adulthood (Freed, Acierno et al. 2003, Garg, Muth et al. 2005, Nesta, Leyne et al. 2005, Kyndt, Gueffet et al. 2007, Pierpont, Basson et al. 2007). Thus, understanding the genetic, cellular and molecular mechanisms that drive valve morphogenesis will offer insights into adult disease and provide druggable targets that can be used to prevent progression of the disease in adults.

Etiology of Myxomatous Valvular Dystrophy and Associated Mitral Valve Prolapse

Myxomatous dystrophy of the cardiac valves is a heterogeneous group of disorders that can manifest in syndromes such as Marfan's Disease, or isolated events affecting only the mitral valve such as mitral valve prolapse. Mitral valve prolapse is the most common form of myxomatous valve disease affecting 2% to 3% of the population and as such, is the leading cause of mitral valve surgery (Levy and Savage 1987). Prolapse is defined as the displacement of one or both

abnormally thickened mitral leaflets into the left atrium during ventricular systole *(Figure 1.1)* (Tamura, Fukuda et al. 1995).

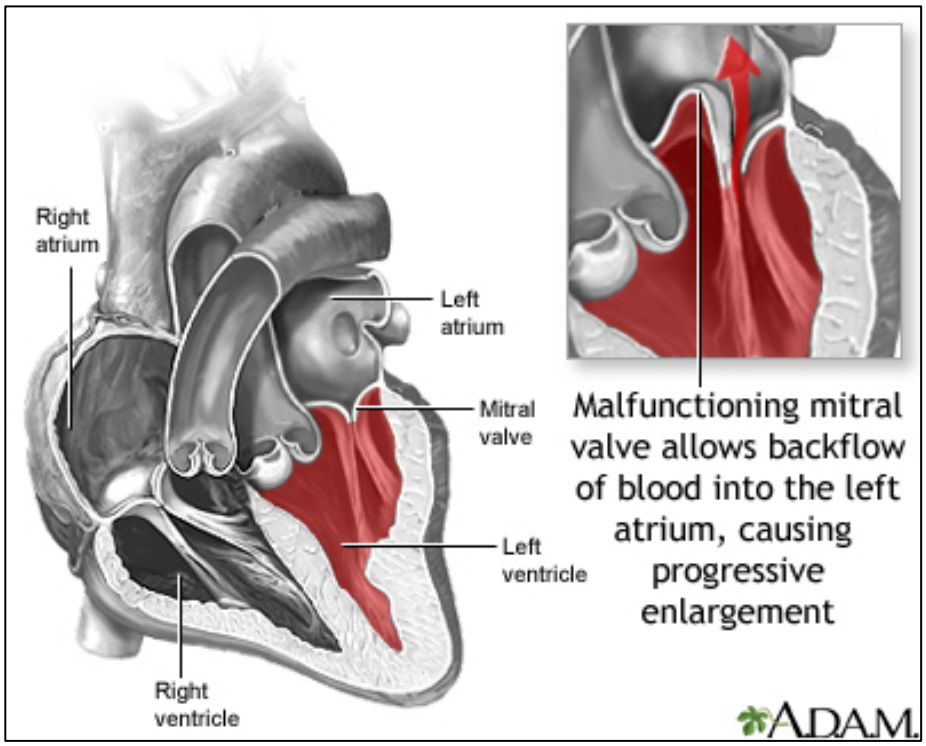

Figure 1.1. Mitral Valve Prolapse. Schematic depicting frontal view of the mammalian heart. Mitral valve labeled on the left side of the heart located between the left ventricle and left atrium. Second image depicts anterior leaflet prolapse. Arrow represents backflow of blood into the left atrium. Image adapted from MedlinePlus, 2015.

Valve abnormalities can often lead to detrimental secondary cardiac diseases including, mitral regurgitation or the backflow of blood into the left atrium, cardiac arrhythmias, mitral stenosis, myocardial hypertrophy, congestive heart failure, and even sudden cardiac death (Kligfield, Levy et al. 1987, Levine, Hagege et al. 2015). Since there are no effective pharmacological treatments that prevent progression of the disease, surgical intervention to replace or repair the mitral valve remains the major mode of treatment (Rajamannan, Gersh et al.

2003, Roger, Go et al. 2012). Current prevalence data estimates that by the age of 70, 11% of men and 6% of women with classic MVP will need mitral valve replacement (Wilcken and Hickey 1988). This is important because it indicates that for most patients there is ample time to intervene if remedial therapies can be found.

Structural changes observed in patients with myxomatous dystrophy and mitral valve prolapse result from myxomatous degeneration of the cardiac leaflets; a process that involves excessive remodeling of the extracellular matrix and subsequent loss of zonal patterning of the matrix. Myxomatous degeneration is morphologically characterized by enlarged, thickened leaflets with fragmented collagen, excessive proteoglycan deposition, hyperplasia, and faulty differentiation of valvular interstitial cells *(Figure 1.2).*

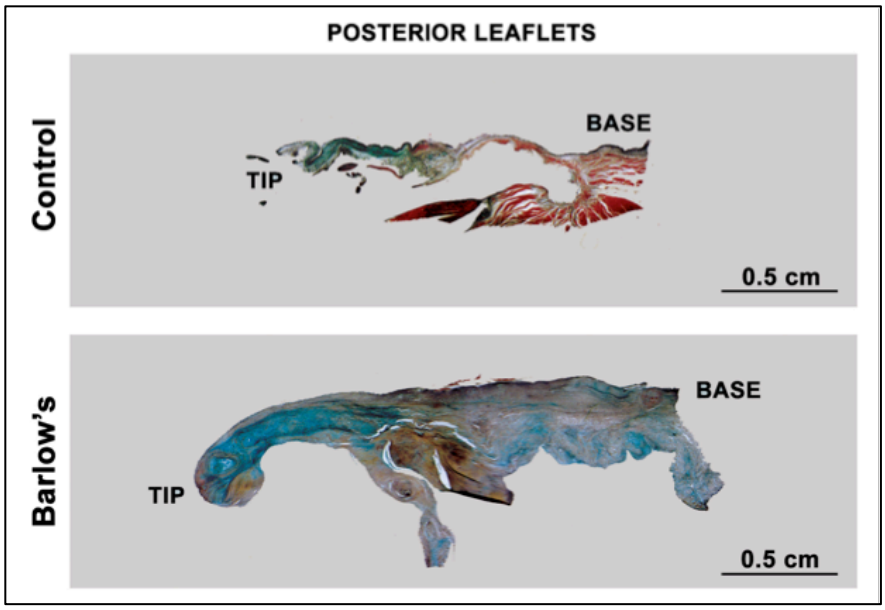

Figure 1.2. Histological Characteristics of Myxomatous Degeneration. Posterior leaflets from human with normal mitral valve (Control) and human with myxomatous mitral valve (Barlow's) stained with Movat's Pentachrome stain. Colors represent different components: black (elastin/nuclei), red (muscle/fibrin), yellow (collagen), blue (proteoglycans). Data generated in Norris lab.

These changes in structure lead to faulty valves that become mechanically weakened over time, thus increasing susceptibility to prolapse. Studies examining human tissue from patients with myxomatous valvular dystrophy reveal increases in "myofibroblasts" or active fibroblasts that express intermediate filaments (actin and desmin) as well as matrix metalloproteinases (MMPs) responsible for enzymatic breakdown of the ECM (Rabkin, Aikawa et al. 2001). This suggests valvular interstitial cells play an important role in matrix remodeling and thus likely play an important role in facilitating disease.

Little is known about the etiology of nonsyndromic mitral valve prolapse and the how valves become myxomatous. This is likely due to a deficiency of data identifying genetic origins for the disease. In contrast, the etiology of

syndromic forms of the disease have been well studied. Marfan's Syndrome, Loeys-Dietz Syndrome, and Shprintzen-Goldberg Syndrome are just a few of the syndromes in which patients present with mitral valve prolapse (Brown, DeMots et al. 1975, Loeys, Chen et al. 2005, Doyle, Doyle et al. 2012). A shared component of each of these syndromes is the dysregulation of TGF-β signaling. In Marfan's Syndrome, autosomal-dominant mutations in the connective tissue gene *FBN1* result in an inability of the ECM to sequester TGF- β, leading to hyperactivity of downstream signaling, including the MEK/ERK pathway (Dietz, Cutting et al. 1991, Milewicz and Duvic 1994). The TGFβ pathway has been implicated in the pathogenesis of MVP in the mouse model of Marfan's, whereby increased pSmad2 signaling followed by increases in cell proliferation has been observed in the mitral valve. The use of a TGF-β antagonist was able attenuate Smad2 signaling and rescue the valve phenotype *in vivo,* suggesting a cause and effect relationship (Ng, Cheng et al. 2004). TGFβ has been shown to affect VIC differentiation and increase expression of α-SMA, a marker for activated fibroblasts, suggesting this pathway may contribute to disease by altering the phenotype of valvular interstitial cells (Walker, Masters et al. 2004). Specifically, noncanonical TGFβ signaling through extracellular signal-regulated kinase (ERK) 1 and 2, and Jun N-terminal kinase-1 (JNK1) are shown to be increased in the Marfan's mouse and can be inhibited by therapies directed against TGFβ. The specific targeting of ERK1/2 activation using RDEA119, an inhibitor of MEK1/2, the upstream activator of ERK1/2, results in amelioration of aortic growth, the

major cause of death in Marfan's syndrome (Holm, Habashi et al. 2011). Although, the effects of RDEA119 on the mitral valve are unknown. Additionally, administration of the angiotensin II type 1 receptor blocker (ARB) Losartan is effective in reducing the aortic dilation rate in human adults with Marfan's syndrome, suggesting ARBs and angiotensin II pathway targeting as a potential therapeutic option for MVP patients (Groenink, den Hartog et al. 2013). Although these studies were performed in the setting of a connective tissue syndrome, these data can provide insights into the pathogenesis of nonsyndromic mitral valve prolapse, whereby a chapter in this dissertation aims to determine if similar mechanisms of disease exists.

Evidence for TGFβ signaling in nonsyndromic myxomatous mitral valve disease has been observed in canine models of the disease, where increased RNA expression of TGFβ and increased pSmad2 is present in diseased valves (Surachetpong, Jiranantasak et al. 2013). Increased TGFβ signaling is evident in human myxomatous mitral valves, where mRNA expression is increased as well as downstream canonical signaling through pSmad2 (Hagler, Hadley et al. 2013). Interestingly, high levels of circulating TGFβ1/2 are present in the majority of human MVP cases and this is correlated with posterior leaflet thickness and the presence and severity of mitral regurgitation (Malev, Zemtsovskii et al. 2012). Mechanistically, TGFβ has been shown to induce proteoglycan expression through the regulation of the transcription factor scleraxis (Scx) (Barnette, Hulin et al. 2013). In support of this finding, Scx null mice exhibit decreased

proteoglycan expression in the cardiac valves, which is positively regulated by TGFβ2. Additionally, expression of Scx is increased in human myxomatous mitral valves, suggesting this as a potential downstream player in the pathogenesis of myxomatous degeneration (Barnette, Hulin et al. 2013). Another possible mechanism for pathogenic TGFβ signaling is the canonical (Smad2/3) and non-canonical (p38, Erk1/2) pathways, which have both been reported to be active and increased in models of myxomatous valve disease. Experiments in cultured VICs from human diseased valves suggest an autocrine/paracrine mechanism whereby angiotensin II receptor 1 blockers (ARB) are sufficient to block TGFβ-induced matrix production that contributes to abnormal valve remodeling (Geirsson, Singh et al. 2012). ARBs act on the angiotension II receptor 1 and preferentially shunt signaling through the angiotension type 2 receptor, thereby attenuating Erk1/2 signaling.

Upstream of TGFβ, increased serotonin [5-hydroxytrptamine (5-HT)] has been implicated in nonsyndromic valve disease and is known to induce TGFβ expression and signaling (Jian, Xu et al. 2002). Specifically, serotonin has been shown to phosphorylate and activate Erk1/2 signaling in many cell types, including VICs, and can upregulate cell proliferation through this pathway (Launay, Birraux et al. 1996, Grewal, Mukhin et al. 1999, Xu, Jian et al. 2002). High levels of circulating serotonin and serotoninergic drugs such as the diet drug fenfluoramine-phentermine, are known to produce hyperplastic valve phenotypes with excess extra-cellular matrix, similar to the phenotype of

nonsyndromic MVP (Connolly, Crary et al. 1997). Additionally, dogs with myxomatous valve disease have been reported to have increased serum serotonin levels suggesting this as a possible initiating mechanism (Arndt, Reynolds et al. 2009). In sheep aortic valve interstitial cell cultures (SAVIC), treatment with either TGFβ or 5-HT resulted in increases in collagen and glycosaminoglycan production by these cells (Jian, Xu et al. 2002). The relevance in human disease has yet to be determined, but valvular interstitial cells in human heart valves express distinct 5-HT receptors, indicating their ability to respond to serotonin (Fitzgerald, Burn et al. 2000, Roy, Brand et al. 2000).

Another suggested pathogenic mechanisms of myxomatous valve disease is the increased presence of reactive oxygen species (ROS), or chemically active molecules produced as a natural byproduct of metabolism that have active roles in cell signaling. Since increased oxidative stress associated with increases in NAD(P)H oxidase catalytic subunits (Nox)2 and 4 have been identified in diseased human mitral valve tissue, it is possible this may play a role in disease pathogenesis. Additionally, in the mitral valves of mice lacking superoxide dismutase-1 (SOD-1), expression of MMP2, CTGF, Nox2, and Nox4 were significantly increased indicating ROS can independently activate pro-fibrotic and matrix remodeling gene expression patterns. Mouse cells treated with anti-oxidants attenuated TGFβ1-induced pro-fibrotic and matrix remodeling (MMPs) gene expression *in vitro* indicating a link between TGFβ activation and ROS (Hagler, Hadley et al. 2013).

A working hypothesis of heart diseases is the re-activation of developmental processes, which facilitate remodeling in adult disease. A well-studied example of this is the expression of natriuetic proteins (ANP,BNP) during cardiac hypertrophy (Sergeeva and Christoffels 2013). Since hypercellularity and expression of mesenchymal markers only present during development (α-SMA, vimentin) have been reported in diseased valve endocardial cells in animal models and human patients, re-activation of EndoMT, an embryonic pathway not present in normal adult valves, has been suggested as a potential disease inducing mechanism which can increase valvular leaflet size (Paranya, Vineberg et al. 2001, Paruchuri, Yang et al. 2006, Liu, Joag et al. 2007). A population of ovine aortic VICs have been observed to co-express the endothelial marker CD31 along with α-SMA. Co-expression of these factors could also be induced *in vitro* by treatment with TGFβ, suggesting a transdifferentiation event may occur in the adult (Paranya, Vineberg et al. 2001). Two distinct populations of endothelial cells from aortic valves have been identified *in vitro*: VECs which invade and transform under TNFα stimulation, and those VECs which are resistant to mesenchymal transformation and remain endothelial. The population that underwent a transformation were shown to have increased MMP9, Notch-1, TGFβ, and BMP-4, suggesting these cells are capable of inducing disease-associated changes (Farrar and Butcher 2014). Additionally, since adult valvular endothelial cells (VEC) are capable of undergoing EndoMT after stimulation *in* vitro, this suggests their capability to

undergo EndoMT *in vivo* as well. Recent *in vitro* work using trans-well assay systems demonstrates VICs secrete factors which can prevent TGFβ-induced EndoMT by VECs. Conversely, conditioned media from VECs was able to attenuate the spontaneous VIC activation, marked by α-SMA and Collagen I expression (Shapero, Wylie-Sears et al. 2015). These results suggest a role for paracrine signaling by VECs and VICs which may regulate VEC EndoMT in the adult. In a tissue engineered *in vitro* model of valve endothelial cell tissue, cyclic mechanical strain can induce EndoMT in the adult porcine valve, where low strain induced EndoMT through a TGFβ-dependent signaling pathway, and high strain induced EndoMT via increased Wnt/β-catenin signaling (Balachandran, Alford et al. 2011). Cultured valvular endothelial cells from sheep were able to undergo EndoMT in response to TGFβ stimulation. This was attenuated by either administration of the angiotensin II type 1 receptor blocker Losartan, or the MEK1/2 inhibitor RDEA119, suggesting TGFβ-induced EndoMT is mediated by pErk1/2 signaling (Wylie-Sears, Levine et al. 2014). While direct evidence for EndoMT processes in the diseased adult mitral valve have not been demonstrated, evidence for the ability and plasticity of VECs to undergo transdifferentiation exists, suggesting re-activation of EndoMT as a potential mechanism by which the mitral valve undergoes myxomatous remodeling (Paruchuri, Yang et al. 2006).

In addition to infiltrating cells from an endothelial origin (EndoMT), cells from an extra-cardiac source have been suggested to contribute to myxomatous

valve disease. Chimeric mice whose bone marrow was replaced with eGFP expressing marrow, demonstrated eGFP-positive cell engraftment into the mitral valve during normal valve homeostasis. Additionally, these hematopoietic-derived cells were shown exhibit synthetic processes characteristic of fibroblasts, including Collagen I expression, indicating a role for these cells in the remodeling and maintenance of the ECM (Hajdu, Romeo et al. 2011). In human myxomatous tissue, increased CD45-positive cells and blood-derived fibrocytes with matrix-altering abilities have been observed (Barth, Koster et al. 2005, Hajdu, Romeo et al. 2011, Geirsson, Singh et al. 2012). These findings suggest a potential role for hematopoietic cells in myxomatous valve disease but requires further validation.

A known, basic principal of biology is that mechanical stimuli can induce mesenchymal cells to remodel their ECM. Therefore, since myxomatous valve disease is characterized by a dysregulation of ECM homeostasis, it is reasonable that abnormal biomechanical loading may play a role in facilitating myxomatous degeneration. Multiple biomechanical forces are exerted on heart valves including, tension, shear, compression, and flexure (Sacks, David Merryman et al. 2009). These loading forces, which occur from the passing flow of blood and coaptation of the leaflets, will vary between valves depending on local pressures and supporting apparatuses. The left side of the heart normally maintains a higher pressure and thus valve location is important for understanding the role of biomechanics in valve disease. The AV valve cells on the left side of the heart (mitral valve) are more stiff, based on their increased expression of α-SMA and

heat shock protein 47 (Hsp47), indicating these cells can respond and adapt to the increased force exerted on the left side of the heart by increasing collagen biosynthesis and cytoskeletal stiffness in order to maintain homeostasis (Sacks and Yoganathan 2007). Importantly, these results indicate VICs are plastic and capable of adapting and responding to their environment. Experiments have demonstrated a role for tensile strain in initiating myxomatous valve disease, whereby increased glycosaminoglycan synthesis was observed in cultured porcine mitral valve cells that were subjected to cyclic stretch and strain in a 3D culture system (Gupta, Werdenberg et al. 2008). Cultured canine valves produce a similar response when subjected to physical strain, where increased expression of a-SMA, MMP-1, MMP-13, and xylosyl transferase (glycosaminoglycan synthetic enzyme) have been detected (Lacerda, Maclea et al. 2012).

The genetics of nonsyndromic MVP are not well understood but familial studies have demonstrated an autosomal mode of inheritance with incomplete penetrance (Weiss, Mimbs et al. 1975, Strahan, Murphy et al. 1983). Recently, two genome wide association studies were performed in a cohort of nonsyndromic MVP patients identifying 6 loci. Two of the candidate genes, *TNS1* (tensin-1) and *LMCD1* (LIM and cysteine-rich domains 1) result in atrioventricular valve regurgitation when morpholino knockdown in zebrafish. Loss of murine Tensin-1, a focal adhesion protein involved in cytoskeletal organization, results in a myxomatous mitral valve in the adult mouse. Both of these genes are important for cell proliferation and cell migration, further

supporting a role for these processes in MVP (Dina, Bouatia-Naji et al. 2015). Freed et al. identified a locus for MVP that maps to a 43 cM region of chromosome 11p15.4 in a large multi-generational family of Western European decent with inherited MVP (Freed, Acierno et al. 2003). The locus described in this study provides the basis for data presented in a following chapter of this dissertation. The genetics of myxomatous valvular dystrophy, which is associated with mitral valve prolapse but affects multiple cardiac valves, have also been described. A familial and genealogical study reveals mutations in the gene *filamin-A* are causal to X-linked, nonsyndromic myxomatous valvular dystrophy. Three missense mutations and a 1944-bp deletion, clustered in exons 16-18 of the *FLNA* gene (filamin-A), were identified in 4 different families in which a common ancestor can be identified (Kyndt, Gueffet et al. 2007). The underlying molecular pathways which involve filamin-A and valve disease are unknown. Understanding the genetics that underlie nonsyndromic myxomatous mitral valve disease and mitral valve prolapse will reveal a molecular basis for the disorder. Since the disease manifests clinically later in life and presents as a severe cardiac event, the identification of genetically susceptible individuals will allow for the prediction of disease progression patterns (Scordo 1998). This is important because these clinically benign individuals can be treated with a therapy that may effectively prevent progression of the disease and other secondary cardiac events.

Filamin-A in Valve Development and Disease

The filamin family consists of three homologous proteins: A, B and C. filamins A and B are widely expressed, while filamin-C expression is predominantly restricted to cardiac and skeletal muscle (Sheen, Feng et al. 2002, Goetsch, Martin et al. 2005). Filamins exist as high molecular mass cytoplasmic proteins and form homo- or hetero-dimeric structures through their last carboxyl-terminal repeat, allowing for the formation of a dynamic V-shaped structure *(Figure 1.3).*

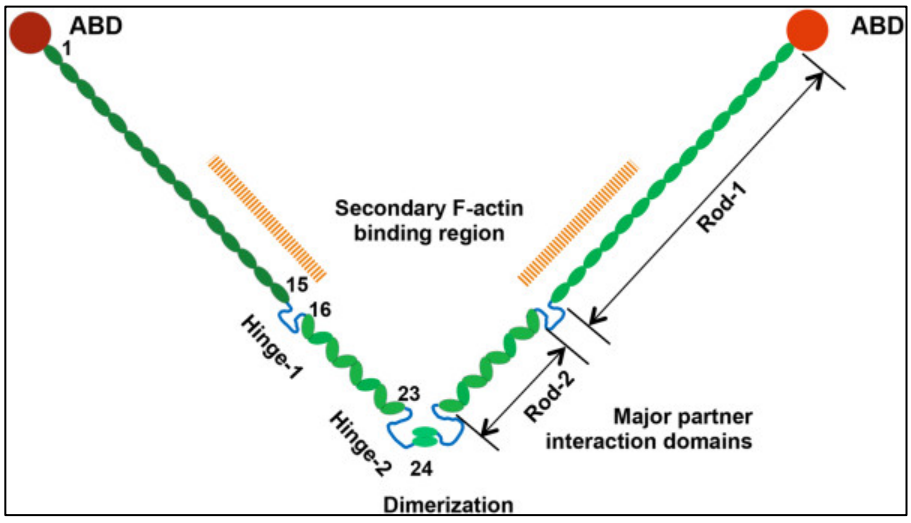

Figure 1.3. Structure of Filamin-A Protein. Filamin-A is a V-shaped homodimer and has an actin-binding domain at the amino terminus (ABD, red). Filamin-A contains an F-actin binding domain, a Rod-1 domain containing repeats 1-15, a Rod-2 domain containing repeats 16-23, and a dimerization domain at repeat 24. Image adapted from (Yue, Huhn et al. 2013).

The filamins have an actin-binding domain at the amino terminus and an integrin-binding domain at the carboxyl terminus (Popowicz, Schleicher et al. 2006). These interactions allow filamins to crosslink and organize actin

filaments into actin networks and tether the cytoskeleton to the cell membrane by means of cell surface integrin receptors (Shizuta, Shizuta et al. 1976, Kim, Sengupta et al. 2008). Serving as a connection between the outside of the cell and the cytoskeleton allows filamins to function in mechano-sensing and thus regulate cell adhesion and migration. Filamin-A has been shown to directly interact with a variety of intracellular proteins and can function as a scaffold for second messengers in signal transduction. Specifically, filamin-A has been shown to directly bind the TGFβ signaling mediators Smad and R-ras (Sasaki, Masuda et al. 2001, Griffiths, Grundl et al. 2011). The interaction between filamin-A and R-ras has been directly linked to the maintenance of vascular permeability, whereby knockdown of R-ras or filamin-A disruptes endothelial barrier function and demonstrates disorganized VE-cadherin at adherens junctions in cultured endothelial cells (Griffiths, Grundl et al. 2011). R-ras has also been shown to mediate and increase cell migration through an integrin-dependent interaction with filamin-A (Gawecka, Griffiths et al. 2010).

Complete genetic removal of filamin-A in the mouse results in embryonic lethality by embryonic day (E) 14 due to vascular hemorrhaging and severe cardiovascular malformations such as: incomplete septation of the outflow tract leading to a common arterial trunk, abnormally enlarged outflow tract valves, atrial and ventricular septal defects, aortic arch disruption, abnormal endothelial organization in blood vessels, and mitral valve thickening. All of these cardiac defects, occurring before E14, indicate a role for filamin-A during heart

development (Feng, Chen et al. 2006, Hart, Morgan et al. 2006). Additionally, filamin-A is highly expressed in non-myocyte cells during cardiac morphogenesis and includes epicardial cells, endocardial cells, and mesenchyme derived from EndoMT in the AV valves. Postnatally, the expression of filamin-A declines in the AV valves and this continues into adulthood, where filamin-A expression is significantly decreased. High filamin-A expression in the adult has been associated with myxomatous degeneration in human tissue (Norris, Moreno-Rodriguez et al. 2010).

A variety of genetic syndromes affecting multiple organ systems have been associated with mutations in filamin-A including fibromuscular dysplasia and otopalatodigital syndrome type 1. Periventricular heterotopia, a brain malformation where cerebral cortex neurons fail to migrate to their proper cortical site, is a disorder caused by loss-of-function mutations in *FLNA.* The dynamic regulation of filamentous actin at the leading edge of migrating neurons is required for migration into the ventricular zone. Mutations in *FLNA* result in the complete immobilization of neurons, suggesting filamin-A is required for cytoskeletal driven migration (Eksioglu, Scheffer et al. 1996). Mutations in filamin-A have also been identified in multiple families with X-linked myxomatous valvular dystrophy and are clustered near the actin-binding domain of the protein (Kyndt, Gueffet et al. 2007, Lardeux, Kyndt et al. 2011). The following chapters aim to identify a role for filamin-A in valve development and disease and use this model to identify potential pathological components of myxomatous valve disease that can be applied to all MVD patients.

Structure and Function of Dchs1

Dachsous 1 (Dchs1) is a large (3503 amino acids) non-classical cadherin that functions in cell-to-cell interactions. Dchs1 is the mammalian homologue to the *Drosophila dachsous* (Ds) gene and in contrast to the mammalian Dchs1, much more is known about how this protein functions (Nakajima, Nakayama et al. 2001). The structure of Ds includes a large extracellular region with 27 tandem cadherin domains and a cytoplasmic domain with sequence similarity to the beta-catenin-binding domain for classical cadherins in mammals *(Figure 1.4)* (Ozawa, Ringwald et al. 1990).

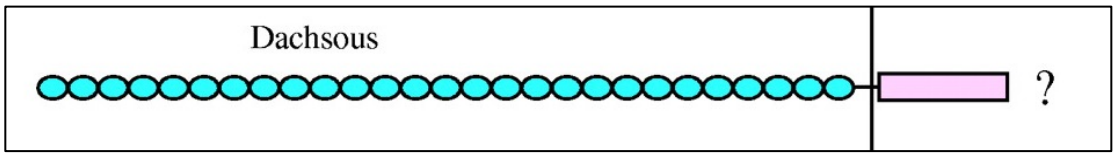

Figure 1.4. Structure of Dachsous. Extracellular domain of Dachsous contains 27 cadherin repeats (blue circles) and a smaller intracellular domain (pink) with an unknown function. Image adapted from (Tanoue and Takeichi 2005).

The similarity between mouse Dchs1 and *Drosophila* Ds is 26%, while the human and mouse proteins have a similarity of 98% (Clark, Brentrup et al. 1995). Studies in *Drosophila* demonstrate a role for Ds in regulating two major pathways: planar cell polarity (PCP) and tissue growth through Hippo signaling (Oh and Irvine 2010). PCP signaling directs the polarized organization of cells within the plane of a tissue. This process is dependent on Ds interaction with another large cadherin, Fat (Clark, Brentrup et al. 1995). The extracellular domain of Ds is required to mediate cell polarity effects, whereby dachsous

functions as a ligand for Fat (Matakatsu and Blair 2006). In mammals, there is evidence to suggest that Dchs1 plays a role in regulating planar cell polarity, but it is unknown whether or not Dchs1 interacts with Fat to regulate this process. The Dchs1 deficient mouse supports a role for Dchs1 in cell polarity with a myriad of developmental defects affecting multiple organ systems including, chochlea stereocilia orientation and length in the ear, kidney growth and branching, polycystic kidneys, sternum growth, intestinal growth, and lung growth. The majority of these defects resulted in shorter and wider growth phenotypes (Mao, Mulvaney et al. 2011). Loss of Fat4, the mammalian homologue of *Drosophila* Fat, in the mouse phenocopies defects seen in the Dchs1 mutant mouse (Saburi, Hester et al. 2008). Additionally, double mutants lacking Dchs1 and Fat4 resemble the single mutants, suggesting both function within the same pathway, possibly as a receptor ligand pair (Mao, Mulvaney et al. 2011). Murine mRNA expression of *Dchs1* by *in situ* hybridization reveals expression in tissues including kidney, lung, intestine, brain and heart. Closer examination of the *in situ*s presented in this study reveal expression in the cardiac valves, although the authors fail to mention or study this in detail (Rock, Schrauth et al. 2005). The following chapters aim to identify a role for Dchs1 in valve development and disease.

CHAPTER 2: DEVELOPMENTAL BASIS FOR FILAMIN-A-ASSOCIATED MYXOMATOUS MITRAL VALVE DISEASE

Introduction

Mutations in filamin-A have been identified as causal in a large family with inherited X-linked nonsyndromic myxomatous valvular dystrophy (Kyndt, Gueffet et al. 2007). Genetic knockout studies have indicated a role for filamin-A in cardiac and vascular development. Two genetic knockout models have been generated and both are embryonic lethal by embryonic day (E) 14 due to vascular hemorrhaging. These mice exhibit additional cardiovascular malformations including incomplete septation of the outflow tract, atrial and ventricular septal defects, aortic arch interruption, vascular permeability, and valve defects (Feng, Chen et al. 2006, Hart, Morgan et al. 2006).

To determine a mechanism by which filamin-A facilitates postnatal valve disease, I used a conditional knockout model, whereby filamin-A is removed from the AV valves. The filamin-A floxed mouse was crossed with a mouse that expresses an endothelial-specific receptor tyrosine kinase (Tie2) promoter directing expression of Cre, in order to target endothelial cells for genetic removal of filamin-A (Kisanuki, Hammer et al. 2001). MVD penetrance is 100% in these mice, making the filamin-A/tie2-Cre cKO mouse a good model to study the disease and its development.

Results

Filamin-A is robustly expressed during cardiac development and restricted to non-myocyte cells. *Figure 2.1* depicts immunohistochemical (IHC) analysis of filamin-A expression during embryonic (E13, E15), fetal (E17), and neonatal (day 1) life. Expression was detected in the endocardium, epicardium, valvular interstitial cells, and myocardial interstitial cells during developmental timepoints but was significantly reduced in the adult. This suggests filamin-A plays a more influential role in developmental processes.

To determine the functional significance of filamin-A in regulating valve biology during development, the filamin-A floxed mouse was bred onto the Tie2-Cre background to generate cKO mice. Since the AV valves are primarily derived from an endothelial origin, this mating strategy provides a model to study the functional consequence of filamin-A loss in valve development. Mice generated from this cross were present in expected Mendelian ratios. Female heterozygote mice exhibited no cardiac defects, while male homozygous mice exhibited 100% penetrance. Filamin-A cKO males exhibit thickening of both the anterior and posterior leaflets of the mitral valve with excess tissue (*Figure 2.2*). Movat's pentachrome and Masson's Trichrome stains performed on cKO and wildtype (Wt) tissue from 2 month old mice show changes in matrix and loss of collagen/proteoglygan organization and zonal interfaces in cKO mitral leaflets. Additional IHC analysis for collagen and hyaluronan binding protein (HaBP) demonstrates complete loss of these boundaries and an increase in proteoglycan production in the cKO animals (*Figure 2.2A*).

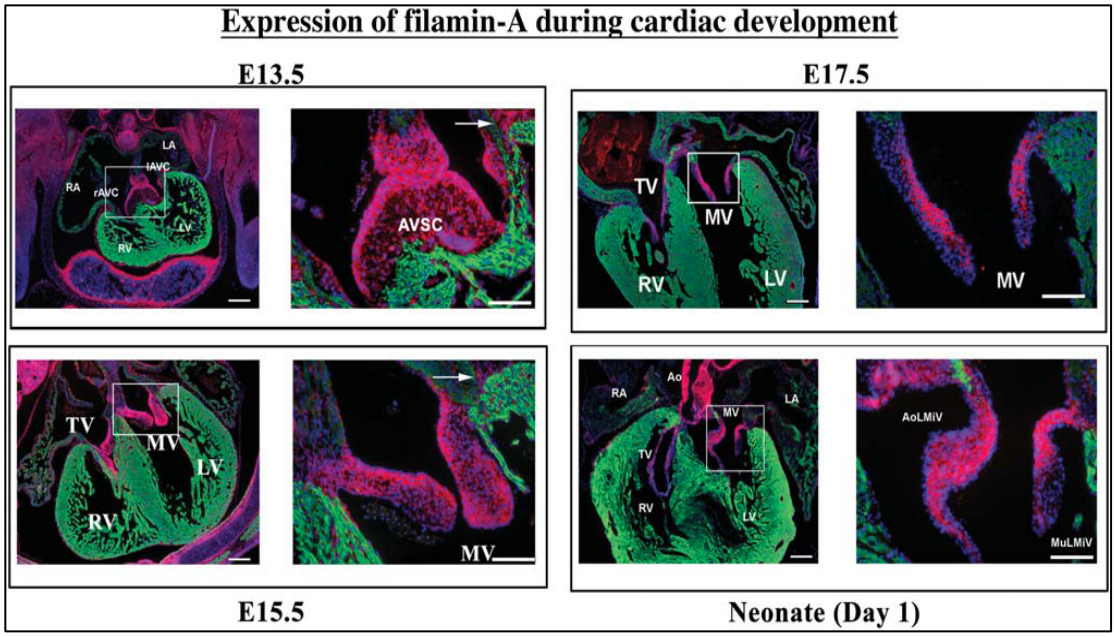

Figure 2.1. Protein Expression of Filamin-A During Cardiogenesis. Immunohistochemistry was performed on E13.5, E15.5, E17.5, and neonatal day 1 hearts for filamin-A (red), MF20/myocytes (green), and nucei (blue). Filamin-A is expressed in non-myocyte cell populations within the heart. High magnification images depict the atrioventricular septal cushions (AVSC), the mitral valve (MV), and the AV sulcus (arrows). Other regions of the heart labeled, left ventricle (LV), right ventricle (RV), tricuspid valve (TV), right atrium (RA), and left atrium (LA).

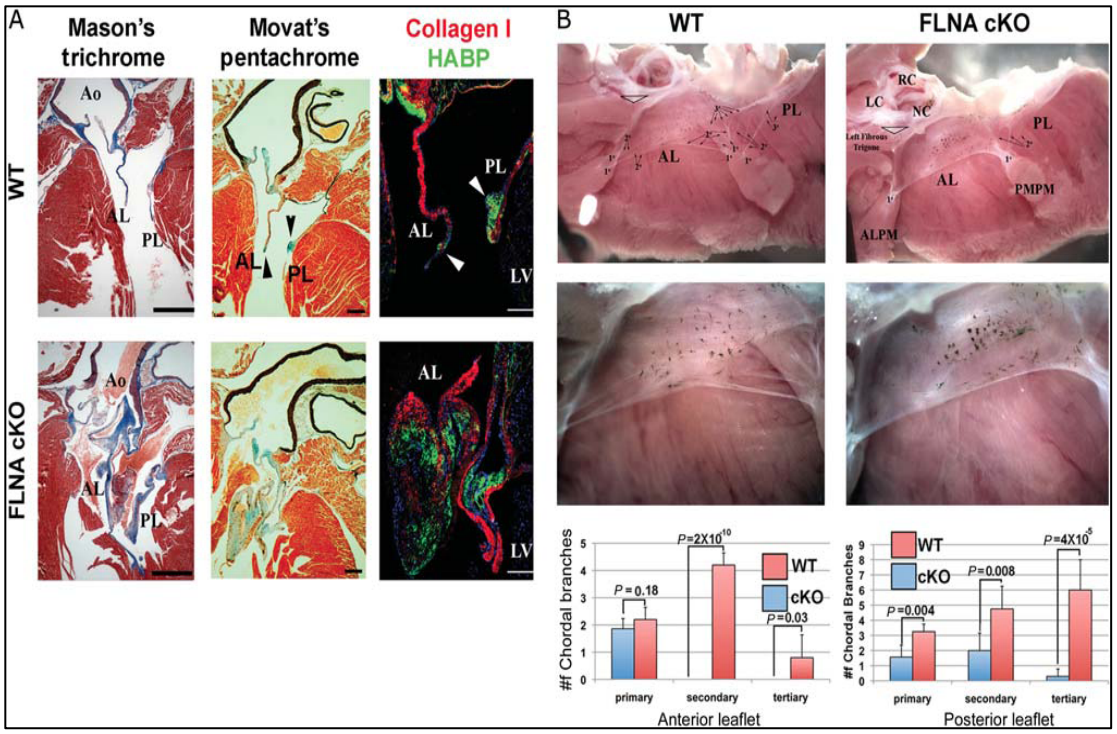

Figure 2.2. Filamin-A cKO Mice Develop Myxomatous Valves. (A) Mason's trichrome, Movat's pentachrome stains showing filamin-A cKO mice have enlarged, excess tissue at 2 months of age. Scale bars: 1 mM. IHC indicate profound disorganization of the collagen (red)/hyaluronan (green) matrix indicative of a myxomatous phenotype. Scale bars = 200 mm. AL, PL, anterior and posterior mitral leaflets. (B) Gross low and high magnification whole mount views of 2-month-old mitral leaflets showing chordae tendineae branching patterns connecting the anterior (AL) and posterior (PL) leaflets to the papillary muscles. Whereas WT leaflets exhibit ordered branching patterns (primary, secondary, and tertiary), the filamin-A cKO mice have a reduction and/or loss in branched chordae. Branching pattern is quantified in the graph. PMPM and ALPM, posterio medial and anterior lateral papillary muscles; LC, RC, NC, left, right and non-coronary aortic leaflets. P-values are denoted. n = 5 for WT, n = 7 for cKO.

Chordae tendineae, which anchor valve leaflets to the papillary muscle, are also endothelial derived and therefore filamin-A deficient in the Tie2-Cre cKO mouse. I additionally examined whether filamin-A plays a role in chord formation. Gorss, morphological analysis of whole mounted hearts reveals thickened primary chordae and loss of chordal branching pattern of the anterior and posterior leaflets of the mitral valve of cKO mice (*Figure 2.2B*). Quantification in *Figure 2.2B,* of the branching pattern based on the number of chordal branches reveals a significant decrease in primary, secondary, and tertiary branching.

To trace the valvular defects back to inception and identify the onset of disease, filamin-A cKO mice were examined during developmental timepoints. Morphological alterations in the mitral valve are not observed until E17, when significant valve enlargement is evident and these changes continued into neonatal timepoints (*Figure 2.3*). Histological sections stained with hematoxalin and eosin stain show enlarged and misshapen leaflets. These sections were used along with AMIRA 3D software to generate 3D reconstructions of mitral valve leaflets at E17 and neonatal day 2. Volumetric quantification of leaflet volume was obtained from the 3D reconstructions and confirms that both the anterior and posterior leaflet of the mitral valve are significantly larger in the cKO.

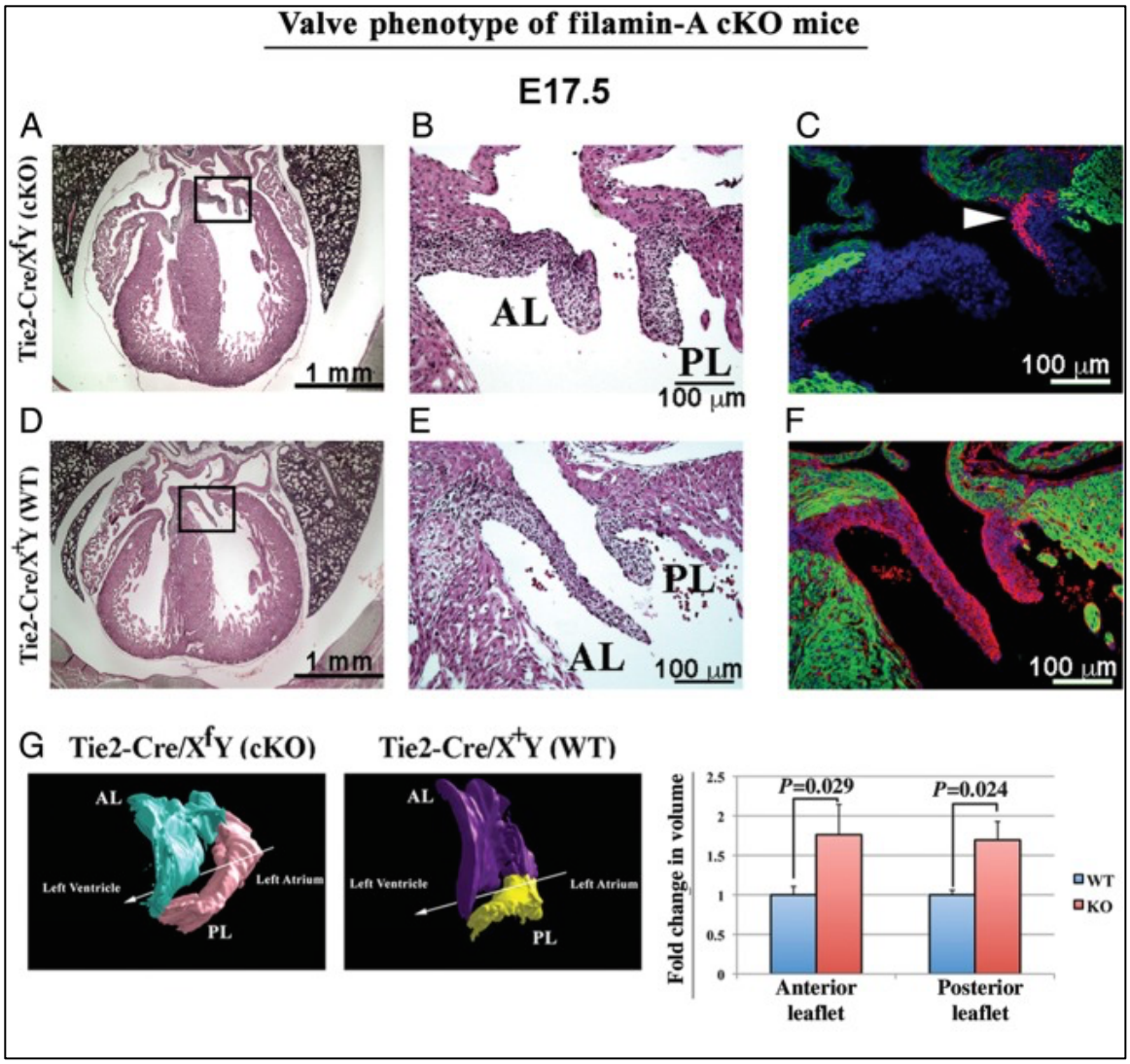
Valve phenotype of filamin-A cKO mice
E17.5
A
B
C
Tie2-Cre/X^fY (cKO)
1 mm
AL
PL
100 μm
100 μm
D
E
F
Tie2-Cre/X^+Y (WT)
1 mm
PL
AL
100 μm
100 μm
G
Tie2-Cre/X^fY (cKO)
Tie2-Cre/X^+Y (WT)
AL
Left Ventricle
Left Atrium
PL
AL
Left Ventricle
Left Atrium
PL
Fold change in volume
P=0.029
P=0.024
2.5
2
1.5
1
0.5
0
Anterior leaflet
Posterior leaflet
WT
KO

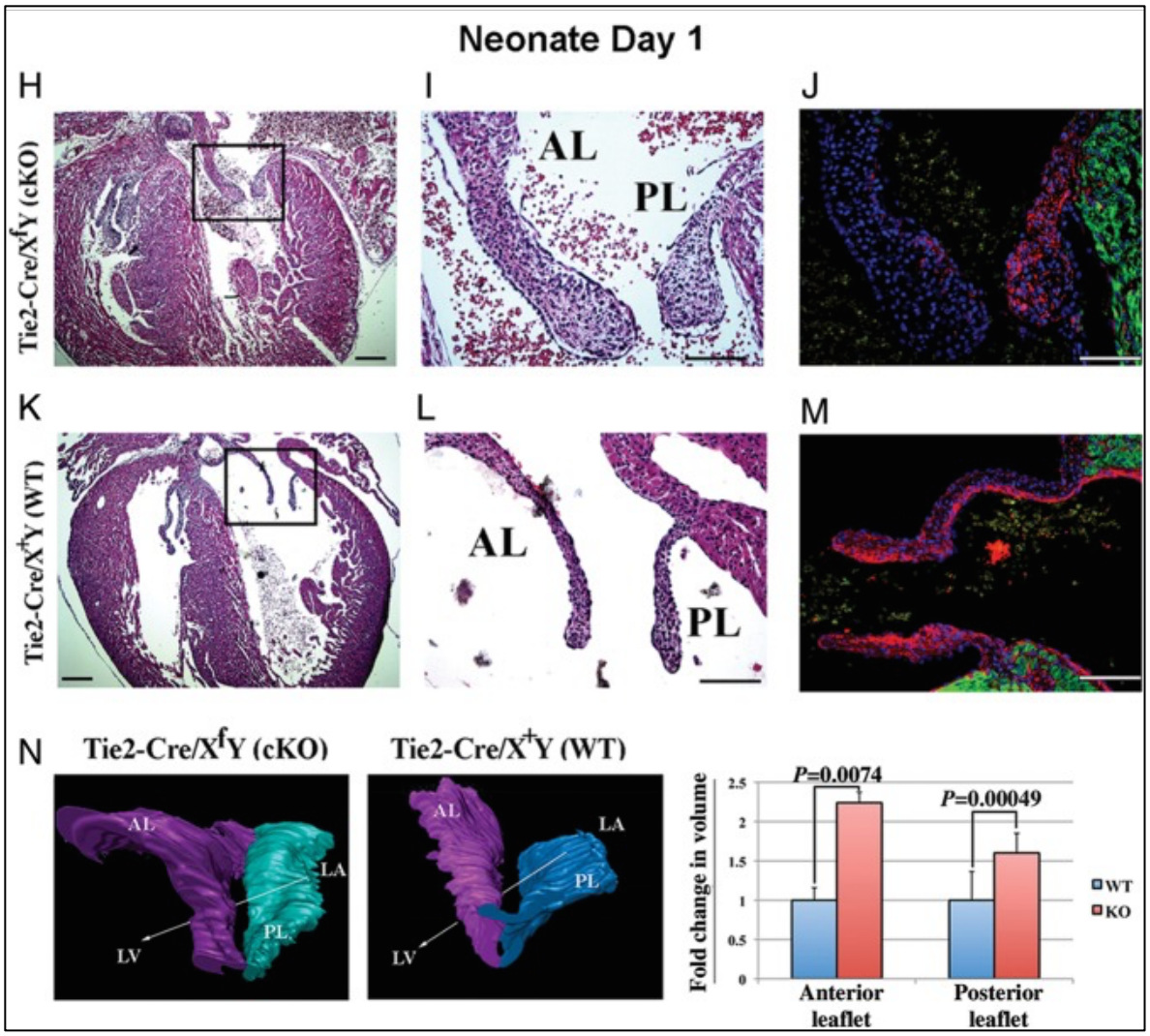

Figure 2.3. Filamin-A cKO mice exhibit enlarged AV leaflets during fetal and neonatal life. (A, B, D, E, H, I, K, and L) The histological assessment of filamin-A conditional KO mice (cKO; Tie2-Cre/X^{f}Y) compared with littermate control animals (Tie2-Cre/X^{+}Y) at E17.5 and neonatal Day 2 using H&E stains. Mitral leaflets of the cKO mice exhibit significant changes in the valve width, length, and shape. (C, F, J, and M) IHC to confirm filamin-A is genetically removed using the Tie2-Cre recombinase mouse line. Little staining of filamin-A (red) is seen in the anterior leaflet of the cKO mouse (AL), whereas significant filamin-A positivity is observed in the posterior leaflet (PL, arrowhead). Green staining is MF20. (G and N) AMIRA 3D reconstructions were performed on the entire mitral leaflet and show shape modifications in the cKO coincident with a significant increase (P-values noted) in volume. Arrows in G and N indicate direction of blood flow. n=3 for each genotype. All samples were littermates, sex, and age matched. Magnification bars: A, D, H, K = 1 mm; B, C, E, F, I, J, L, M = 100 mm.

To validate that this finding is in fact a direct effect of loss of filamin-A and not due to secondary defects in the genetic removal of filamin-A from all endothelial and endothelial-derived cells in the entire animal, the filamin-A floxed mouse was bred onto an NfatC1-Cre background in which NfatC1 is only expressed in endothelium within the developing heart (Wu, Wang et al. 2011). Filamin-A NfatC1-Cre cKO mice exhibit a similar phenotype to the Tie2-Cre cKO mice, indicating loss of filamin-A form either of these genetic lines results in developmental defects in valve size and shape.

Potential mechanisms by which loss of filamin-A leads to developmental defects and valve enlargement were examined. There were no appreciable differences in cell proliferation (ki67 and PCNA), apoptosis, or total cell number (*Figure 2.4*). Proliferating cells were primarily localized to the endocardium and sub-endocardial mesenchyme and did not overlap with filamin-A-deficient cells. To determine whether matrix production was contributing to valve enlargement, ECM components were examined. IHC analysis of collagen, versican, and hyaluronan were not significantly changed between genotypes, suggesting matrix production was not a contributing factor to valve enlargement in the cKO (*Figure 2.5*). As cell proliferation and matrix production do not appear to be directly involved in the valve enlargement phenotype at E17.5, attention was turned back to the patients with X-linked myxomatous valvular dystrophy (XMVD). I hypothesized that analysis of the mutations may provide insight into biological activities by which the native protein functions.

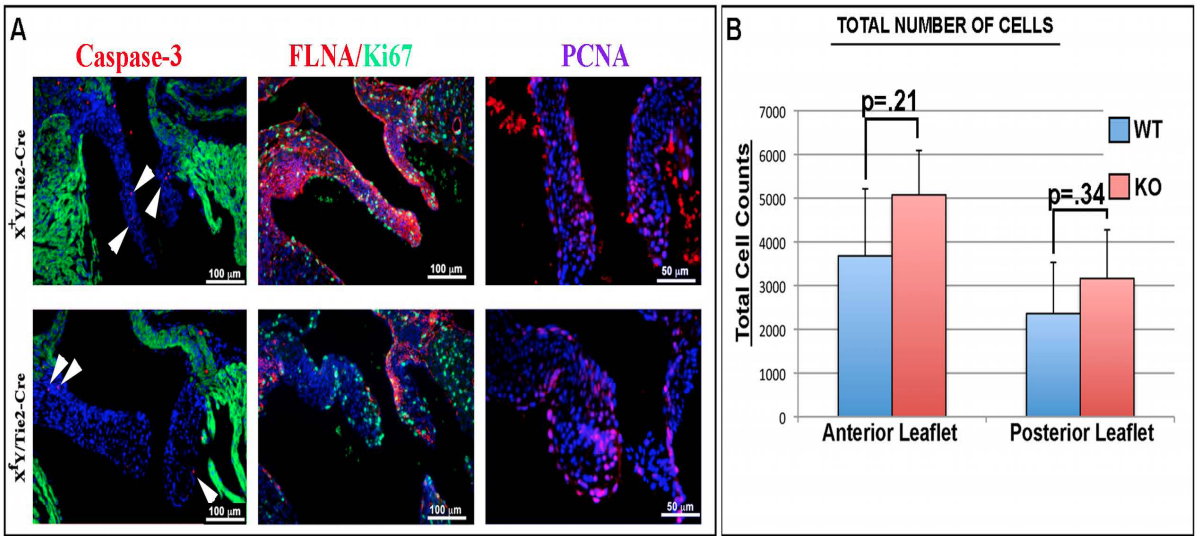

Figure 2.4. Proliferation, Apoptosis, and Total Cell Number Remain Unchanged in Filamin-A cKO Valves. (A) IHC for Activated Caspase-3 (red) and MF20 (green) shows minimal number of cells undergoing apoptosis. Co-staining for Filamin-A (red) and Ki67 (green) shows no changes in proliferating cells or proliferating cells which express filamin-A. PCNA (purple) confirms proliferating cells between genotypes. (B) Total number of cells were counted in both the anterior and posterior leaflets. There was no significant difference between the number of cells between wildtype and filamin-A cKO mice.

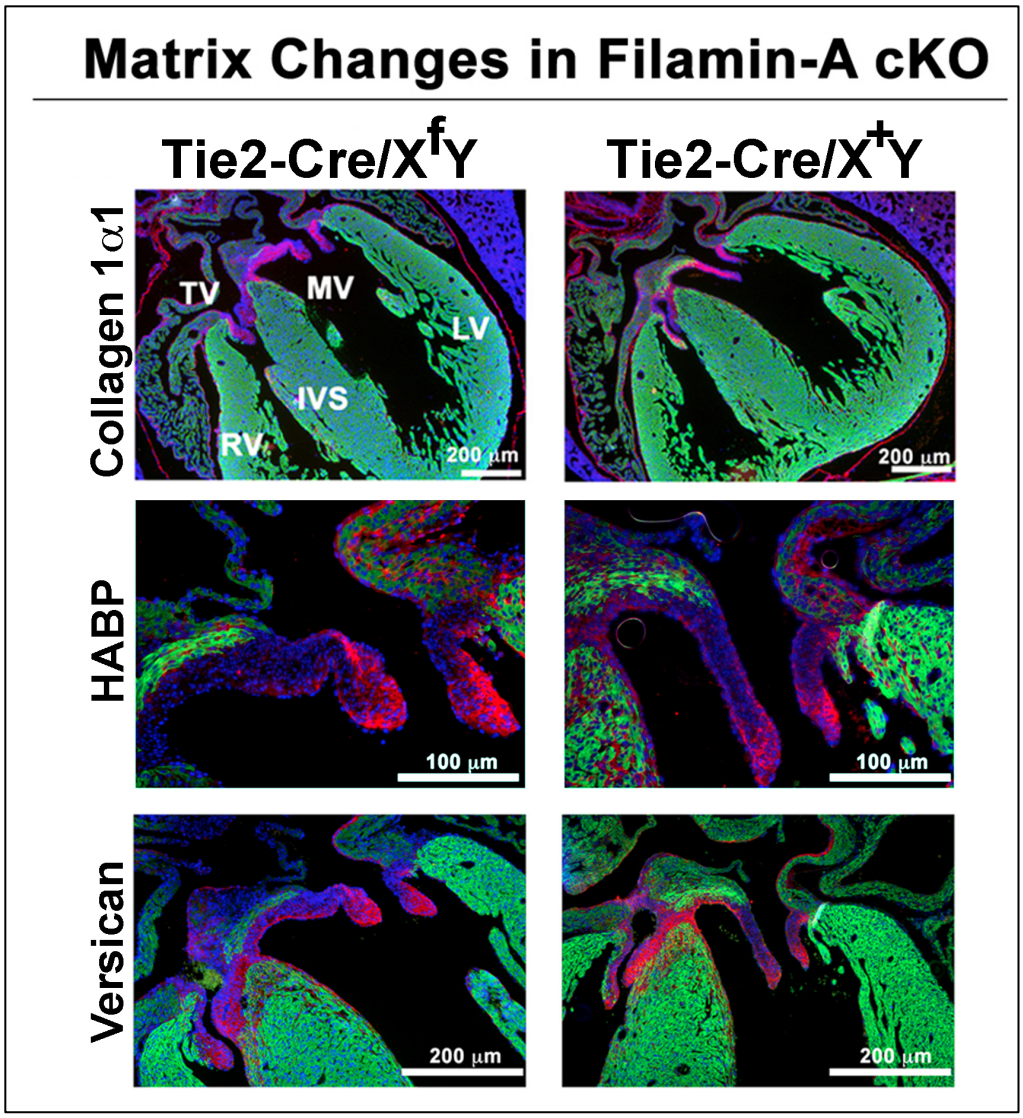

Figure 2.5. Matrix changes in Filamin-A cKO. IHC for Collagen 1, Hyaluronan Binding Protein (HaBP), versican (all red), MF20 (myocardium/green), and nuclei (blue) show no significant changes in matrix expression at E17 between wildtype (Tie2-Cre/$X^{+}Y$) and cKO (Tie2-Cre/$X^{f}Y$).

Three dimensional *in silico* modeling of the amino end of filamin-A indicate the XMVD patient mutations are inwardly oriented on filamin-A repeats, suggesting these residues may be involved in the formation of a protein-docking interface (*Figure 2.6*). Upon closer examination, this region contains potential recognition sites for the enzyme transglutaminase 2 (TG2). Additionally, the sequence near the P637Q mutation (WPQEA) is nearly identical to defined TG2 interacting sequences (APQQEA) found in fibrillin-1 (Khew, Panengad et al. 2010). Thus I examined potential interactions between TG2 and filamin-A.

TG2 has been previously shown to post-translationally modify intracellular and extracellular proteins (collagen, fibrillin, and filamin-A) through covalent attachment of bioamines such as serotonin (Watts, Priestley et al. 2009, Walther, Stahlberg et al. 2011). The functional consequence of this modification is unknown, but other work suggests this modification results in changes in cytoskeletal activity (Watts, Priestley et al. 2009). Since filamin-A is directly linked to the cytoskeleton, we hypothesized that intracellular interactions between filamin-A, TG2 and internalized serotonin in interstitial cells may be important in regulating the valve tissue size by stimulating contractile-dependent matrix compaction during the late stages of valve development. To test this hypothesis, expression patterns of filamin-A, TG2, tryptophan hydroxylase-1 (tph-1; rate limiting enzyme in serotonin biosynthesis), and the serotonin transporter (SERT; main mechanism for internalizing serotonin) were analyzed to determine potential overlap in protein expression during valve development.

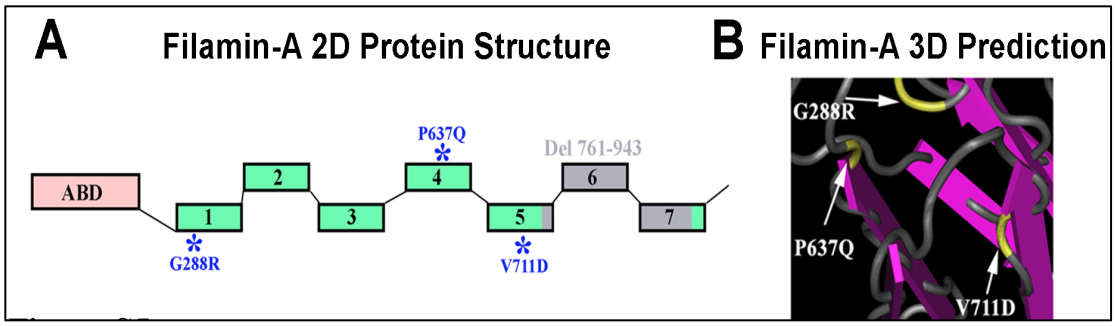

Figure 2.6. 3D *in silico* Modeling of Filamin-A Point Mutations. (A) The amino end of filamin-A and the location of the XMVD point mutations (blue) and deletion (gray), Actin-binding domain (ABD). (B) *In silico* 3D model generated using Cn3D software. The mutation residues are depicted in yellow and labeled with arrows. Mutated residues are located at an inward facing pocket region.

At E13.5 filamin-A is expressed in all non-myocyte cells throughout the heart including the cardiac cushions. Whereas the expression of TG2 protein at this timepoint is absent, SERT is found in a punctate pattern in the AV septal complex and tph1 is primarily found in endocardial and sub-endocardial mesenchyme of the developing leaflets. Thus, overlap of expression of these proteins at E13.5 is not apparent. Co-expression of these proteins begins around E15.5, and by E17.5 filamin-A, TG2, tph1, and SERT are each expressed in the developing mitral and tricuspid leaflets, being primarily restricted to interstitial valve cells (*Figure 2.7*). No overlap in expression of these proteins is observed in the adult mouse.

ICC was performed to examine whether intracellular serotonin co-localizes with the filamin-A/Actin cytoskeleton during valve development and whether this localization is dependent on TG and/or SERT activity. Primary fetal mitral interstitial valve cells were incubated with biotinylated serotonin. Serotonin signal is detected in an overlapping pattern with both filamin-A (*Figure 2.8*) and Actin. To demonstrate that this overlap in expression patterns is dependent on serotonin transporter and TG activity, experiments were performed in the presence of either clomipramine (SERT antagonist) or cystamine (pan TG antagonist). As shown in *Figure 2.8*, SERT antagonism resulted in loss of co-localization of serotonin with filamin-A in addition to disruption of the filamin-A cytoskeletal network as observed by lack of stress fibers and diffuse filamin-A staining. This depolymerization of the filamin-A/Actin network was also observed when using an additional SERT inhibitor, fluoxetine. Perturbing TG activity using cystamine also disrupted the interaction

between serotonin and filamin-A (*Figure 2.8*). These findings demonstrate that intracellular serotonin and TG activity are required for serotonin co-localization with filamin-A/actin as well as the importance of this interaction in the maintenance and/or formation of stress fibers.

In order to validate a direct interaction between filamin-A and serotonin, co-immunoprecipitation experiments were performed either in the presence or absence of the TG inhibitor, cystamine. As demonstrated in Figure *2.9*, filamin-A immunoprecipitates with serotonin in vivo (lane1), which is blunted (50%) by the addition of cystamine. It was suprising to observe such a modest inhibition of filamin-A/serotonin interactions in the presence of cystamine. One possibility is that this covalent interaction has already occurred in vivo, thus precluding a more significant effect of the TG inhibitor. To test this potential and to verify the filamin-A–serotonin interaction is dependent on TG activity, reciprocal co-IP reactions using a chemically synthesized biotinylated-serotonin were performed (*Figure 2.9*). During the reaction, all samples received biotinylated serotonin either in the presence or absence of cystamine. Samples were co-immunoprecipitated with a filamin-A antibody, run on a Western and detected with a streptavidin-HRP antibody. Two bands at the corresponding molecular weight of filamin-A are detected only in the absence of cystamine, demonstrating TG activity is required for this reaction to occur. These data demonstrate a TG2-mediated interaction between intracellular serotonin and filamin-A in mitral valve fibroblasts in vitro and in vivo and suggest their functional importance in forming and/or maintaining stress fibers.

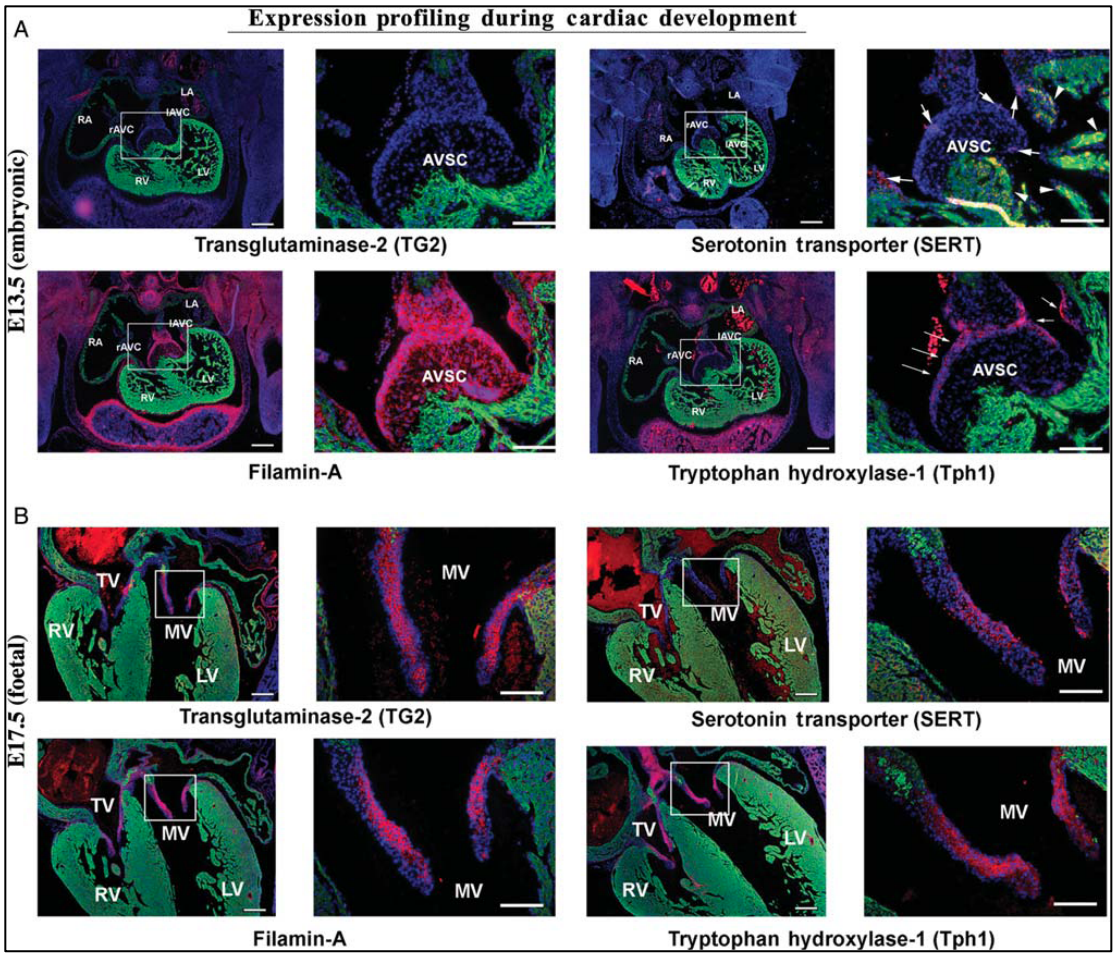

Figure 2.7. Co-expression of Filamin-A, TG2, SERT, and Tph1 During Fetal Valve Development. IHC's were performed to determine overlap of the expression of filamin-A, TG2, SERT, and tph1 during cardiac development. For each immunostain, MF20 is green, nuclei-blue, and specific protein is in red. (A) At E13.5, no significant overlap of expression is observed between each of the proteins. No detectable expression of TG2 is seen. Only punctate expression of SERT is observed in the developing valves (arrows), as well as expression in the endocardium and myocytes (arrow heads). Tph1 is expressed in the developing cushions but is restricted to the endocardium and subendocardial mesenchyme (arrows) filamin-A is expressed in all non-myocyte cells at this stage. (B) By E17.5, each protein shows significant overlap in expression patterns being primarily restricted to the interstitial valve fibroblast. Scale bars: low magnification = 200 mm, high magnification = 100 mm.

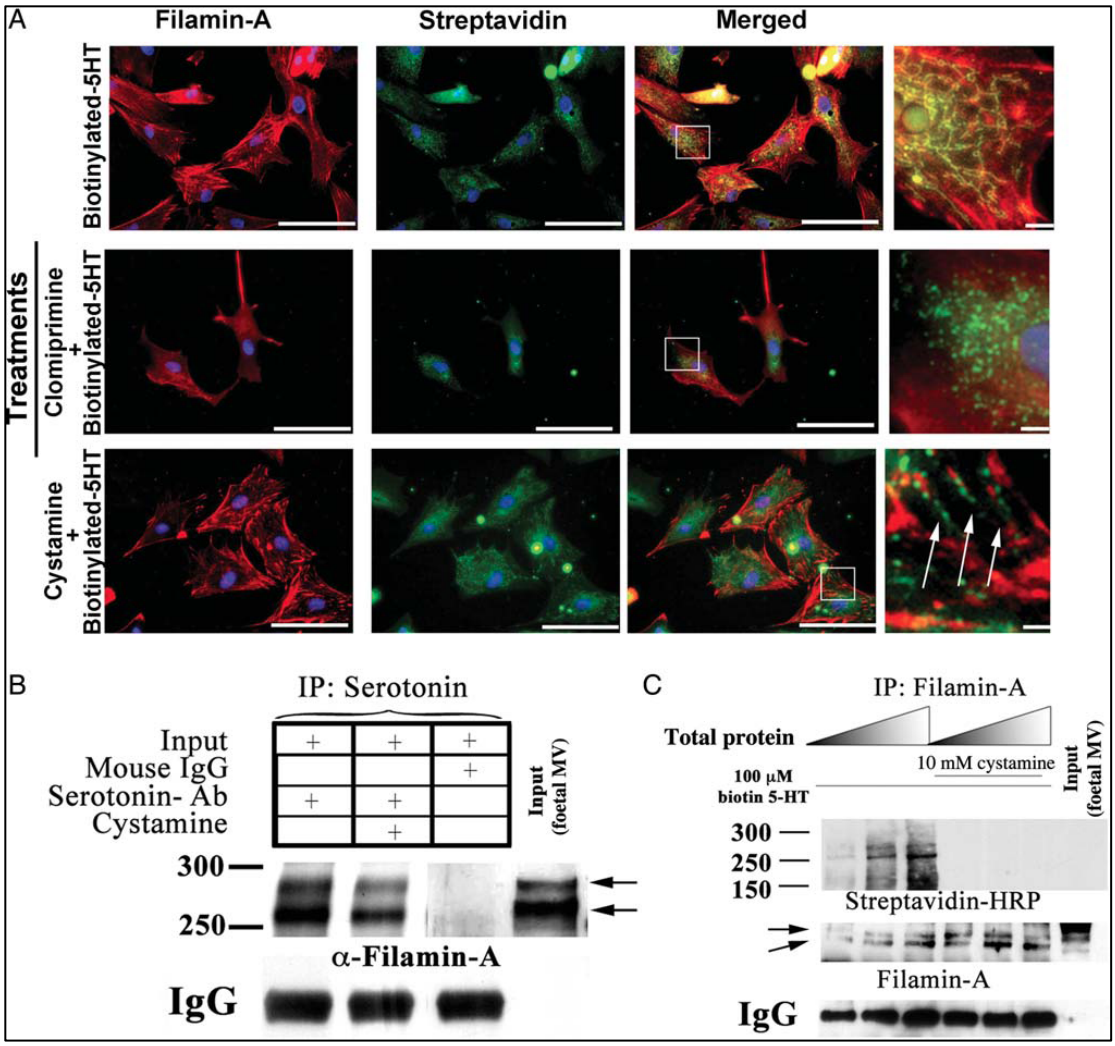

Figure 2.8. Internalized Serotonin Interacts with Filamin-A and Promotes Stress Fiber Formation. (A) Primary fetal mitral valve fibroblasts were supplemented with biotinylated serotonin (biotinylated-5HT) either in the presence of a SERT inhibitor (clomiprimine) or a TG inhibitor (cystamine), or no inhibitor. Cells were fixed and stained for filamin-A, and/or streptavidin (to detect biotinylated-5HT). In controls (biotinylated-5HT treatment only), serotonin appears to decorate the filamin-A cytoskeletal networks (yellow staining in the merge samples). Blocking internal transport (Clomiprimine) or TG2 activity (cystamine) resulted in a disruption of this interaction suggesting internalization and/or TG2 activity are required for serotonin incorporation into the cytoskeleton. Additionally, loss or depolymerization of stress fibres (arrows) is apparent in clomipramine- or cystamine-treated cells, respectively. Blue-Nuclei. (B) Fetal mitral valve lysate was used in TG2 enzymatic assays (in the presence or absence of cystamine). Co-IP's demonstrate physical interaction between serotonin and filamin-A with a reduction in binding upon TG2 inhibition. (C) Serotonin is incorporated into filamin-A in cultured fetal mitral valve fibroblasts and is dependent on TG2. Assays were performed as described in (B) except filamin-A antibody was used to IP filamin-A and a-streptavidin-HRP was used to detect biotinylated serotonin. Input represents starting material. Two forms of filamin-A are present in the valves (FLNA-1/2).

This approach has defined a novel interaction between filamin-A and serotonin that is specific for fetal valve development *in vivo*. Perturbing these interactions appears to result in failed co-localization of filamin-A and serotonin, and causes a loss of stress fibers. Owing to the importance of stress fibers in promoting cellular-dependent contractility, I next examined whether the serotonin–filamin-A interaction is required for retaining contractile function of valve interstitial cells. This was tested in the context of matrix remodelling/gel compaction assays, which are accepted tools for monitoring cytoskeletal-dependent matrix condensation/organization. Fetal mitral valve fibroblasts were entombed within collagen or fibrin gels and allowed to freely compact over time. I initially tested the serotonin pathway and its role in promoting matrix compaction using collagen gels (*Figure 2.9*). Following polymerization of the gels at Day 0, the gels were released from the wells to be free-floating and stimulated with increasing doses of serotonin. After Day 1, valve fibroblasts receiving a dose of 10 mM serotonin showed a significant increase in matrix compaction (*Figure 2.9A*). The maximal effect of serotonin was observed at the 10 mM dose. A statistical increase in serotonin-mediated compaction was observed from Days 1 to 3, demonstrating serotonin is required for promoting fetal valve cell contractility and extracellular matrix compaction. Whether intracellular serotonin was required for this cellular behavior was interrogated by blocking serotonin transporter function using two highly specific inhibitors: clomipramine and fluoxetine (data not shown). Addition of either drug plus 100

mM of exogenous serotonin resulted in a significant inhibition of compaction, demonstrating a requirement for intracellular serotonin in matrix compaction and not a result of serotonin receptor engagement. In the three-dimensional matrix system, no changes in proliferation and/or apoptosis were detected (consistent with pervious reports of this assay system) indicating the changes observed are not due to differences in cell numbers (data not shown) (Stegemann and Nerem 2003). Although we cannot rule out cell surface serotonin receptor (e.g. 5-HT1, 5-HT2) engagement as having a contribution, this data demonstrate that intracellular serotonin is the primary and major mode for promoting matrix compaction. As serotonylation of filamin-A requires intracellular TG activity, I hypothesized that blocking this activity should result in failed matrix compaction. To test this hypothesis, cells/gels were incubated in the presence of 100 mM serotonin and increasing doses of the TG inhibitor, cystamine. Blockade of TG activity resulted in attenuation of matrix compaction (*Figure 2.9C*), consistent with the observations that intracellular serotonin/filamin-A interactions provide a primary means for remodeling the extracellular matrix. To further validate the interdependency of filamin-A/serotonin/TG interactions, I performed matrix compaction assays using freshly isolated E17.5 filamin-A cKO mitral valve interstitial cells in the presence of serotonin. As shown in *Figure 2.9D*, filamin-A-deficient cells are unable to effectively respond to serotonin treatment and result in the abrogation of matrix compaction.

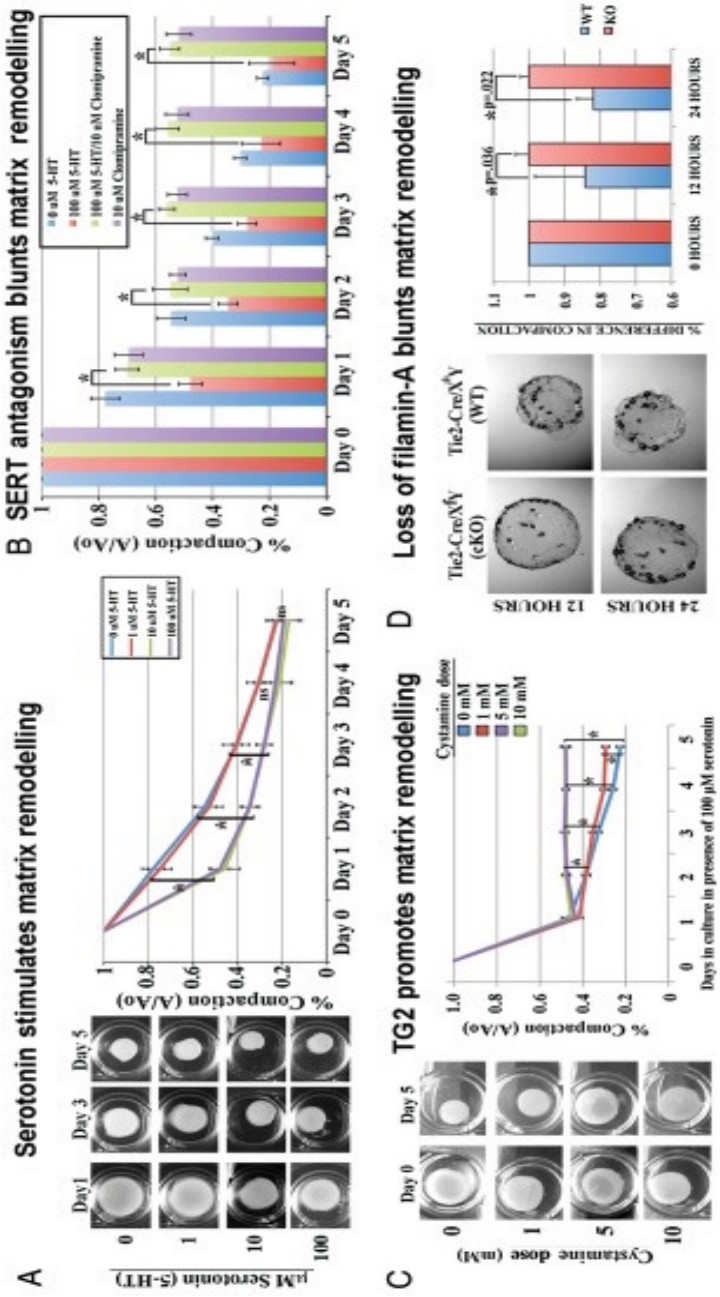

Figure 2.9. Perterbation of Filamin-A-Serotonin Interactions Blunt Matrix Remodeling.
(A) Serotonin significantly increased the ability for valve fibroblasts to condense collagen over a 5-day period. Actual gels are represented in (A) to demonstrate effect of exogenous addition of Serotonin. (B and C) Serotonin-induced compaction (in the presence of 100 mM serotonin) was blunted using a SERT inhibitor (clomiprimine) and a TG inhibitor (cystamine), demonstrating internalized serotonin and TG activity are required for matrix condensation. (A/Ao, final area of gel divided by initial area). *Statistical significance: P , 0.05. ns, not significant. N=12 for each condition. (D) E17.5 anterior mitral leaflets were removed from cKO and littermate WT mice placed in fibrin compaction assays in the presence of serotonin. Filamin-A cKO cells exhibit _20% reduced ability to efficiently compact the matrix (compare left panels to right panels) in the presence of 100 mM serotonin with P-values denoted. n = 20 constructs analysed for each.

Discussion

Myxomatous valvular dystrophy of the cardiac valves is a disease that consists of leaflet enlargement, breakdown of the extra-cellular matrix, and loss of the zonal boundaries which define the layers of the valvular leaflets. As a result, the leaflets are unable to properly close during ventricular systole resulting in prolapse and mitral regurgitation. Little is known about the pathogenic mechanisms that underlie development of this disease. These data indicate a developmental origin for the disease, whereby faulty developmental processes during post-EndoMT stages result in enlarged myxomatous valves in the adult mouse by 2-months of age. The myxomatous phenotype observed in these mice at fetal and adult stages mimics the clinical phenotype observed in the XMVD patients by echocardiography (Kyndt, Gueffet et al. 2007, Lardeux, Kyndt et al. 2011). Additionally, these reports indicate defects in chordae tendineae in these patients; therefore chord formation was examined in the filamin-A model of disease. Consistent with the patients, I observed thickened chords with defects in the number of chords and their branching patterns in the filamin-A cKO. The matricellular protein Periostin, has previously been reported to also direct chordae tendineae formation by promoting differentiation of mesenchymal cells into fibroblasts post-EndoMT (Norris, Potts et al. 2009). Though it is possible filamin-A and perisotin may interact to direct this process, a specific link between these two proteins has yet to be defined.

This work has identified a developmental origin for the post-natal myxomatous phenotype observed in the filamin-A cKO mouse. These profound

defects in valve size and shape are observed at E17. This indicates a role for filamin-A in the post-EndoMT phase, when the valvular leaflets undergo compaction and organization of the ECM components. In order to define the molecular mechanisms by which filamin-A regulates this process, I performed a 3D *in silico* modeling of the disease causing filamin-A point mutations. The point mutations are clustered at the amino end of the filamin-A protein, which contains a consensus binding motif for the enzyme TG2. TG2 catalyzes thiol and calcium-dependent-transamidation reactions, resulting in the formation of a covalent bond between a peptide bound glutamine and a primary amine group (Sane, Kontos et al. 2007). Previous work has shown TG2 catalyzes a reaction between serotonin and other cytoskeletal proteins including filamin-A (Watts, Priestley et al. 2009). Based on the importance of serotonin in contributing to cellular contractility as well as valvular pathologies and the presence of TG2 consensus interacting motifs in a region spanning mutations in filamin-A that cause human valvular disease, I hypothesized that co-operative interactions between serotonin, filamin-A and TG2 are important for cell contractility-dependent matrix organization (Connolly, Crary et al. 1997, Shively, Roldan et al. 1999, Chester, Misfeld et al. 2001, Gustafsson, Tommeras et al. 2005, Connolly, Bakay et al. 2009). These data show that the expression of these components overlap during late stages of valve development in valvular interstitial cells, and that the disruption of any component in this complex results in functional deficits in the valvular cells ability to remodel the surrounding matrix *in vivo* and *in vitro*. The formation of stress fibers are required for generation of traction

forces capable of remodeling and compaction, indicating an important role for the cytoskeleton. This data supports the idea that the covalent interactions between serotonin and filamin-A are necessary for this process to occur. Therefore, the defects observed in the filamin-A cKO mice and in the patients with filamin-A mutations may be a result of deficient stress fiber formation and/or stability.

While the TG2 knockout mouse has not been extensively studied, the serotonin transporter knockout mice display valvular phenotypes similar to what I have shown in out filamin-A cKO mouse and in the filamin-A patients (Pavone, Spina et al. 2009). The phenotype in the SERT knockout mice is hypothesized to be a result of excess circulating serotonin leading to hyperactivity of the serotonin receptors. This increase in serotonin receptor activity is thought to promote TGFβ signaling and thus may contribute to the valve phenotype seen in these mice (Mekontso-Dessap, Brouri et al. 2006, Disatian and Orton 2009, Pavone, Spina et al. 2009). This is similar to patients with valve disease who have excess circulating serotonin and those patients who received the ergot deriviative drug, FenPhen, which is a SERT inhibitor and serotonin receptor agonist (Connolly, Crary et al. 1997, Connolly, Bakay et al. 2009). Studies done in canine models of myxomatous valve disease have found a downregulation of the SERT and increased levels of the serotonin receptor, further suggesting these components play a role in valve disease (Oyama and Levy 2010). It is possible that the filamin-A mice may downregulate the SERT

and/or promote increased activation of serotonin-induced TGFβ signaling but this requires further investigation. This is the first identification of a role for serotonin in valve development, since a role for serotonin in cardiac development has not been studied.

During fetal valve development, the AV valves undergo a phase of remodeling where valvular interstitial cells become aligned and the ECM becomes organized and compacted. The cellular and molecular mechanisms that drive this process are largely unknown (de Vlaming, Sauls et al. 2012). Other studies have shown the actin and microtubule cytoskeleton is required for matrix remodeling to occur (Canty, Starborg et al. 2006, Butcher, Norris et al. 2007). Additionally, Tensin1, a focal adhesion protein involved in cytoskeletal organization, has been identified as a candidate gene in a genome wide association study performed in nonsyndromic MVP patients. Loss of Tensin1 in mice results in myxomatous mitral valves, further supporting a role for the cytoskeleton in myxomatous valve disease (Dina, Bouatia-Naji et al. 2015). A mechanism by which the cytoskeleton drives matrix organization is dependent on linkage between the actin network and integrin receptors that provide mechanical cues back to the cell (D'Addario, Arora et al. 2001, Banerjee, Yekkala et al. 2006). One of the main proteins that establishes this connection is filamin-A. This study demonstrates a role for filamin-A in valve development and subsequent myxomatous valve disease, whereby filamin-A deficient cells exhibit a contractile dysfunction *in vitro* and *in vivo* resulting in failed compaction of

both fibrin gels (*in vitro*) and valve leaflets (*in vivo*). Understanding the relationship between integrin beta-1, filamin-A, serotonergic system, stress fiber formation and contractility as an extension and future direction of this study will provide new insights in to valve development and disease.

CHAPTER 3: MUTATIONS IN DCHS1 CAUSE MITRAL VALVE PROLAPSE

Introduction

Mitral valve prolapse is functionally defined as the abnormal billowing of one or both leaflets into the left atrium during ventricular systole. Histologically, the leaflets of the mitral valve are enlarged and exhibit myxomatous degeneration characterized by fragmented collagen, increased proteoglycan accumulation, hyperproliferation, and faulty differentiation of valvular interstitial cells. While the etiology of the disease is largely unknown, familial studies demonstrate an autosomal mode of inheritance with incomplete penetrance (Weiss, Mimbs et al. 1975, Strahan, Murphy et al. 1983). Freed et al. identified a locus, *MMVP2,* that maps to a 43 cM region of chromosome 11p15.4 in a large multi-generational family of Western European decent with autosomal dominant inheritance of MVP (Freed, Acierno et al. 2003). Here I show data that refines this locus and identifies genetic mutations in the gene *DCHS1* that segregate with MVP. *In vitro* experiments define this as a loss of function mutation enabling the use of a heterozygote mouse model to study the disease. I have characterized this mouse model and demonstrate functional, histological, and molecular changes which phenocopy MVP patients. Defects in cell migration, alignment, and adhesion provide mechanistic insight into how Dchs1 functions in mammals. Additionally, enhanced pERK1/2 is observed at the neonatal timepoint which preceeds myxomatous changes, and persists into adulthood, suggesting ERK1/2 may provide the initial que that directs myxomatous degeneration. This provides a potential therapeutic target which may prevent the progression of MVP.

Results

Previous work which provides the basis for this study, identified the *MMVP2* locus mapped to a 4.3 cM region of chromosome 11p15.4 in a large family of western-European descent, with autosomal dominant inheritance of mitral valve prolapse and age-dependent penetrance (Freed, Acierno et al. 2003). This large family consists of 41 individuals in five generations. From this family, DNA and echocardiography was performed on 28 individuals, identifying 12 with MVP, 3 with nondiagnostic minimal leaflet displacement, and 13 as unaffected. The proband (arrow) of this family had severe mitral regurgitation, thickened mitral leaflets, and heart failure resulting in mitral valve repair surgery (*Figure 3.1c*). Using specific diagnostic criteria developed by Levine, R.A. and colleagues, family members with >2mm leaflet displacement in the parasternal long-axis view by echocardiography, were classified as affected with MVP (*Figure 3.1a, c*) (Perloff and Child 1987, Levine, Stathogiannis et al. 1988, Levine, Handschumacher et al. 1989).

Our colleagues at The Center for Human Genetic Research at Harvard University performed tile capture and high throughput sequence analysis of genomic DNA from four affected family members (notated with a red star) in the large pedigree shown in *Figure 3.1a*. As a result of this analysis, 4,891 single nucleotide variants (SNV) and insertion/deletion polymorphisms were identified within the target region.

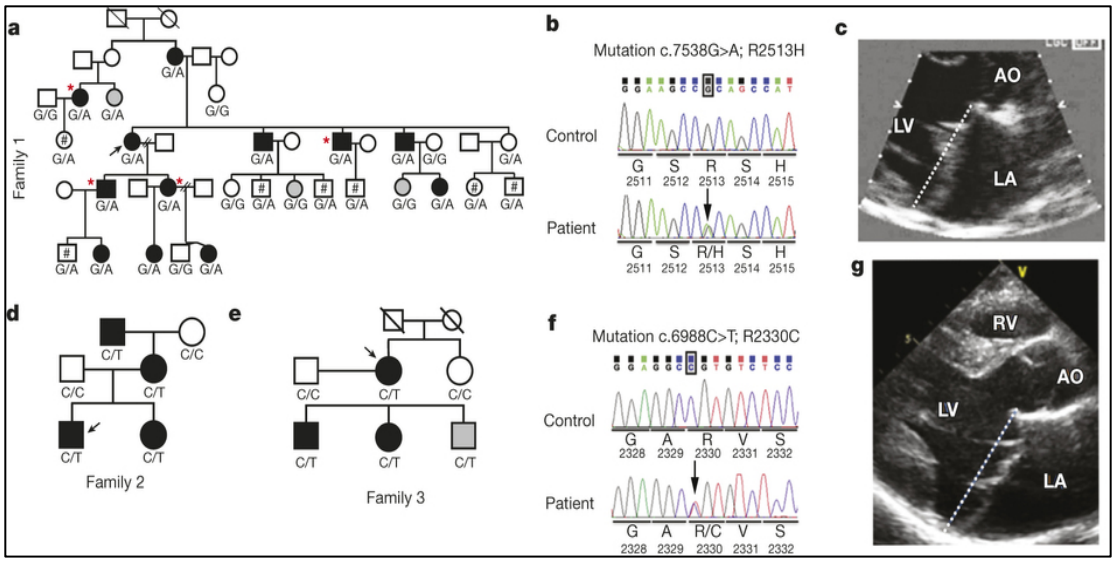

Figure 3.1. Pedigree, Mutation, and Phenotype. Black circles and squares represent affected family members, white circles and squares are unaffected family members, and grey circles and squares are non-diagnostic members with minimal leaflet displacement. Arrows point to probands and if no genotype is shown, those members were unavailable for study (a) Pedigree of the large family with inherited nonsyndromic MVP linked to chromosome 11. #, individuals under 15 years of age, *, individuals sequenced. (b) Chromatogram depicting c.7538G>A (p.R2513H). (c) Two-dimensional echocardiographic parasternal long-axis view of family 1 proband. Dashed line represents annulus. (d,e) Family 2 and 3 pedigrees. (f) Chromatogram of DNA sequence c.6988C>T (p.R2330C). (g) Two-dimensional echocardiographic parasternal long-axis view of family 2 proband. These data were generated by our collegues from the Leducq Foundation.

The SNV pool was narrowed based on three criteria, those that were protein-coding, those that were rare coding variants not present in the general population determined by comparisons against individuals in NHLBI Exome sequencing Project database, and those variants that were predicted to be protein damaging by PolyPhen-2, LRT, and MutationTaster (Adzhubei, Schmidt et al. 2010, Schwarz, Rodelsperger et al. 2010). These criteria led to the identification of three heterozygote protein-altering variants shared by the four sequenced family members: two missense SNVs in *DCHS1,* p.P197L and p.R2513H, and one missense SNV in *APBB1,* p.R481H. APBB1 is an amyloid beta (A4) precursor protein-binding, family B, member 1 gene that is not expressed in the murine heart based on *in-situ* data generated from our collegues, and the APBB1 knockout mouse is not reported to have any cardiac defects (*Figure 3.2)* (Guenette, Chang et al. 2006). Additionally, Zebrafish morpholino knockdown experiments for APBB1 reveal no cardiac phenotype (Performed by David Milan's group). Together, this suggests that the APBB1 Variant likely does not contribute to MVP in this family. To determine the functional effect of *DCHS1* variants, the zebrafish model system was used for its simple genetic system and ability to rapidly reveal gene functions that are difficult to uncover in other systems. The zebrafish, *Danio rerio*, has been successfully used to define mutations implicated in human disease, and therefore represents an appropriate model system to examine these mutations (Chaki, Airik et al. 2012, Golzio, Willer et al. 2012). Zebrafish have two homologues to the human *DCHS1* gene, *dachsous1a* and *dachsous 1b.*

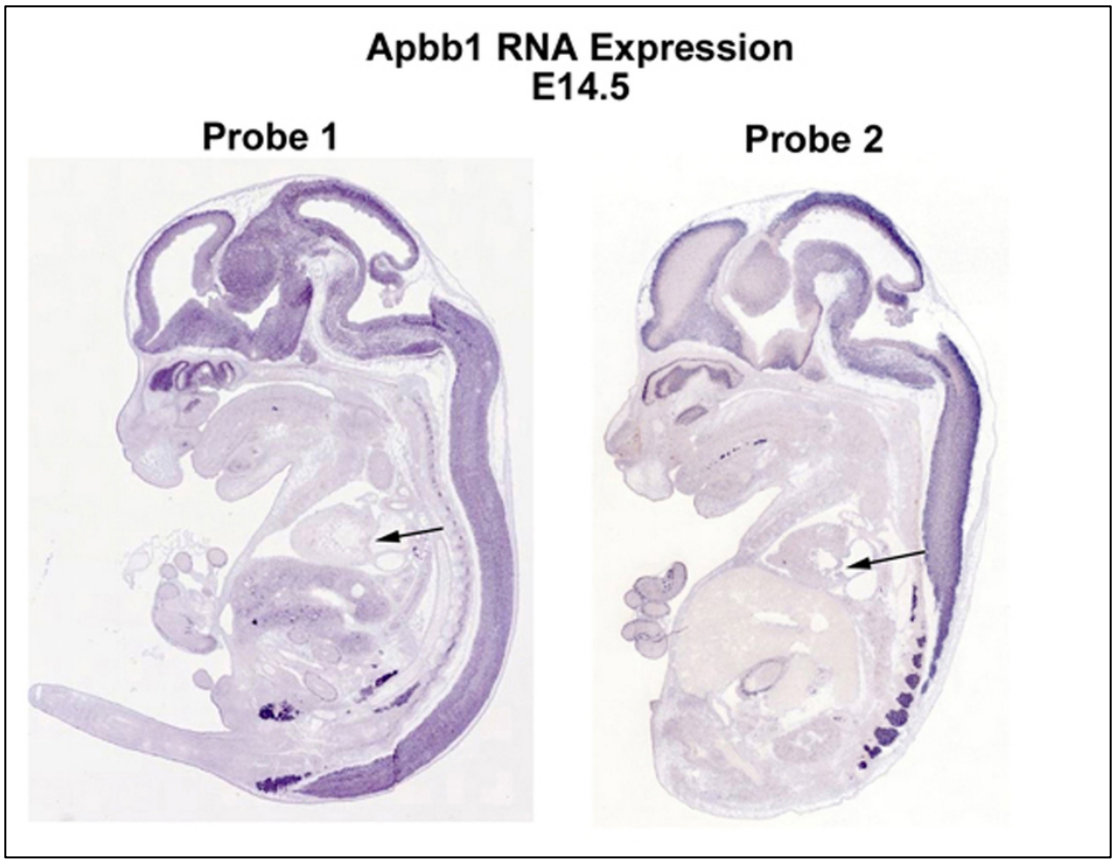

Figure 3.2 *Apbb1* RNA is Not Expressed in the Murine Heart. Two different antisense probes were used to detect Apbb1 RNA expression, which is evident as cranial and neural expression at E14.5. No expression was detected in the heart or the mitral valve (arrow). These data were generated by our colleagues part of the Leducq Foundation.

Dachsous1b is located in a region of chromosome 10 in the zebrafish that is syntenic to the *DCHS1* region of human chromosome 11. All zebrafish data was generated by collaboration with David Milan's group. As shown in *Figure 3.3a,b,* Knockdown of *dachsous1a* did not result in a cardiac phenotype, however knockdown of *dachsous1b* resulted in significant changes in cardiac morphology. Control zebrafish hearts undergo a cardiac looping event and develop an atrioventricular constriction (AVC), which is functionally similar to valve primordial in mammals, by 48 hours post-fertilization (hpf). In *dachsous1b* knockdown fish, this looping process is disrupted, resulting in disturbed AVC formation. In the control fish, blood flow is unidirectional flowing from the atrium into the ventricle. In contrast, the *dachsous1b* knockdown fish exhibits a regurgitation phenotype, whereby the AVC is ineffective at preventing blood from leaking backwards into the atrium. Approximately 76% (*n*=170) of *dchs1b* morphants exhibit AVC defects when injected with a high dose of morpholino (1.5ng), compared to controls which exhibited spontaneous cardiac defects in 0.5% of fish (*n*=205) (*Figure 3.3c).* Whole mount *in situ* hybridization demonstrates *dchs1b* mRNA is highly expressed at the atrioventricular junction at 48 and 72hpf, which corresponds to the defects seen in this region at the 72hpf timepoint (*Figure 3.4*). Additional whole mount *in situ* hybridizations for genes associated with atrioventricular ring development were performed at 48 and 72 hpf. Expansion of *bmp4* expression into the ventricle in *dchs1b* knockdown embryos was observed at 48hpf compared to the restricted atrioventricular ring expression observed in controls (*Figure 3.5*).

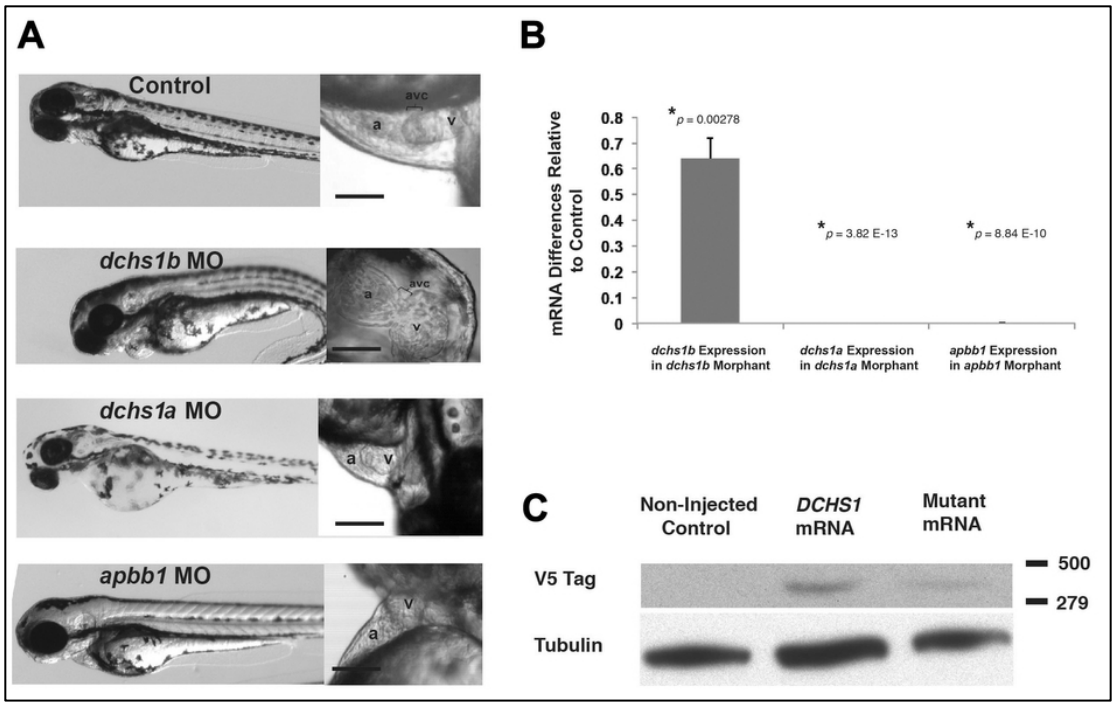

Figure 3.3. Measurement of Endogenous and Exogenous Gene Expression in *D. rerio.* (a) Morpholino knockdown embryos with close up of heart. (b) To assess efficiency of morpholino knockdown, 20 embryos were collected 72 h after injection, mRNA was collected, and quantitative PCR was performed with three technical replicates. David Milan's group demonstrates that morpholino (MO) knockdown of each indicated gene results in reduced mRNA expression, after normalization to beta-actin expression, compared to mock-injected controls (two-sided Student's *t*-test). *P* values are noted on graphs. (c) Western blotting of 20 pooled embryos injected with *DCHS1* mRNA demonstrates the production of protein. Mutant mRNA refers to the compound mutant P197L/R2513H. These data were generated by our colleagues part of the Leducq Foundation.

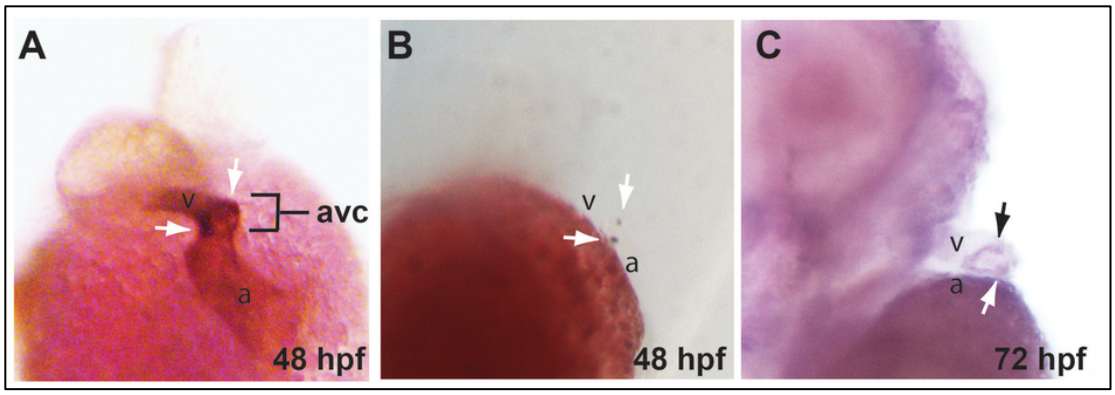

Figure 3.4. *Dachsous 1b* Expression at the Atrioventricular Junction. Whole mount *in situ* hybridization reveals *dachsous 1b* expression at the atrioventricular canal (AVC) at 48 hpf (a,b) and 72 hpf (hpf). Purple is *dachsous 1b* expression and brown is counterstain. These data were generated by our colleagues part of the Leducq Foundation.

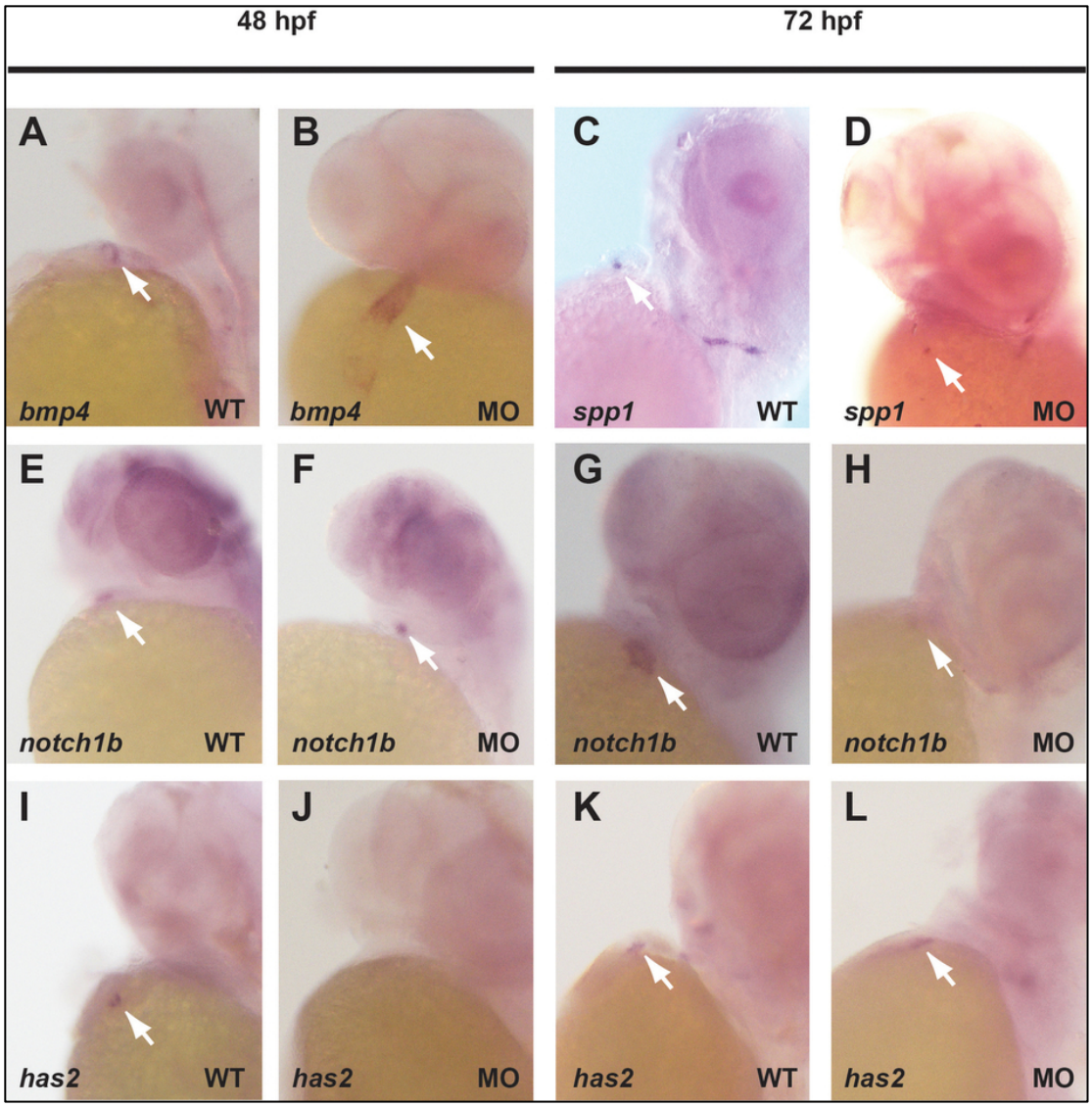

Figure 3.5. ***Dachsous 1b*** **Knockdown Alters Atrioventricular Ring Development Markers.** *In situ* hybridization at 48 hpf and 72 hpf, as indicated, was performed for known atrioventricular ring markers. In contrast to WT (a) *bmp4* expression is expanded into the ventricle at 48 hpf in *dchs1* knockdown embryos at 48 hpf (b), *spp1* and *notch1b* expression was largely unperturbed (c–f), and *has2* expression was not detected at 48 hpf, and is faint at 72 hpf in *dchs1* knockdown, compared to identically handled and stained controls (i–l). These data were generated by our colleagues part of the Leducq Foundation.

Additionally, *has2* expression was lost at 48 hpf and only faintly detectable at 72 hpf in the *dchs1b* knockdown embryo compared to controls, while *notch1b* and *spp1* were unchanged between embryos (*Figure 3.5*). To test the pathogenicity of the mutation in this model, rescue experiments were performed by injecting wildtype human DCHS1 or p.P197L/p.R2513H mutant mRNA with a lower dose of morpholino (0.75 ng) in order to reduce the toxicity of combined RNA and morpholino injection. The wildtype human DCHS1 mRNA was able to rescue the AVC phenotype, whereas injection of the mutant DCHS1 mRNA (p.P197L/p.R2513H) failed to rescue the phenotype (*Figure 3.6*). Injection of the mutant DCHS1 mRNA alone did not cause any AVC defects, indicating this mutation is not dominant-negative, supporting the loss-of-function mechanism.

In order to determine if genetic variation in *DCHS1* plays a role in MVP outside of the large family identified in *Figure 3.1,* our collaborators sought to identify additional families with mutations in *DCHS1.* By evaluating a cohort of MVP patients, two additional families were identified with inherited nonsyndromic MVP segregating with the novel p.R2330C mutation in *DCHS1* (*Figure 3.1 d-g).* The proband of family 2, a 21-year-old male, underwent mitral valve repair surgery due to severe mitral valve prolapse and mitral regurgitation. From this surgery, our lab was able to obtain valve cells from resected tissue for experiments described in this chapter and use the rest of the posterior leaflet tissue sample for histological analysis.

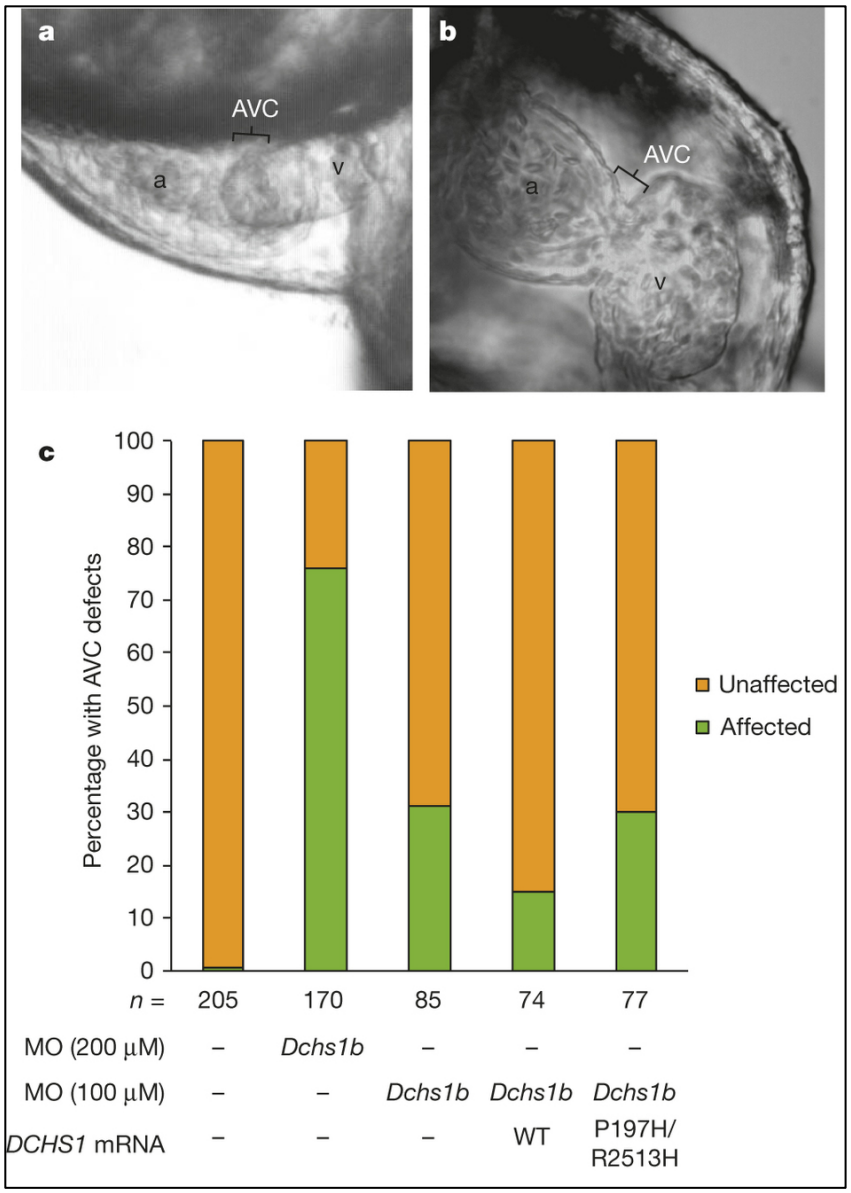

Figure 3.6. *Dchs1b* is Required for Zebrafish AVC Development. a, By 72 hpf, zebrafish hearts develop a constriction in the atrioventricular canal (AVC) that separates the atrium (a) from the ventricle (v). b, Knockdown of *dchs1b* results in absence of the atrioventricular constriction (bracket). c, Approximately 75% of *Dchs1b* morphants exhibit AVC defects (**P* = 1 × 10^{-62}). *DCHS1* human mRNA rescues the *dchs1b* morpholino AVC phenotype, whereas human mutant *DCHS1* mRNA (P197H/R2513H) fails to rescue the phenotype (***P* = 0.009). The total number of fish analysed was 611 and statistical values were obtained using Fisher's exact test. These data were generated by our colleagues part of the Leducq Foundation.

Movat's pentachrome staining of this patient sample revealed myxomatous tissue with expansion of proteoglycans and disruption of the normal matrix boundaries that define the leaflet structure (*Figure 3.7*). The proband's sister, evaluated at age 27 and also heterozygous for the p.R2330C mutation, demonstrated classical MVP with thickened leaflets and moderate regurgitation. The father and maternal grandmother were unaffected and do not carry the mutation. The mother (age 49) and maternal grandfather (age 76) are both affected with mild MVP and both carry p.R2330C. In family 3, the proband (*Figure 3.1e*) had moderate to severe heart failure owing to severe mitral regurgitation with posterior leaflet prolapse requiring surgery at age 72. The proband's sister, age 69, is unaffected and negative for the p.R2330C mutation. The son (age 52) and the daughter (age 53) are both affected with MVP and both carry p.R2330C. The second son (age 55) also carries p.R2330C, however his MVP status is indeterminate due to due to mild left ventricular inferior wall hypokinesis that tethers the leaflets down into the left ventricular cavity21, masking leaflet prolapse motion towards the left atrium.

To determine the functional consequence of the *DCHS1* mutations, human embryonic kidney (HEK) cells were transfected with wildtype *DCHS1* or human mutant *DCHS1* (p.P197L/p.R2513H) constructs and protein levels detected by western blot. Expression of mutant *DCHS1* was reduced by 60% in comparison to wildtype *DCHS1* but exhibited no significant change in mRNA levels. This suggests the *DCHS1* variants result in protein instability (*Figure 3.8a,b,c).*

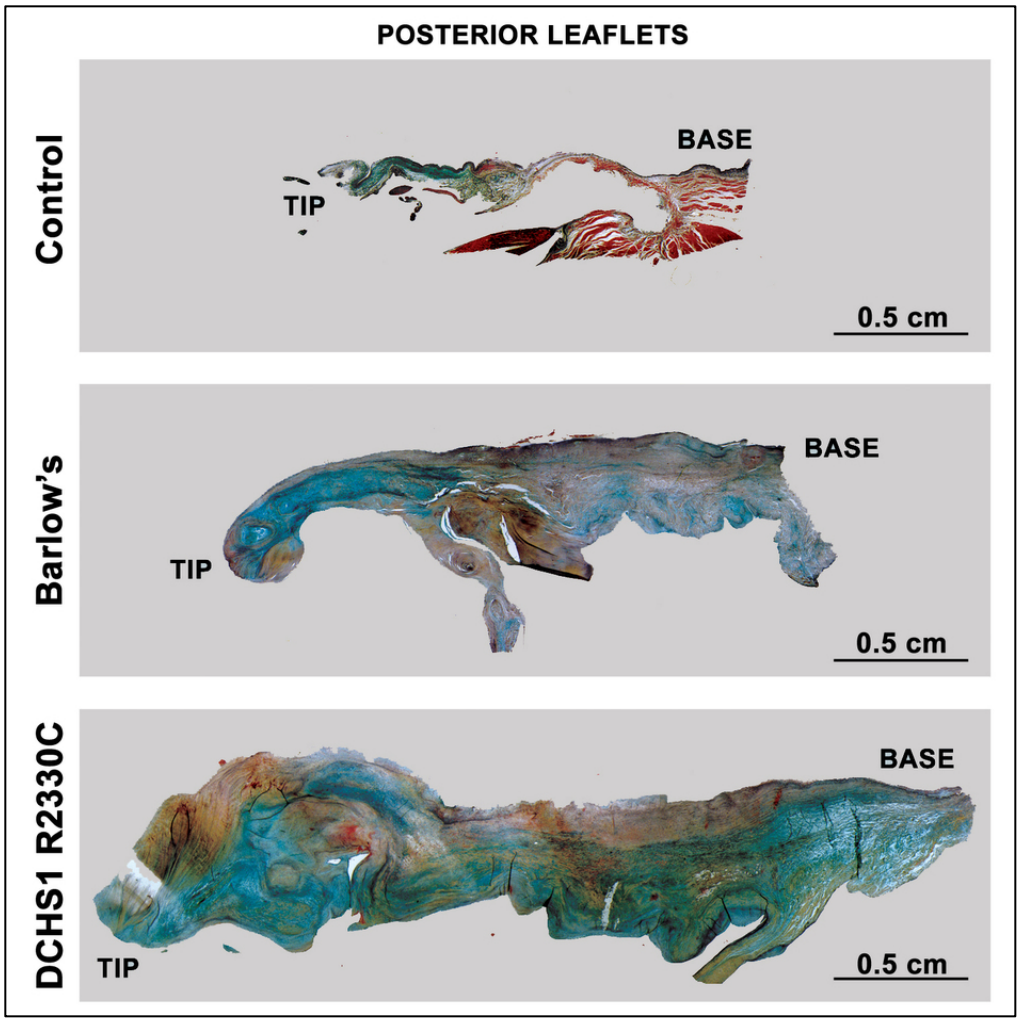

Figure 3.7. Histopathology of Human Posterior Leaflets. Movat's pentachrome stain was performed on human posterior leaflet section from control, Barlow's with MVP, and DCHS1 R2330C. Disruption in matrix organization and expansion of the proteoglycan rich layer (blue) is observed in the Barlow's and DCHS1 samples. Black, elastin; red, fibrin and cardiac muscle; yellow, collagen; blue, proteoglycans.

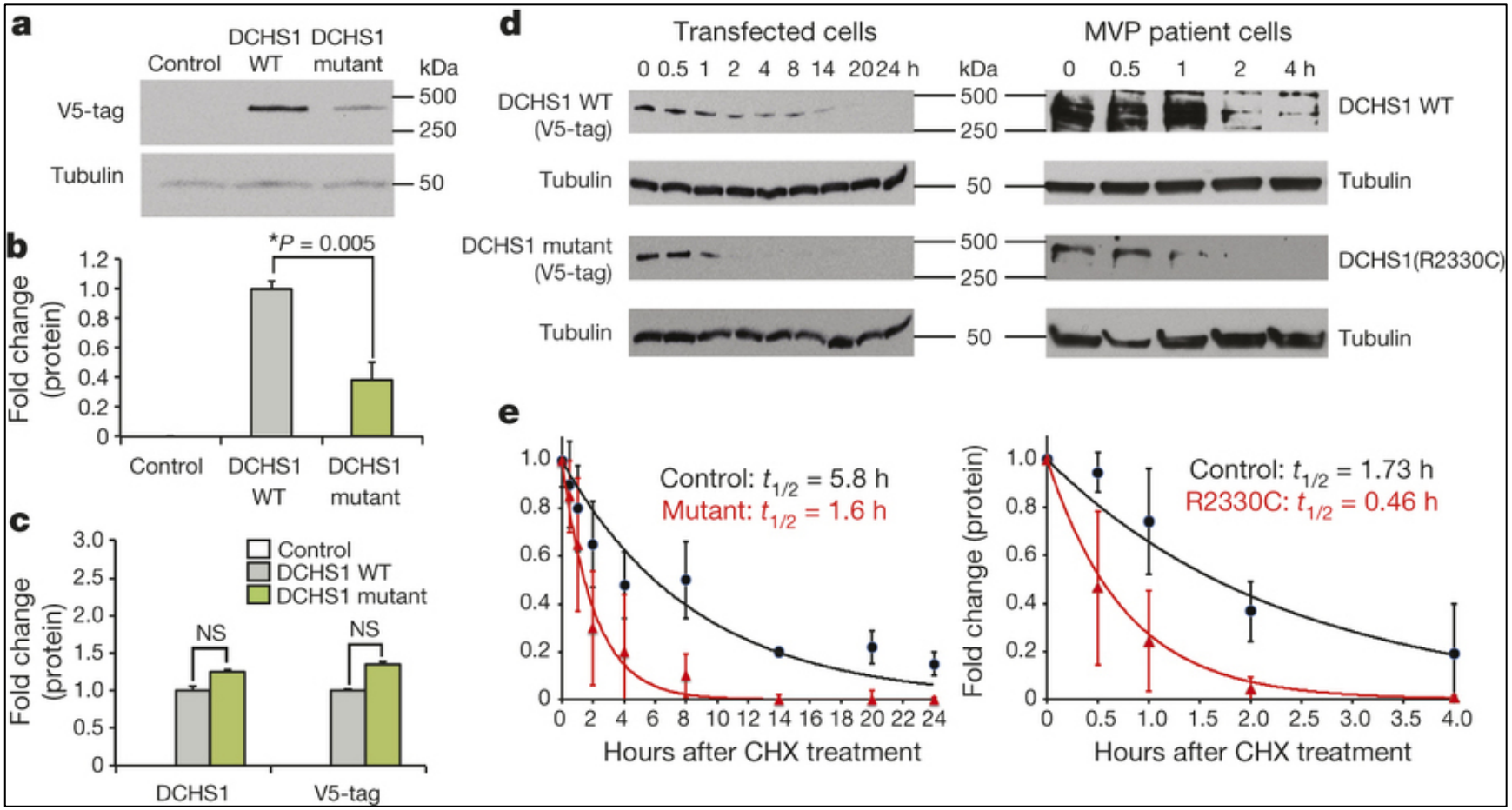
a
Control
DCHS1 WT
DCHS1 mutant
kDa
V5-tag
500
250
Tubulin
50
b
*P = 0.005
Fold change (protein)
1.2
1.0
0.8
0.6
0.4
0.2
0
Control
DCHS1 WT
DCHS1 mutant
c
Fold change (protein)
3.0
2.5
2.0
1.5
1.0
0.5
0
Control
DCHS1 WT
DCHS1 mutant
NS
NS
DCHS1
V5-tag
d
Transfected cells
0 0.5 1 2 4 8 14 20 24 h
kDa
DCHS1 WT (V5-tag)
500
250
Tubulin
50
DCHS1 mutant (V5-tag)
500
250
Tubulin
50
MVP patient cells
0 0.5 1 2 4 h
DCHS1 WT
Tubulin
DCHS1(R2330C)
Tubulin
e
Control: $t_{1/2}$ = 5.8 h
Mutant: $t_{1/2}$ = 1.6 h
1.0
0.8
0.6
0.4
0.2
0
0 2 4 6 8 10 12 14 16 18 20 22 24
Hours after CHX treatment
Control: $t_{1/2}$ = 1.73 h
R2330C: $t_{1/2}$ = 0.46 h
Fold change (protein)
1.0
0.8
0.6
0.4
0.2
0
0 0.5 1.0 1.5 2.0 2.5 3.0 3.5 4.0
Hours after CHX treatment

Figure 3.8. DCHS1 Mutation is Loss of Function. (a–c), Western blot, (p.P197L/p.R2513H) mutant *DCHS1* results in a 60% decrease in protein with no change in RNA expression. (d), Left panel, DCHS1 wild-type (WT) or mutant (p.P197L/p.R2513H) transfectants treated with cycloheximide (CHX) for specified times followed by western blot analyses. Right panel, cycloheximide on control (DCHS1 WT) or MVP patient (p.R2330C) MVICs. Tubulin, loading control. (e) Calculated protein half-lives. WT and mutant transfectants half-life = 5.8 h versus 1.6, respectively (left). Control and mutant *DCHS1* half-life is 1.73 h versus 0.46 h, respectively (right). Analyses performed in triplicate and repeated four times. Error bars, standard deviations; *P* values calculated using two-tailed Student's *t*-test.

Transfected cells were treated with cycloheximide, an inhibitor of protein biosynthesis, 48 hours after transfection and then harvested at multiple timepoints to assess exponential protein decay. The half-life of wildtype *DCHS1* protein in transfected cells was 5.8 hours, while the half-life of the mutant *DCHS1* protein (p.P197L/p.R2513H) was 1.6 hours (*Figure 3.8a-c).* Both the p.P197L and p.R2513H constructs were evaluated individually, but only the construct harboring the R2513H mutation resulted in significantly reduced protein levels, implicating this as the pathogenic mutation in the family (*Figure 3.9*). Cycloheximide experiments examining protein stability were also performed in mitral valvular interstitial cells recovered from the proband in family 2 harboring the p.R2330C mutation. Consistent with the findings in cells transfected with the p.R2153H mutation, these p.R2330C mutant cells have a significantly decreased protein half-life at 0.46 hours, compared to the control valvular interstitial cells which exhibited a protein half life of 1.73 hours (*Figure 3.8 d,e).* These studies indicate both the p.R2153H and the p.R2330C mutations are loss of function and result in loss of *DCHS1* protein stability. In order to study the consequences of loss of function *DCHS1* in a mammalian model, I chose to evaluate the Dchs1 heterozygote (*Dchs1*$^{(+/-)}$) mouse for phenotypic similarities to the MVP patients.

The homozygous Dchs1 knockout mouse results in neonatal lethality around neonatal day 0 (P0) in addition to multi-organ impairment, including polycystic kidneys, skeletal growth abnormalities, lung branching abnormalities,

and other phenotypes consistent with polarity defects (Mao, Mulvaney et al. 2011). I was interested in examining the *Dchs1*$^{(+/-)}$ mouse since loss of one *Dchs1* allele mirrors the effect of loss of function *DCHS1* mutations in the patients, where only one allele of *DCHS1* is functional. Histological examination of this mouse reveals enlarged and elongated mitral leaflets compared to the wildtype control. Additional immunohistochemical stainings for collagen I and Hyaluronan Binding Protein (HaBP), the major structural components of the mitral leaflets, reveal matrix disorganization and increases in proteoglycan deposits, which are classic characteristics of myxomatous degeneration (*Figure 3.9*). These structural changes were quantified by micro-MRI analysis and 3D reconstructions generated from MRI slices. Volumetric analysis of the 3D reconstructions demonstrated increased thickening and volume in the posterior leaflet of the mitral valve in the *Dchs1*$^{(+/-)}$ (*Figure 3.9*). Anterior volumentric measurements were variable with some large increases in volume, but together were not significant. Functional assessment of these mice by echocardiography reveals mitral valve prolapse with a pronounced involvement of the posterior leaflet, which is elongated and shifts leaflet coaptation anteriorly as observed in the proband from family 1 (*Figure 3.9*). Other parameters measured by echocardiography including ejection fraction, fractional shortening, left ventricular mass, left ventricular volume in diastole and systole, were unchanged (*Figure 3.10*). Together these data reveal the *Dchs1*$^{(+/-)}$ mice phenocopy the MVP patients structurally and functionally, and that Dchs1 heterozygosity results in mitral valve prolapse in mice.

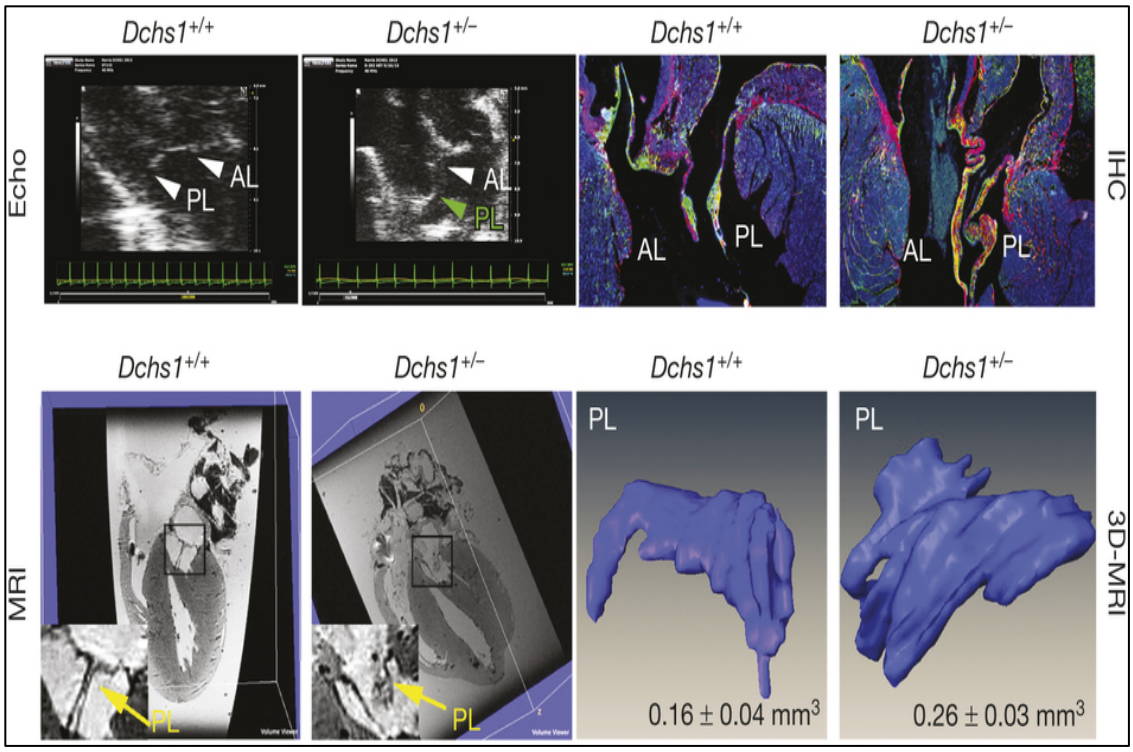

Figure 3.9 *Dchs1* Deficiency causes MVP and myxomatous Phenotype in Adult Mice. Echocardiography (Echo), MRI, histopathology and 3D reconstructions performed on 9-month old male *Dchs1*$^{+/+}$ and *Dchs1*$^{+/-}$ mouse hearts. Echo, posterior leaflet prolapse in *Dchs1*$^{+/-}$ (green arrow) (n = 6 per genotype). Immunohistochemistry (IHC), *Dchs1*$^{+/-}$ (n = 5) anterior, posterior leaflets (AL, PL) exhibit myxomatous degeneration and expansion of proteoglycan expression compared to *Dchs1*$^{+/+}$ (n = 7), collagen (red), proteoglycans (green). MRI show posterior leaflet (PL) thickening in *Dchs1*$^{+/-}$ (arrow-inset) compared to control littermates. 3D reconstructions of MRI: *Dchs1*$^{+/-}$ mice exhibit thickened and elongated leaflets compared to *Dchs1*$^{+/+}$. (Two-tailed Student's t-test was used to calculate P values; P = 0.01, n = 4 per genotype).

Cardiac Function (Echocardiography)

Measurement	Mode	Parameter	Units	Dchs1 +/+ (N=6)	STD	Dchs1 +/- (N=6)	STD	p-value
IVS;d	M-Mode	Depth	mm	0.8208935	0.187955	0.9096155	0.140668	0.170463
IVS;s	M-Mode	Depth	mm	1.290918667	0.243251	1.369591167	0.200513	0.393879
LVID;d	M-Mode	Depth	mm	4.282772333	0.515571	4.045031833	0.217379	0.28511
LVID;s	M-Mode	Depth	mm	2.887339833	0.33268	2.735737167	0.362674	0.544435
LVPW;d	M-Mode	Depth	mm	0.914783667	0.210393	0.961298	0.215238	0.691322
LVPW;s	M-Mode	Depth	mm	1.293790333	0.237193	1.385096	0.238861	0.252632
Calculation		**Units**						
EF		%		60.5315595	7.808571	61.0498945	8.235624	0.934765
FS		%		32.317489	5.734886	32.5702855	5.939884	0.955876
LV Mass		mg		148.9330448	42.74011	150.7559685	40.75343	0.891865
LV Mass (Corrected)		mg		119.1464358	34.19209	120.6047747	32.60275	0.891865
LV Vol;d		ul		83.76315083	23.58335	72.14675683	9.354702	0.261482
LV Vol;s		ul		32.456727	9.786065	28.5946545	8.983466	0.570045

Figure 3.10. Cardiac Function is Not Altered in *Dchs1*$^{(+/-)}$ Mice. M-mode analyses were performed to determine whether cardiac structure and/or function were perturbed in the *Dchs1*$^{+/-}$ mice. No statistically significant differences were observed in either cardiac structure or calculated cardiac function (n = 6 for each genotype). IVS, interventricular septum; d, diastole; s,

systole; LVID, left ventricular internal dimension; LVPW, left ventricular posterior wall; EF, ejection fraction; FS, fractional shortening; LV, left ventricle.

Echocardiograms of affected family members reveal children affected by MVP who are also clinically benign with no signs of mitral regurgitation (Freed, Acierno et al. 2003). Additionally, since the *DCHS1* mutations are present at conception and therefore during development, I hypothesized there is a developmental origin for the disease. Expression analysis examining mRNA and protein expression reveal robust expression of *Dchs1* during embryonic and fetal timepoints. *In situ* hybridization and Immunohistochemical experiments show *Dchs1* expression in endocardial cells and mesenchymal cells of the developing cushions at E11.5, E12.5, and E13.5, and in the endocardial cells and valvular interstitial cells of the leaflets at E15.5, E17.5, and P2 (*Figure 3.11*). A closer examination of Dchs1 protein expression by IHC reveals Dchs1 is expressed as a gradient from atrialis to ventricularis, in the mitral leaflets during development (*Figure 3.12 a)*. On a cellular level Dchs1 expression is asymmetric and localized to one side of the cell in cultured cells by ICC (*Figure 3.12 b*). Functional assessment of loss of Dchs1 during development showed no appreciable change at embryonic timepoints (E11.5-E13.5), but changes in leaflet shape were observed by histology at fetal timepoints (E15.5-E17.5) in both the $Dchs1^{(+/-)}$ and $Dchs1^{(-/-)}$. The more severe phenotype was observed in the $Dchs1^{(-/-)}$ mouse indicating a gene dosage effect (*Figure 3.13 a*). From histological sections at E17.5, 3D reconstructions of the mitral leaflets were generated using Amira software, allowing for a more accurate visualization of the mitral valve and

quantitative measurements of leaflet volume.

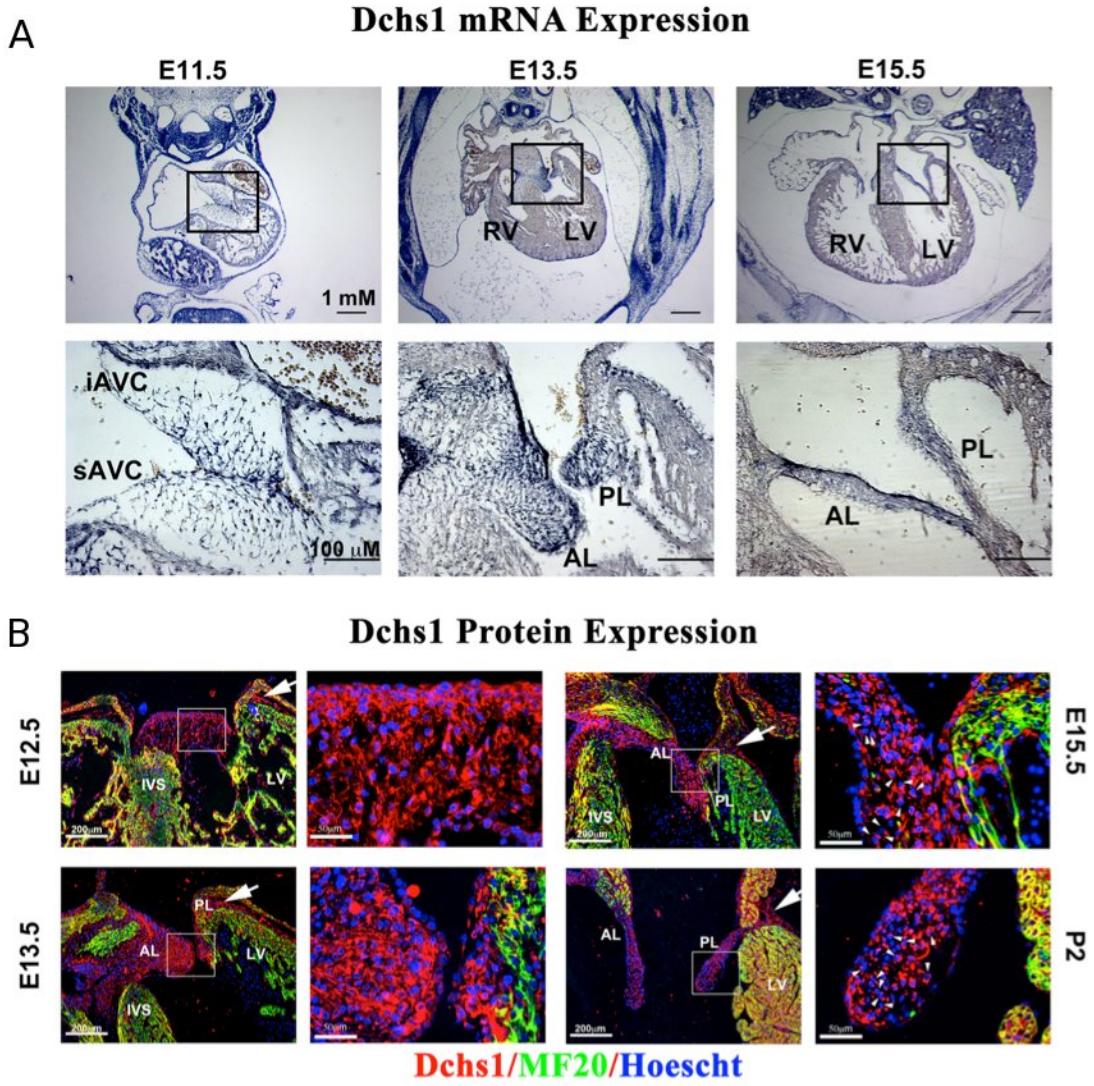

Figur 3.11. Dchs1 RNA and Protein Expression During Valvulogenisis. (a) *in situ* hybridization of Dchs1 mRNA expression of mouse sections at E11.5, E13.5, and E15.5 reveals robust expression at all timepoints in the cushions and mitral valve. (b) IHC for Dchs1 (red), MF20 (green, myocardium), and Hoechst (blue, nuclei) in E12.5, E13.5, E15.5, and P2 mouse sections show expression in cushions and mitral leaflets at all timepoints. RV, right ventricle; LV, left ventricle; iAVC, inferior atrioventricular cushion, sAVC, superior atrioventricular cushion.

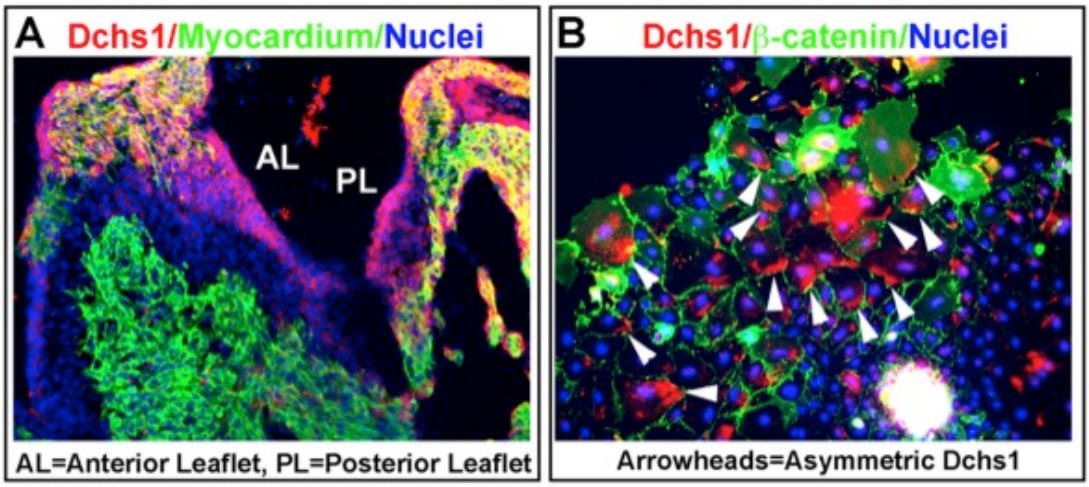

Figure 3.12. Asymmetric Localization of Dchs1 *in vivo* and *in vitro*. (a) IHC for Dchs1 (red), MF20 (green, myocardium), Hoechst (blue, nuclei) on E14.5 wildtype mouse sections shows gradient of Dchs1 expression from atrialis to ventricularis regions of the leaflets. (b) ICC on wildtype mouse explants for Dchs1 (red), b-catenin (green, cell membrane), hoechst (blue, nuclei) demonstrate asymmetric Dchs1 expression on the cellular level.

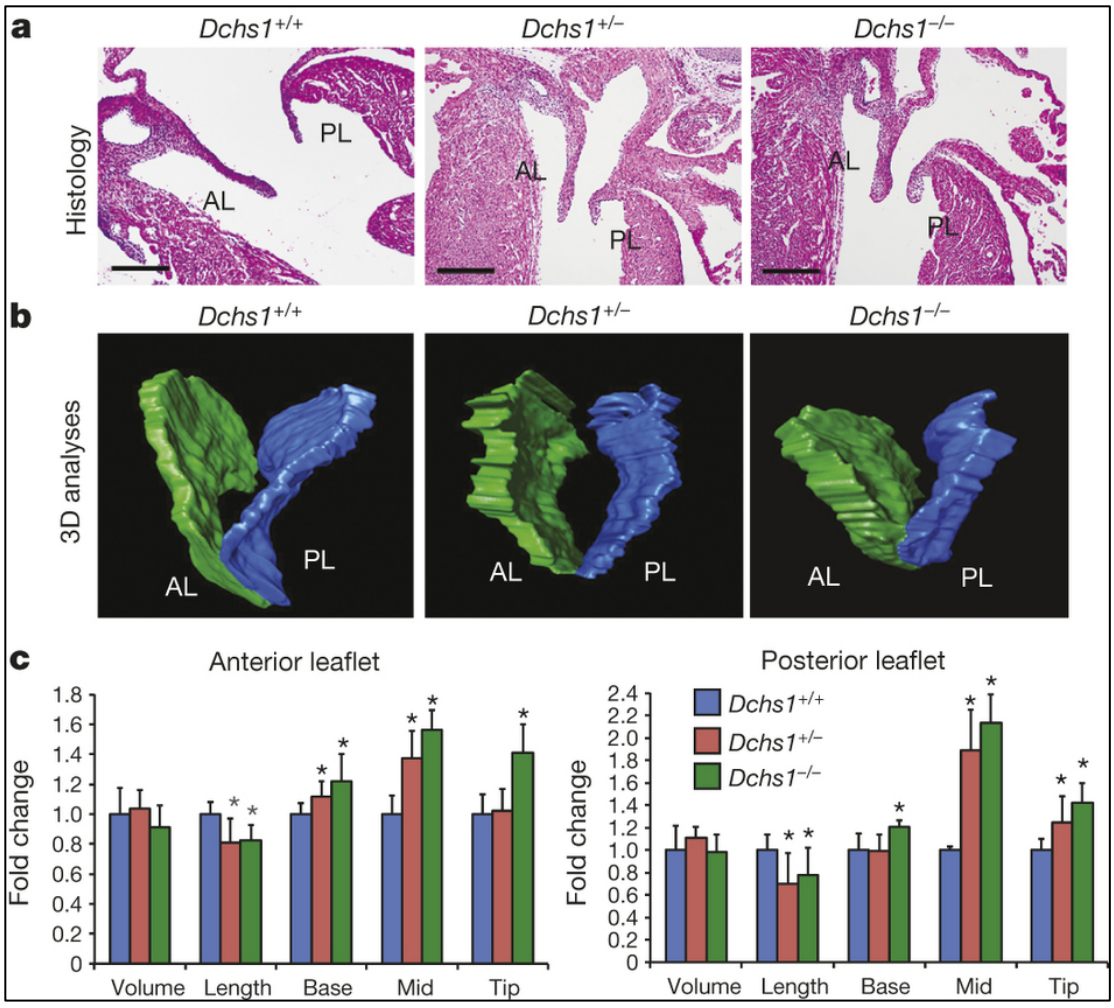

Figure 3.13. Loss of Dchs1 Results in Developmental Defects. (a, b) Haematoxylin and eosin and 3D reconstructions of E17.5 *Dchs1*$^{(+/+)}$, *Dchs1*$^{(+/-)}$ and *Dchs1*$^{(-/-)}$ mouse hearts showing thickening of anterior and posterior leaflets (AL, PL) in *Dchs1*$^{(-/-)}$ mice compared to *Dchs1*$^{(+/+)}$.*Dchs1*$^{(+/-)}$ valves display an intermediate phenotype. (c) Quantification of valve dimensions showing *Dchs1*$^{(-/-)}$ (green bars) and *Dchs1*$^{(+/-)}$ (red bars) anterior and posterior lengths were significantly reduced compared to *Dchs1*$^{(+/+)}$ (blue bars) leaflets. *Dchs1*$^{(-/-)}$ and *Dchs1*$^{(+/-)}$ valves displayed increased thickness throughout the leaflets compared to *Dchs1*$^{(+/+)}$. Scale bars, 100 μm. n = 5 per genotype and two-tailed Student's t-test was used to calculate P values; *$P < 0.01$.

Between genotypes, volumes of both the anterior and posterior leaflets were unchanged (*Figure 3.13 b,c*). Quantification of valve dimensions, being length and width at the base, mid, and tip of the leaflets, reveal statistically significant increases in thickness at all three points of measurement and a decrease in leaflet length of the *Dchs1*$^{(+/-)}$ and *Dchs1*$^{(-/-)}$. These morphological changes indicate Dchs1 is required for directing anatomical patterning and leaflet shape during development.

Studies in *drosophila* have demonstrated a role for Dchs1 in directing cell polarity and orientation of cells and hairs of the wing (Cho and Irvine 2004). Based on these findings, I examined whether Dchs1 is required for valvular interstitial cell alignment and orientation, as a mechanism by which Dchs1 regulates leaflet shape. The anterior leaflets of Dchs1 mice at P0 were isolated and histologically examined by hematoxylin and eosin staining. Vector maps were generated by drawing a line across the longest axis of each cell within the valvular interstitum and the orientation of each cell in relation to the axis of the leaflet was quantified. In a wildtype leaflet, the majority of valvular interstitial cells are oriented along the same plane. In contrast, the *Dchs1*$^{(-/-)}$ mouse exhibits randomized orientation of cells with a significant decrease in the number of cells properly aligned. The *Dchs1*$^{(+/-)}$ mouse exhibits an intermediate phenotype, with significantly less cells properly aligned compared to the wildtype (*Figure 3.14*). These data suggest Dchs1 directs the orientation of valvular interstitial cells in the mitral valve. Additionally, I proposed that Dchs1 regulates the patterning of the mitral valve by directing cell migration.

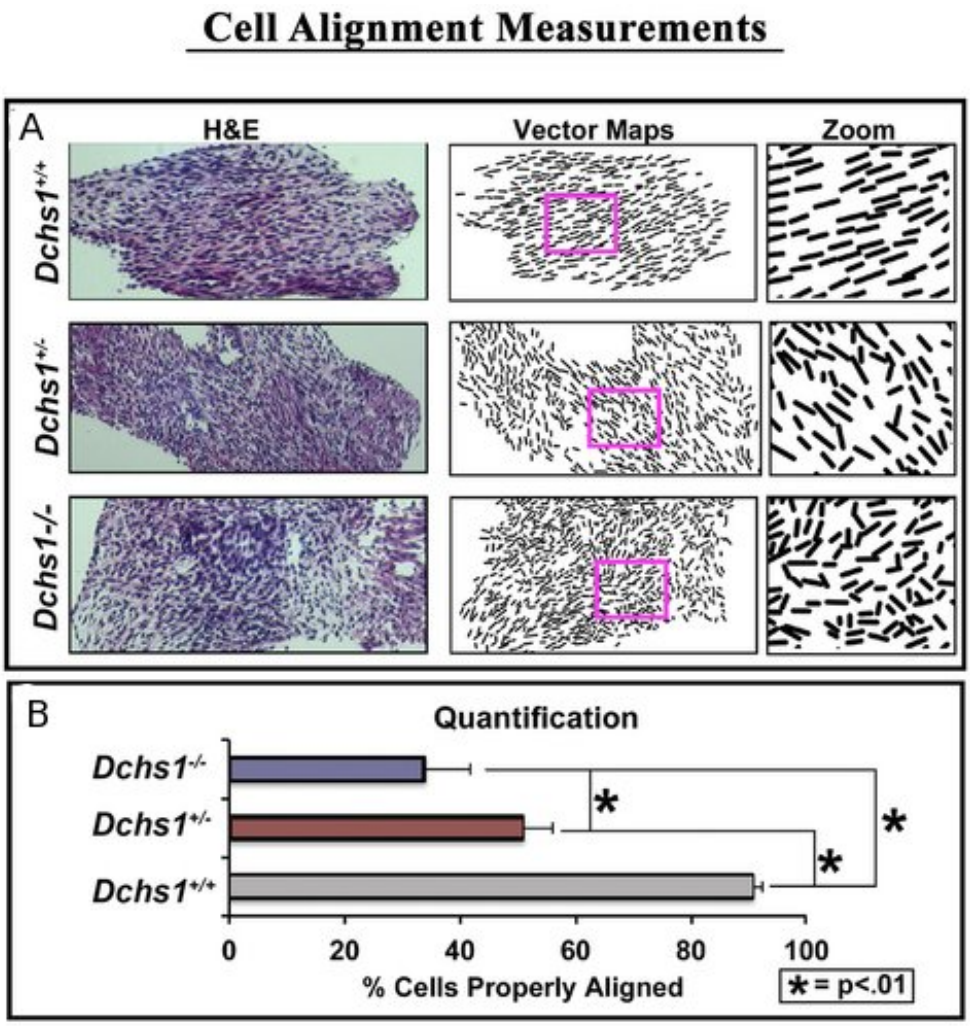

Figure 3.14. Interstitial Cell Alignment is Disrupted in the *Dchs1*$^{(+/-)}$ Mouse at E17.5 (a) Isolated anterior leaflets were embedded and sectioned at 5μm from *Dchs1*$^{(+/+)}$, *Dchs1*$^{(+/-)}$ and *Dchs1*$^{(-/-)}$ hearts. Vector maps were generated from histological stains (hematoxylin and eosin) by drawing a line across the longest axis of the cell to show orientation and alignment of cells in relation to each other. Boxes in each images represent location of zoomed image which demonstrates alignment defects in the *Dchs1*$^{(+/-)}$ and *Dchs1*$^{(-/-)}$ leaflets. (b) Quantification of % of cells properly aligned was determined by the number of cells that deviate >10 degrees from the proximal-distal axis. 90% of the cells within the wildtype are properly aligned, compared to a 50% reduction seen in the *Dchs1*$^{(+/-)}$ and even further reduction in the *Dchs1*$^{(-/-)}$. (P values <0.01).

To examine the role for Dchs1 in cell migration, we performed experiments using murine mitral leaflet explants and examined cell migration *in vitro*. Net migratory distance was assessed at 24 hours (T_2) minus the initial (T_1) distance traveled from the explant, taken at 0 hours. Cells from both the anterior and posterior leaflets of *Dchs1*$^{(+/-)}$ mice migrated 1.5 times faster than wildtype cells (*Figure 3.15*). Since loss of Dchs1 results in increased migratory behavior *in vitro*, I wanted to determine if this had an effect *in vivo*. Epicardial-derived cells (EPDC) begin their migratory journey from the outer surface of the heart, through the AV sulcus, and into the posterior leaflet of the mitral valve around E13. To determine if Dchs1 directs this migration of EPDCs into the posterior leaflet, *in vivo* lineage-tracing studies were performed on *Dchs1*$^{(+/+)}$ and *Dchs1*$^{(-/+)}$ mice at P0. Crossing the WT1-Cre/ROSA-eGFP25 line onto both *Dchs1*$^{(+/+)}$ and *Dchs1*$^{(-/+)}$ backgrounds allowed visualization of patterning defects of epicardial-derived cells (EPDCs) during migration into the posterior leaflet. *Figure 3.16* demonstrates that EPDCs in the wildtype migrate as a single sheet of cells, sub-endocardially, along the atrialis aspect of the leaflet. Migratory defects are observed in the *Dchs1*$^{(+/-)}$ where EPDC infiltration is increased and the sheet-like migration pattern of cells is disrupted and randomized. 3D reconstructions were generated from the immunohistochemical stainings performed on these mice, allowing for the quantification of leaflet volume which consists of cells from an endothelial origin (GFP negative) and cells from an epicardial origin (GFP positive) (*Figure 3.16 a-e*). EPDC volume was significantly increased in the posterior leaflet of the *Dchs1*$^{(+/-)}$, while total leaflet volume remained unchanged.

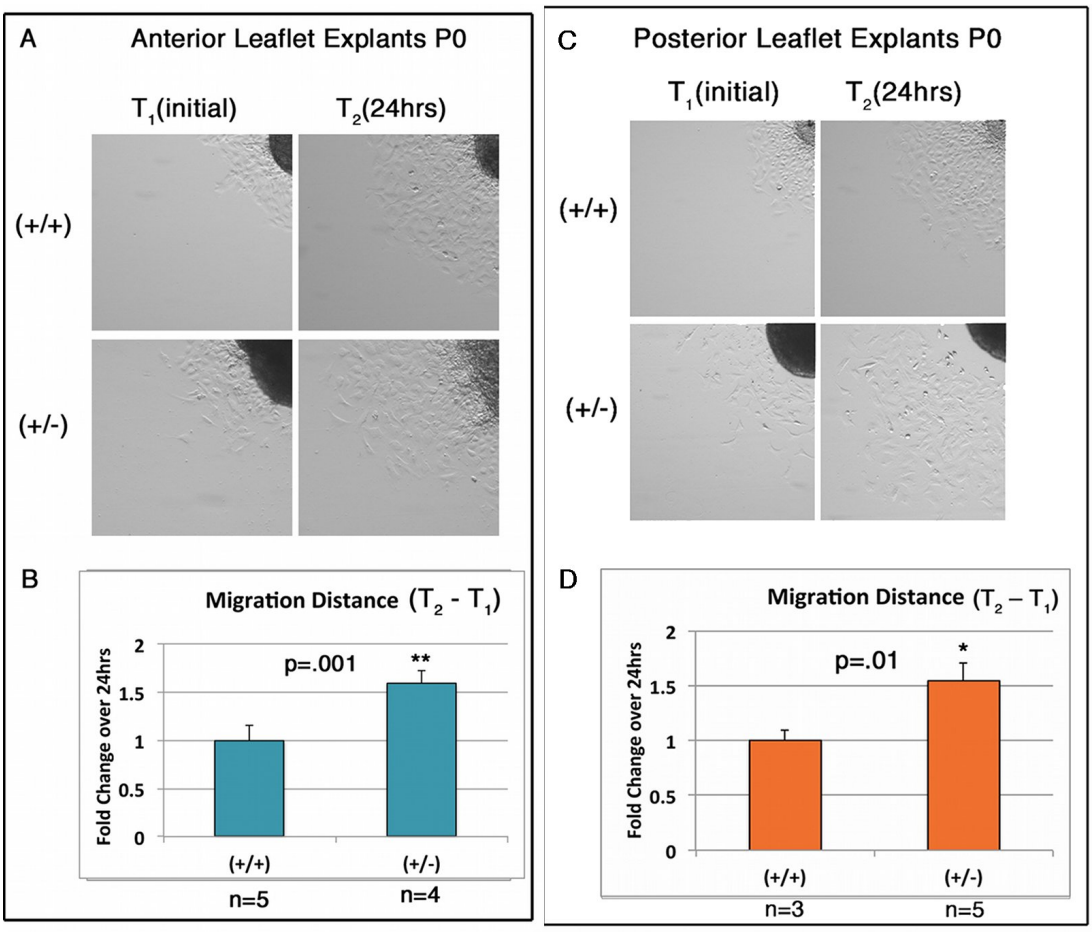

Figure 3.15 Dchs1 Deficient Mice Exhibit Migration Defects *in vitro.* (a, c) Anterior leaflets were explanted and interstitial cells were allowed to migrate out for 24 hours. (d,e) distance traveled from explant was measured at multiple points around the explant and mean distance traveled was quantified as T_1 (initial) – T_2 (24hrs). Cells from *Dchs1*$^{(+/-)}$ mice, exhibited increased migratory behavior. Anterior p=0.01, Posterior p= 0.001.

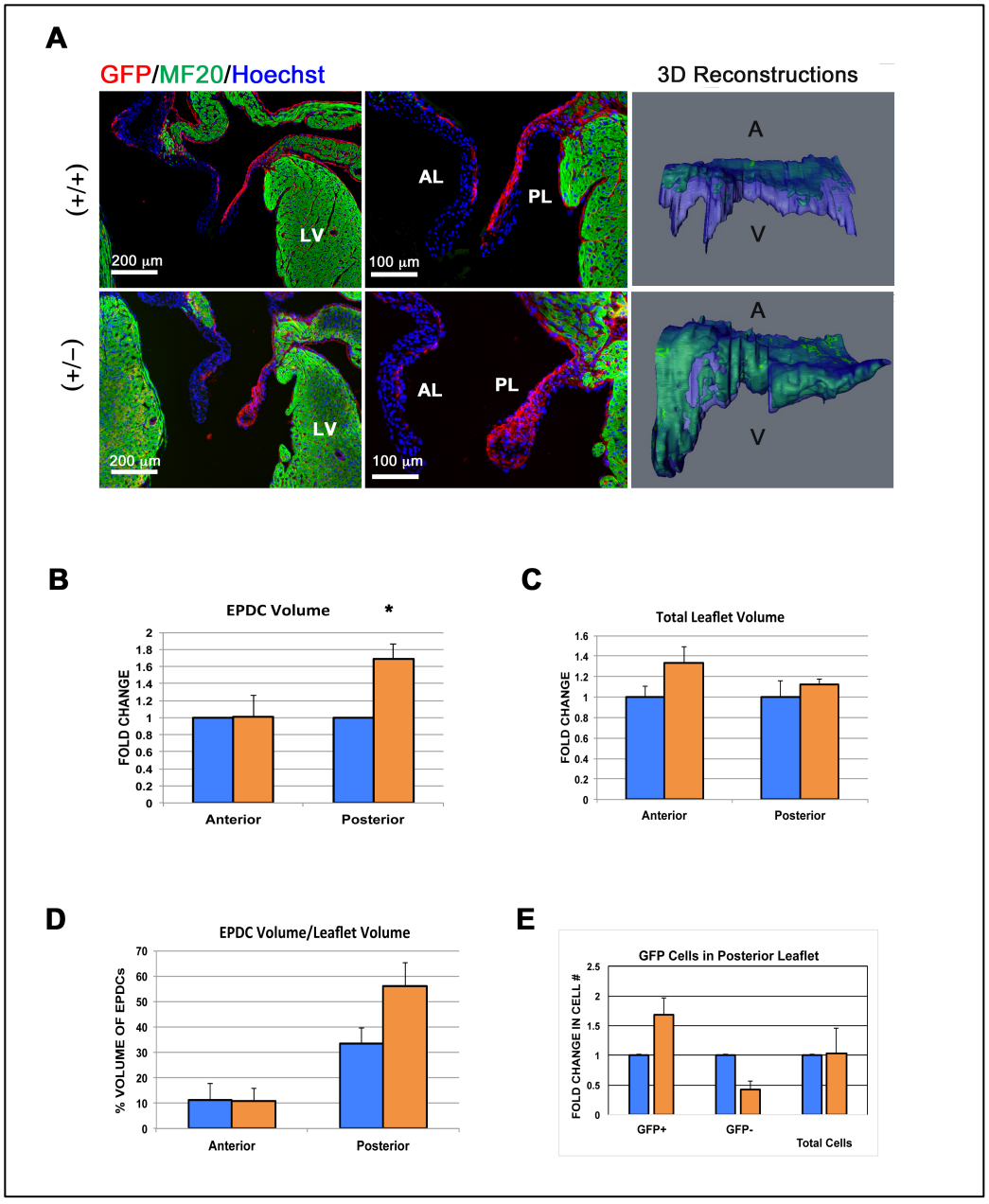

Figure 3.16. Loss of Dchs1 Results in Altered EPDC Migration *in vivo.* (a) WT1-Cre/ROSA-eGFP25 lineage traced mice were crossed with *Dchs1*$^{(+/+)}$ and *Dchs1*$^{(+/-)}$, and sacrificed at P0. IHC for GFP (red) and MF20 (green) reveals defects in migrational patterning in the posterior leaflet (PL). anterior leaflet (AL); Left ventricle (LV). 3D reconstructions of IHC sections through the entire posterior leaflet (blue) show more EPDCs (green) and increased migration in the posterior leaflet. (b,c) EPDC volume was increased in the posterior leaflet of the *Dchs1*$^{(+/-)}$, while total leaflet volume remained unchanged. (d) EPDC volume to leaflet volume is also increased in the *Dchs1*$^{(+/-)}$ (e) The number of GFP positive and GFP negative cells were counted in the posterior leaflet and compared among genotypes. The total number of cells remains unchanged, while increased GFP+ cells (EPDCs) and decreased GFP- (endothelial derived cells) cells were observed.

The ratio of EPDC volume to leaflet volume is also increased in the posterior leaflet of *Dchs1*$^{(+/-)}$ mice indicating the majority of the posterior leaflet is derived from EPDCs. The number of cells within the posterior leaflet was quantified revealing no change in total cell number between genotypes. The percentage of cells from an epicardial origin were increased while the percentage of cells from an endocardial origin were decreased in the *Dchs1*$^{(+/-)}$ mice (*Figure 3.16 e*). Additionally, the migrational properties of patient cells harboring the p.R2330C *DCHS1* mutation were examined by seeding these cells into wells with a hydrogel (*Figure 13.17*). The hydrogel was dissolved after cells became adherent, and the rate of migration into the open space was calculated based on percentage of area covered over time. The migrational speed of *DCHS1* mutant cells was significantly faster at the 6, 12, and 24-hour timepoints in comparison to normal human valvular interstitial cells (*Figure 3.17 b*).

Cellular adhesion is known to regulate migration by promoting collective cellular migration, where groups of cells can migrate together in a specific direction. This collective migration is observed during normal developmental, wound healing, cancer invasion, and this is also observed in normal EPDC migration into the posterior leaflet of the mitral valve during murine development (Matsui, Ishikawa et al. 2015). Disruptions in collective EPDC migration are observed in the *Dchs1*$^{(+/-)}$ mouse resulting in irregular valve architecture and patterning. I hypothesize that Dchs1 regulates cell migration by promoting cellular adhesion.

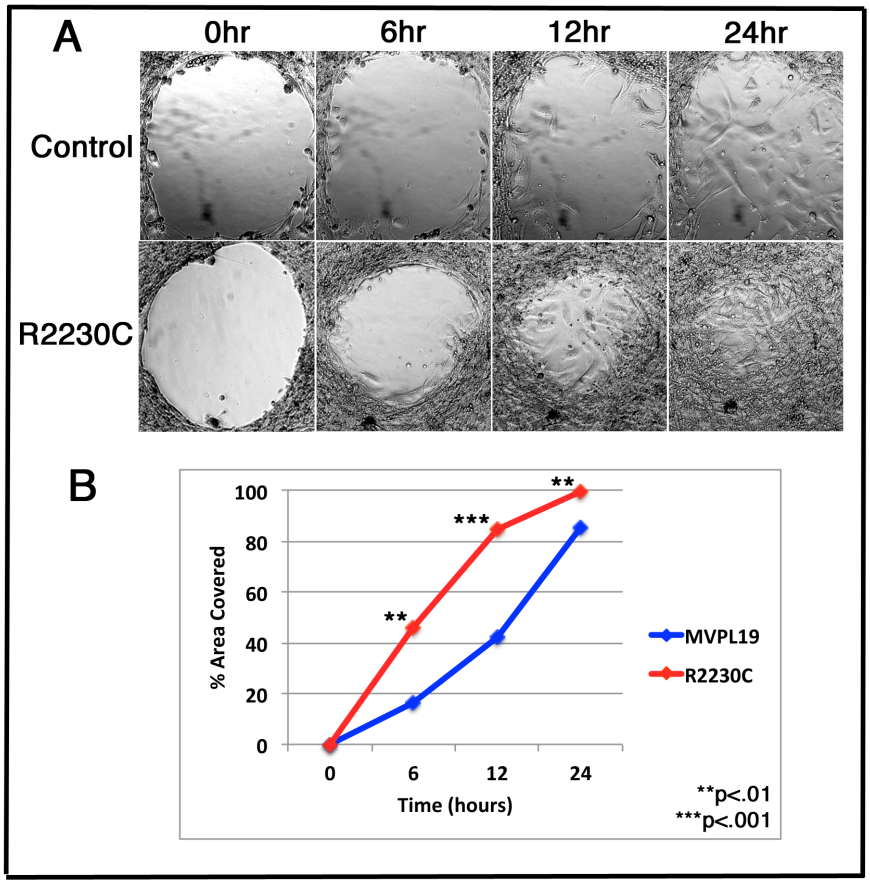

Figure 3.17 MVP Patient Cells With the DCHS1 Mutation Exhibit Increased Migration. (a) Patient valvular interstitial cells with the R2330C *DCHS1* mutation and control valvular interstitial cells were seeded into hydrogel migration assay plates. (b) Migration rate was quantified by % area covered over time at 0, 6, 12, and 24 hours. *DCHS1* mutant valvular interstitial cells (red line) migrated at a significantly faster rate at 6, 12, and 24 hours, compared to control cells (blue line). Control N=8; R2330C N=9.

To test this hypothesis, *in vitro* adhesion assays were performed using human VICs harboring the p.R2330C mutation and normal human VICs. Spectrophotometer (OD 540) readings of crystal violet indicate a loss of adhesive properties in mutant *DCHS1* cells compared to control cells (*Figure 3.18*).

To further investigate changes in adhesive properties, specifically cell-to-cell interactions, with loss of Dchs1, I examined adherens junction localization, stability and expression by ICC in mitral valve explants used in previous migration assays. Adherens junctions are cell-to-cell adhesion complexes made up of core cadherins linked to the cytoskeleton through cytoplasmic proteins (Harris and Tepass 2010). *Figure 3.19* demonstrates a change in N-cadherin localization, a major structural component of adhernes junctions, in the *Dchs1*$^{(+/-)}$ anterior and posterior leaflet explants. In wildtype mice, N-cadherin is localized to the cellular membrane at regions of cell-to-cell contact and this localization is maintained as the valve cells migrate collectively away form the explant. While expression of N-cadherin is maintained in the *Dchs1*$^{(+/-)}$ explants, the cell-to-cell localization is lost and in contrast to the wildtype, these cells migrate individually and not as a collective sheet of cells. These data indicate Dchs1 is required for adherens junction localization and potentially, the stabiliziation of these complexes.

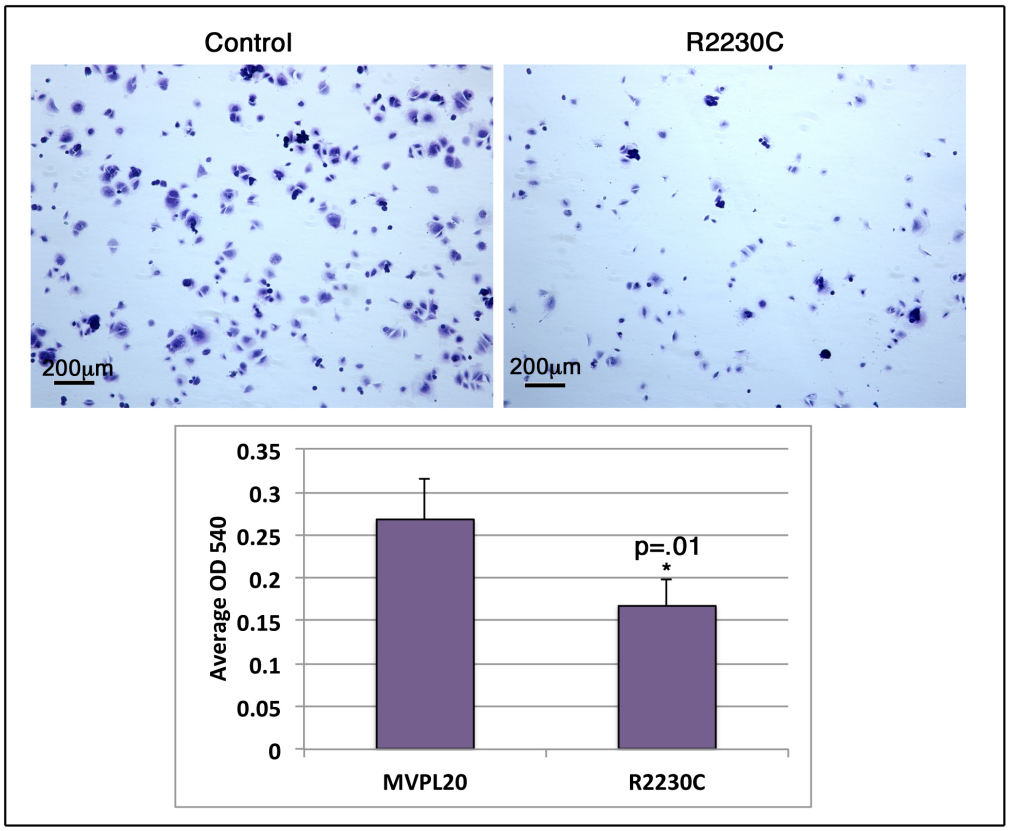

Figure 3.18 *DCHS1* p.R2330C Mutation Results in Decreased Adhesion of Valvular Interstitial Cells. Human valvular interstitial cells were seeded in equal numbers and allowed to adhere for 2 hours, then washed and stained with crystal violet. The number of cells adherent were quantified by spectrophotometer readings at 540 nm. Fewer *DCHS1* mutant cells were able to adhere after 2 hours than control cells (MVPL20). N=5; p=0.01

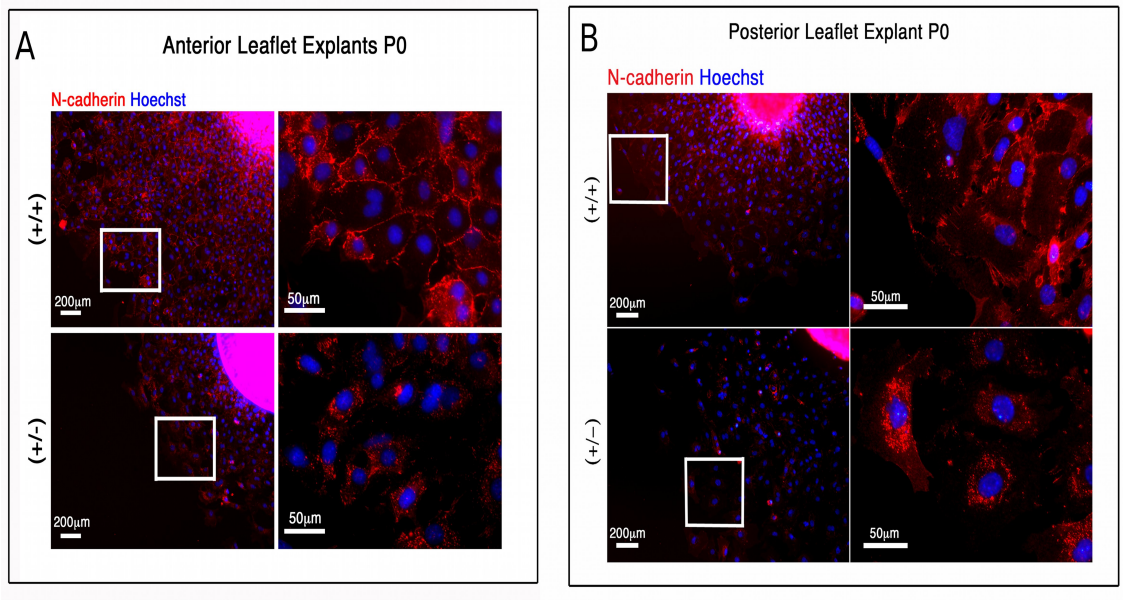

Figure 3.19 N-Cadherin Localization Disrupted in *Dchs1*$^{(+/-)}$ Migratory VICs. Anterior (a) and posterior (b) explants were used for previously described migration assays and then fixed for ICC. Cells were stained for N-cadherin (red) and Hoechst (nuclei/blue). In the wildtype, VICs in both anterior and posterior explants expressed N-cadherin at cell-to-cell junctions. *Dchs1*$^{(+/-)}$ migrational cells exhibited mis-localization of N-cadherin not at cell junctions.

In addition to cellular adhesion, the presence of a substrate on which cells migrate is likely to influence migrational behavior. Collagen IV, a component of the basement membrane, is expressed in the AV cushions and the mitral valve during murine development (*Figure 3.20*). Expression of collagen IV is restricted to endocardium and the atrialis aspect of the leaflets, consistent with the observed migrational pattern of EPDCs into the posterior leaflet.

To determine if collagen IV expression is changed in the *Dchs1*$^{(+/-)}$ mouse and/or EPDC migration is influenced by collagen IV expression, I examined the expression profile of Collagen IV in wildtype and *Dchs1*$^{(+/-)}$ mitral valves by IHC. *Figure 3.21* demonstrates loss of Dchs1 is associated with a loss in collagen IV expression at neonatal day 0. In the wildtype mouse, EPDC migration is primarily localized to regions of collagen IV expression and is disrupted in the *Dchs1*$^{(+/-)}$, suggesting the basement membrane may be important for directing EPDC migration.

As another mechanism by which Dchs1 regulates leaflet shape, I examined whether loss of Dchs1 resulted in changes in cell proliferation and apoptosis. Proliferation was examined at P0 by Ki67 expression and apoptosis by cleaved-caspase 3 expression in wildtype and *Dchs1*$^{(+/-)}$ mice bred onto the WT1-Cre/ROSA-eGFP25 background. From these experiments, the total number of proliferating cells in the posterior leaflet was significantly increased in the *Dchs1*$^{(+/-)}$. Since these experiments were performed in the Wt1-lineage trace mouse, distinction between the cellular origins of proliferating cells can be determined by GFP expression (*Figure 3.22 a,b*).

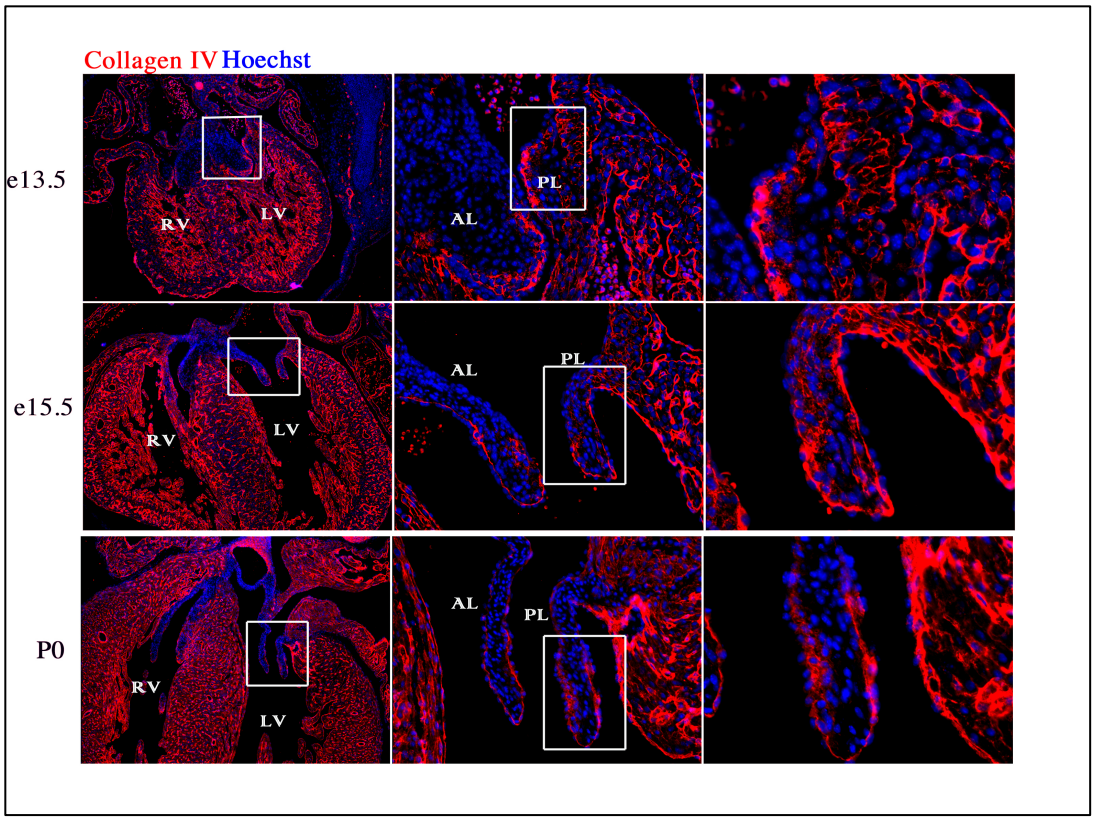

Figure 3.20. Collagen IV Expression During Valvulogenisis. IHC for collagen IV (red) and hoechst/nuclei (blue) performed on wildtype sections at E13.5, E15.5, and P0. Boxes represent areas where higher magnification images were taken. RV, right ventricle; LV, left ventricle; AL, anterior leaflet; PL, posterior leaflet. Collagen IV is localized to the endocardium of the mitral valve and the atrialis aspect of the posterior leaflet during development.

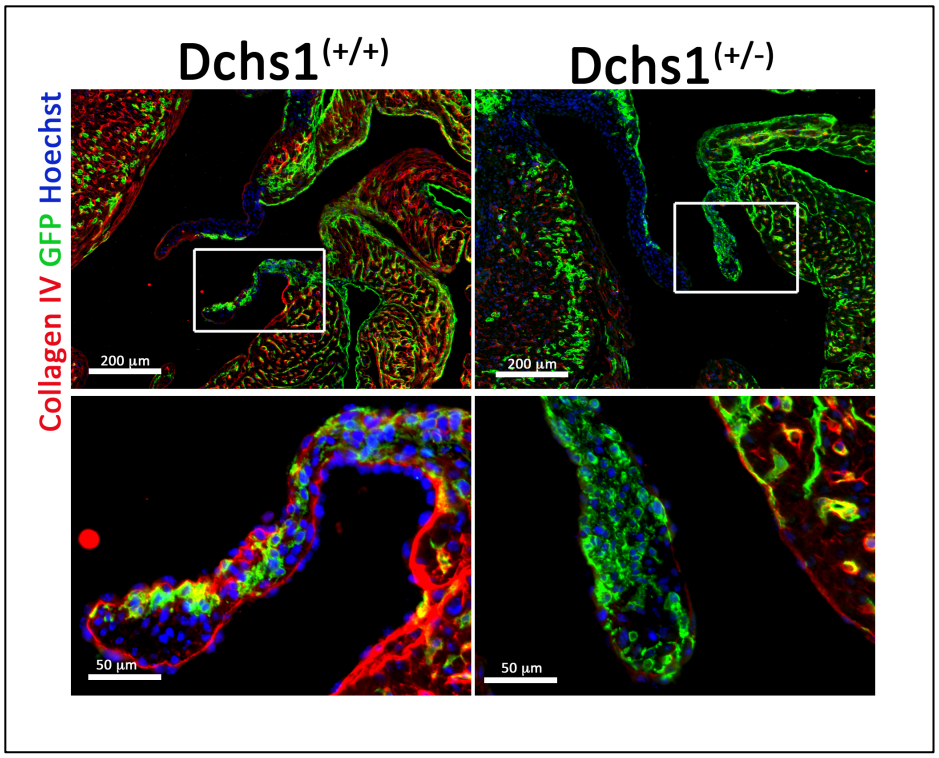

Figure 3.21. EPDC Migration Defects Concurrent with Loss of Collagen IV. IHC for Collagen IV (red), GFP (EPDCs, green), and Hoechst (nuclei,blue) on *Dchs1*$^{(+/+)}$ and *Dchs1*$^{(+/-)}$ sections at P0. High magnification image is of the posterior leaflet. EPDCs migrate along collagen IV expression in wildtype leaflets, while this pattern is lost in the *Dchs1*$^{(+/-)}$.

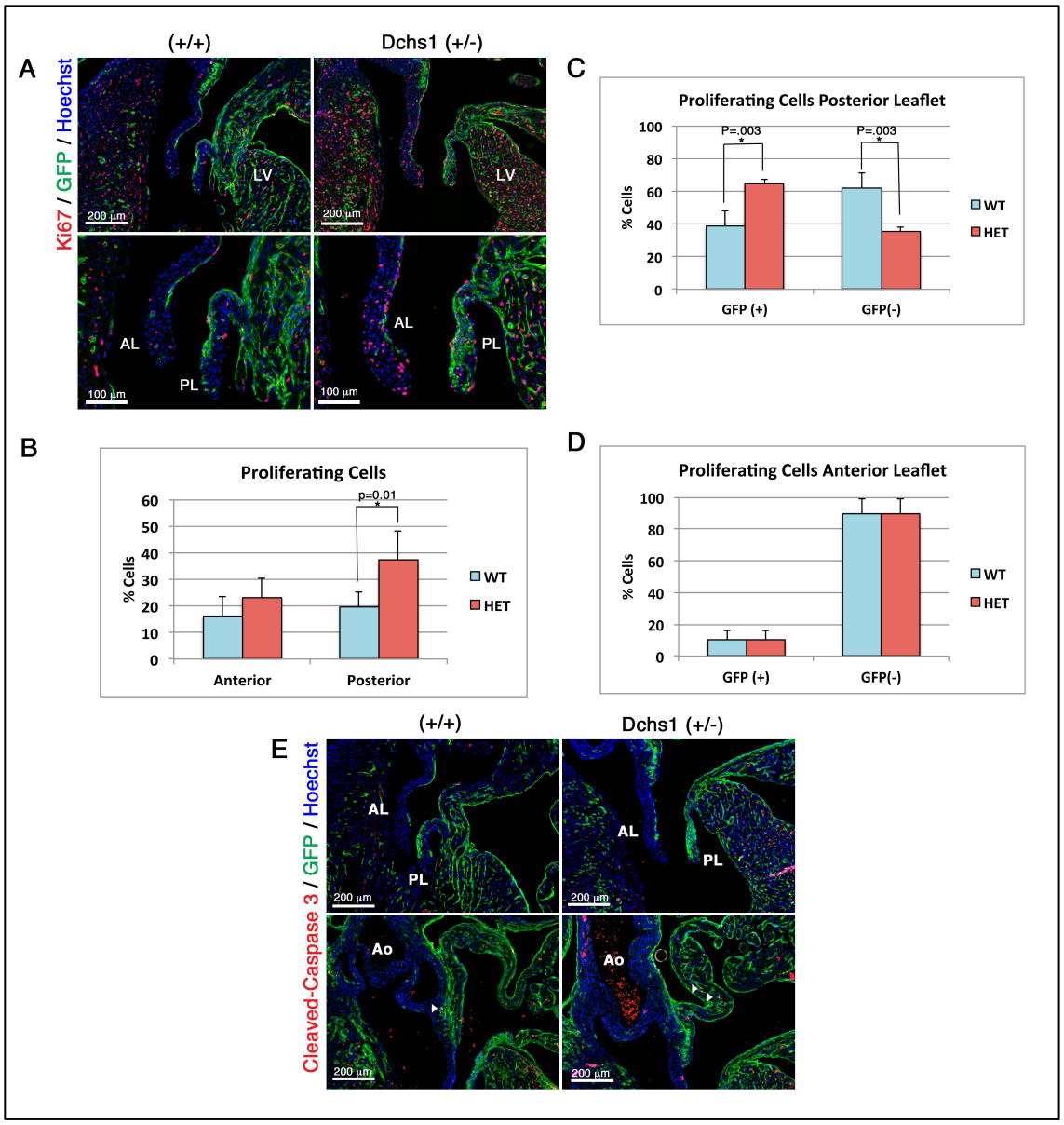

Figure 3.22. Proliferative and apoptotic profile of EPDCs and endocardial-derived cells at P0. (a) IHC performed in *Dchs1*$^{(+/+)}$ and *Dchs1*$^{(+/-)}$ sections at neonatal day 0, for Ki67 (red, proliferation), GFP (green, EPDCs), and Hoechst (blue, nuclei). AL, anterior leaflet; PL, posterior leaflet; LV, left ventricle. (b)Percentage of proliferating cells determined by counting the number of Ki67+ cells divided by the total number of cells. The percentage of proliferating cells in the posterior leaflet were increased in *Dchs1*$^{(+/-)}$ sections. (c,d) Proliferating cells in the posterior and anterior leaflets of *Dchs1*$^{(+/+)}$ and *Dchs1*$^{(+/-)}$ animals were counted based on those positive for GFP and negative for GFP in the WT1-Cre/ROSA-eGFP25 background. (e) IHC performed in *Dchs1*$^{(+/+)}$ and *Dchs1*$^{(+/-)}$ sections at neonatal day 0, for cleaved-caspase 3 (red, apoptosis), Hoechst (blue, nuclei). Apoptotic cells were rare in the mitral valve. Positive control staining was observed in the aorta (Ao).

In the posterior leaflet, proliferating cells from the epicardial-origin (GFP+) were significantly greater in the *Dchs1*$^{(+/-)}$. Concurrently, a decrease in the number of proliferating cells from the endocardial-origin (GFP-) was also observed (*Figure 3.22 c*). Apoptotic cells were rare in both genotypes, and not perceived to be a contributing factor to valve shape or size at this timepont (*Figure 3.22 d*). These data demonstrate Dchs1 is required for maintenance of the proper proliferative profile in the posterior leaflet of the mitral valve during neonatal timepoints, and this may contribute to the pathogenesis of MVP in adulthood.

The data in this chapter have presented a developmental basis for Dchs1-related valve disease, in which Dchs1 is required to direct valve architecture and shape. In order to identify pathogenic pathways that may lead to myxomatous valves in the adult, I examined the MEK/Erk signaling pathway. Current literature implicates increased TGFβ signaling in the pathogenesis of MVP in the context of connective tissue syndromes including Marfan's syndrome (mutations in FBN1), Loyes-Dietz syndrome (mutations in TGFβ Receptor 1/2), and Sphrintzen-Goldberg syndrome (mutations in SKI) (Ng, Cheng et al. 2004, Loeys, Chen et al. 2005, Doyle, Doyle et al. 2012). In Marfan's syndrome, use of a TGFβ antagonist was able attenuate Smad2 signaling and rescue the valve phenotype *in vivo,* suggesting a cause and effect relationship (Ng, Cheng et al. 2004). TGFβ is known to activate numerous signaling pathways, and therefore it is likely noncanonical signaling may contribute to the pathogenesis of MVP. Noncanonical TGFβ signaling through extracellular signal-regulated kinase

(ERK) 1 and 2, and Jun N-terminal kinase-1 (JNK1) are shown to be increased in the Marfan's mouse and can be inhibited by therapies directed against TGFβ. The specific targeting of ERK1/2 activation using RDEA119, an inhibitor of MEK1/2, the upstream activator of ERK1/2, results in amelioration of aortic growth, the major cause of death in Marfan's syndrome (Holm, Habashi et al. 2011). To determine if MEK/Erk signaling is dysregulated in MVP patients with the *DCHS1* p.R2330C mutation, western blot analysis was performed on VICs obtained from the proband of family 2 who underwent mitral vale surgery (*Figure 3.23*). Significant increases in pErk/Erk and its upstream activator pMEK/MEK were detected in patient samples with the *DCHS1* p.R2330C mutation, indicating this pathway is relevant to human nonsyndromic MVP. Additionally, human patient cells exhibit increased proteolytic activity of MMP2, as shown by zymography (*Figure 3.24*).

In order to determine if MEK/Erk signaling is dysregulated in the *Dchs1*$^{(+/-)}$ model of MVP, IHC and westerns were performed on adult mice. IHC for phospho-Erk1/2 (pErk1/2) shows elevated signaling in the anterior and posterior leaflet of the mitral valve in *Dchs1*$^{(+/-)}$ mice (*Figure 3.25 a,b*). Isolated anterior leaflets were harvested for western blot analysis of phospho to total Erk1/2. Significant increases in pErk1/2 to total Erk1/2 were observed in the adult *Dchs1*$^{(+/-)}$ mouse (*Figure 3.25 c,d*). To determine if this signaling is pathogenic to the development of a myxomatous phenotype, pErk1/2 was examined at P0, a timepoint when myxomatous changes are not yet present.

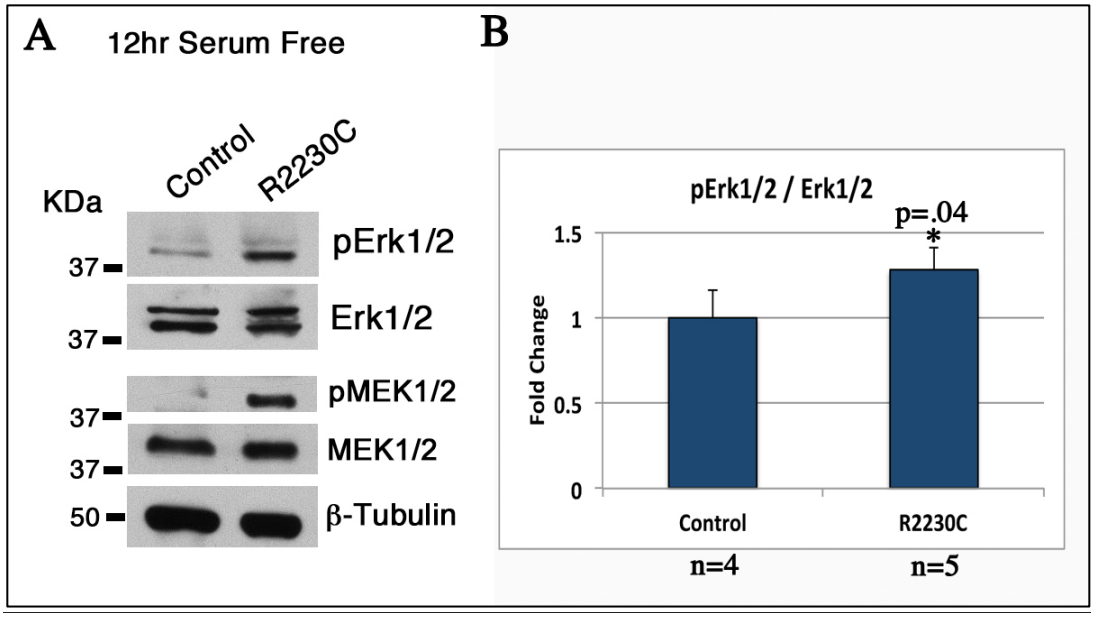

Figure 3.23. Incresed MEK/Erk Signaling Present in Human Cells with *DCHS1* Mutation. (a) Western blot analysis of control and *DCHS1* R2330C mutant cells normalized to β-tubulin. (b) Quantification by densitometry shows significant increases in pErk/Erk in mutant cells compared to control cells. (P=0.04, control n=4, mutant n=5)

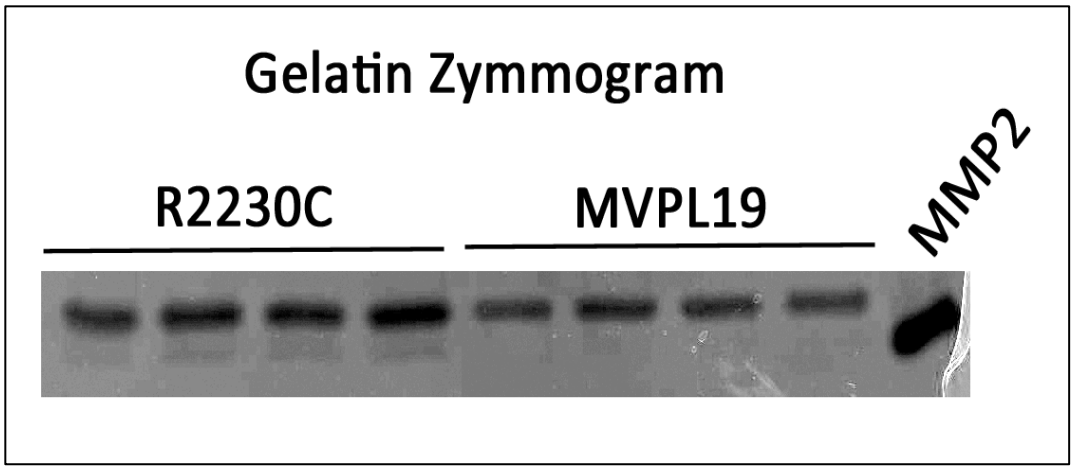

Figure 3.24. Increased Enzymatic Activity of MMP2 in *DCHS1* Mutant Cells. Gelatin Zymmography was performed using equal amounts of conditioned media from cultured human patient valvular interstitial cells with the *DCHS1* mutation (p.R2330C) and human control (MVPL19). Cells were plated using equal numbers of cells. The last lane is a control and consists of purified MMP2.

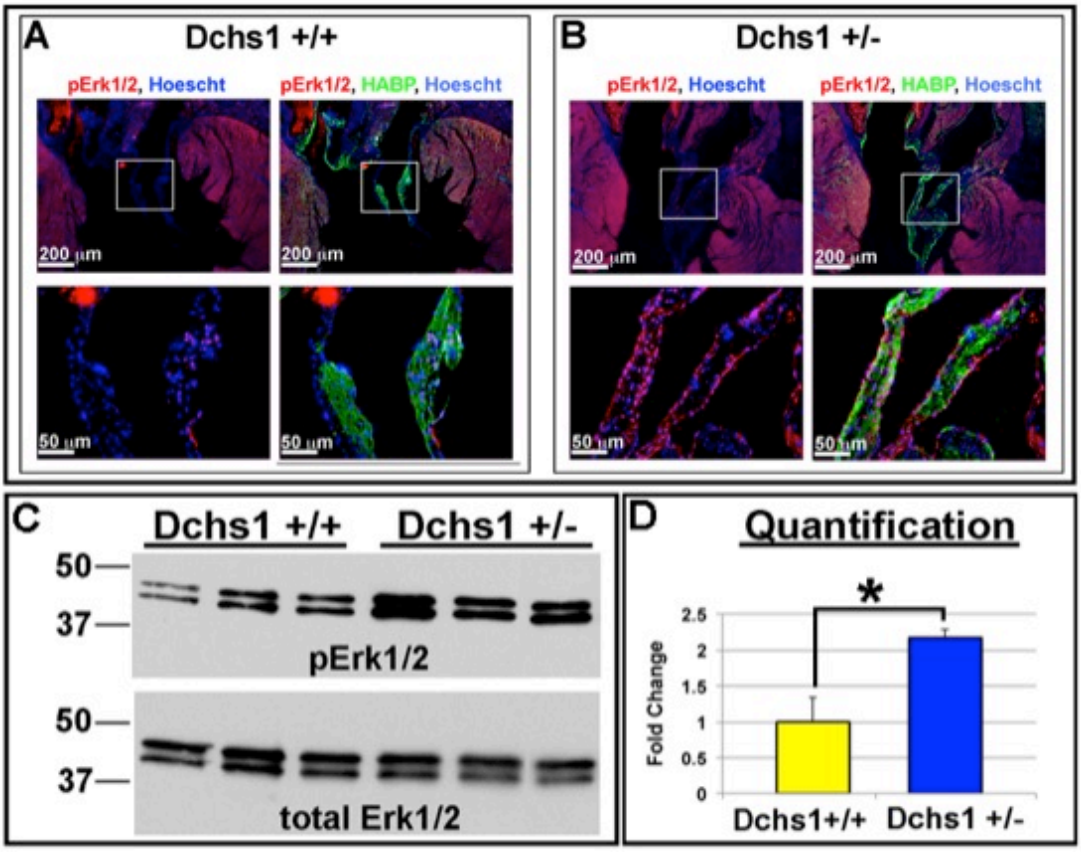

Figure 3.25. Increased Erk1/2 Activity in *Dchs1*$^{(+/-)}$ Adult Mice. (a, b) Wildtype and *Dchs1*$^{(+/-)}$ 9 month old mouse sections stained by IHC for pErk1/2 (red), HaBP (green), and Hoechst (blue, nuclei) show increased pErk1/2 in *Dchs1*$^{(+/-)}$ mitral leaflets. (c,d) Western blot analysis on individual anterior leaflets reveal significant increases in phospho/total protein per individual leaflet. ($P<0.01$).

By IHC, increases in pErk1/2 are observed in the *Dchs1*$^{(+/-)}$ mouse mitral leaflets at P0, concurrent with increased α-smooth muscle actin (α-SMA), a marker for myofibroblasts (*Figure 3.26*). These changes in cellular signaling and activity precede myxomatous changes in the adult, shown in *Figure 3.26* by collagen I and HaBP stainings. Quantification of phospho to total Erk1/2 protein levels were obtained by western blot performed on isolated anterior and posterior leaflets, one leaflet per sample. Significant increases in pErk/Erk were observed in the posterior leaflets of the *Dchs1*$^{(+/-)}$ mouse at P0 (*Figure 3.27*). These changes in pErk1/2 signaling occur before myxomatous degeneration and persist into adulthood, suggesting this pathway may be pathogenic to the development and progression of myxomatous degeneration and MVP.

Since increases in EPDC migration into the posterior leaflet are observed concurrent with increases in pErk1/2, I examined the possibility that these cells are expressing pErk1/2 and contributing to signaling changes in the *Dchs1*$^{(+/-)}$. pErk1/2 activity is observed at neonatal day 0 in both EPDCs and endocardial-derived cells in the *Dchs1*$^{(+/-)}$ but not in the *Dchs1*$^{(+/+)}$ where pErk1/2 activation is only present in the endocardial derived cells (*Figure 3.28*). This indicates valvular EPDCs that lack an allele of Dchs1 are functionally different than those from a wildtype mouse. Additionally, overall pErk1/2 activity appeared to be increased in the heart, including in the myocardium of the *Dchs1*$^{(+/-)}$.

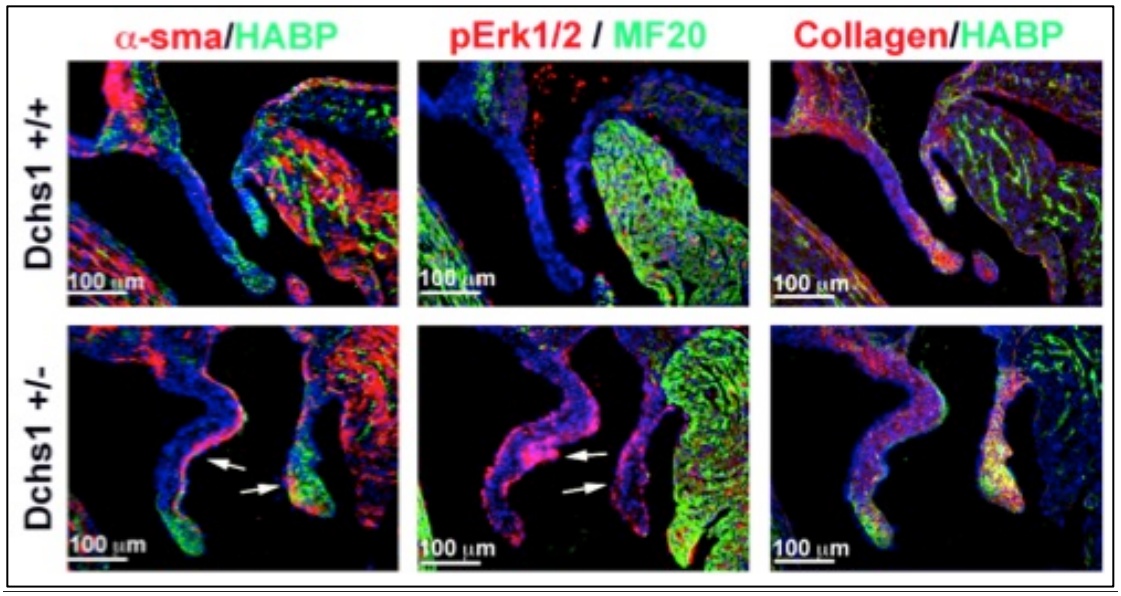

Figure 3.26. Increased pErk1/2 Signaling and Myofibroblast Activity Precede Myxomatous Changes in the *Dchs1*$^{(+/-)}$ Mouse. IHC was performed on P0 *Dchs1*$^{(+/+)}$ and *Dchs1*$^{(+/-)}$ mice for α-SMA (red) and HaBP (green), pErk1/2 (red) and MF20 (green, myocardium), and, Collagen I (red) and HaBP (green). Increased pErk1/2 and α-SMA (white arrows) is observed in the *Dchs1*$^{(+/-)}$ mouse compared to the *Dchs1*$^{(+/+)}$ before myxomatous changes have occurred.

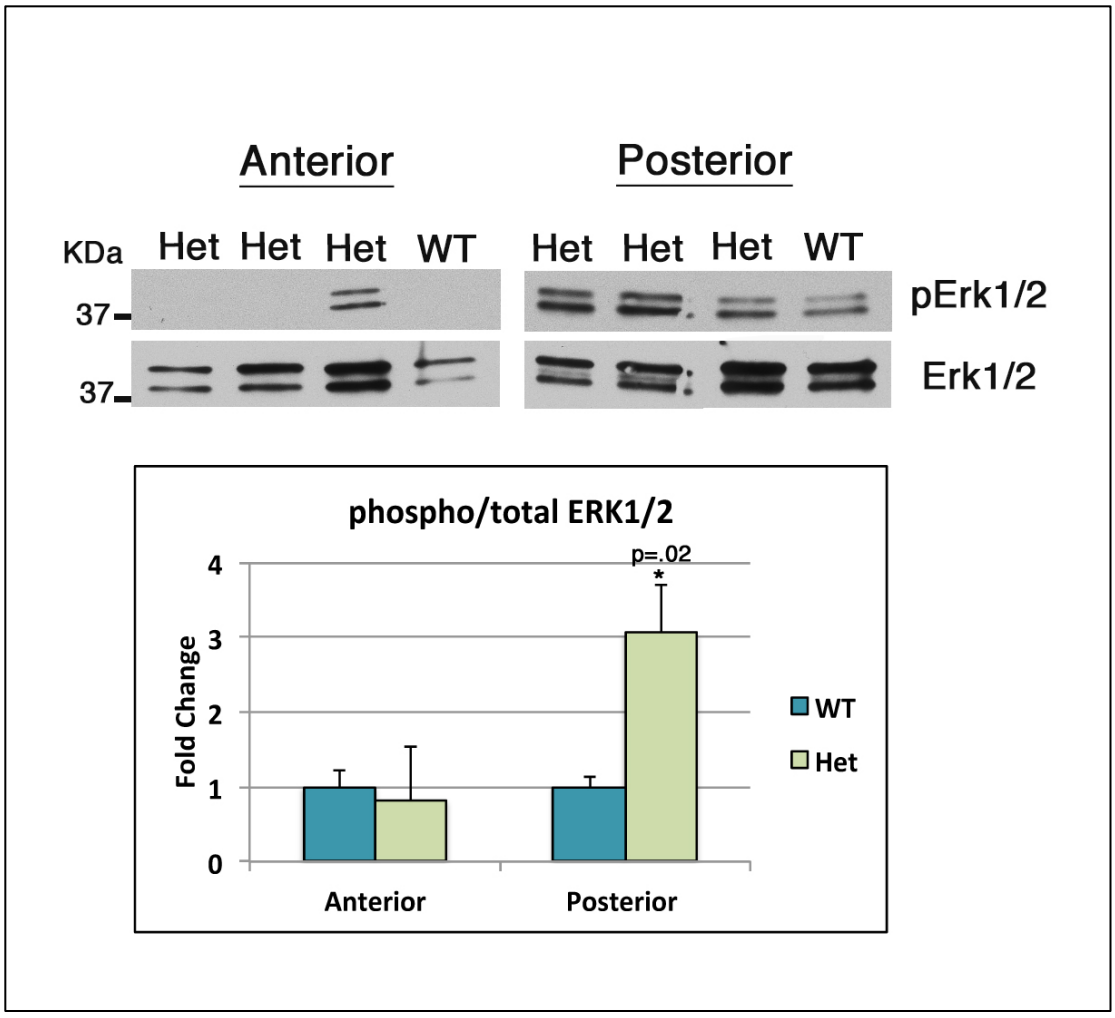

Figure 3.27. Quantification of Phospho/Total Protein Levels of Erk1/2 in P0 Anterior and Posterior Mitral Leaflets. Isolated mitral anterior and posterior leaflets were harvested at P0 for western blot analysis. One leaflet per sample was used to detect levels of pErk/Erk, quantified by densitometry. Significant increases in pErk/Erk were observed in the posterior leaflet (p=0.02, Anterior n=7, Posterior n=5)

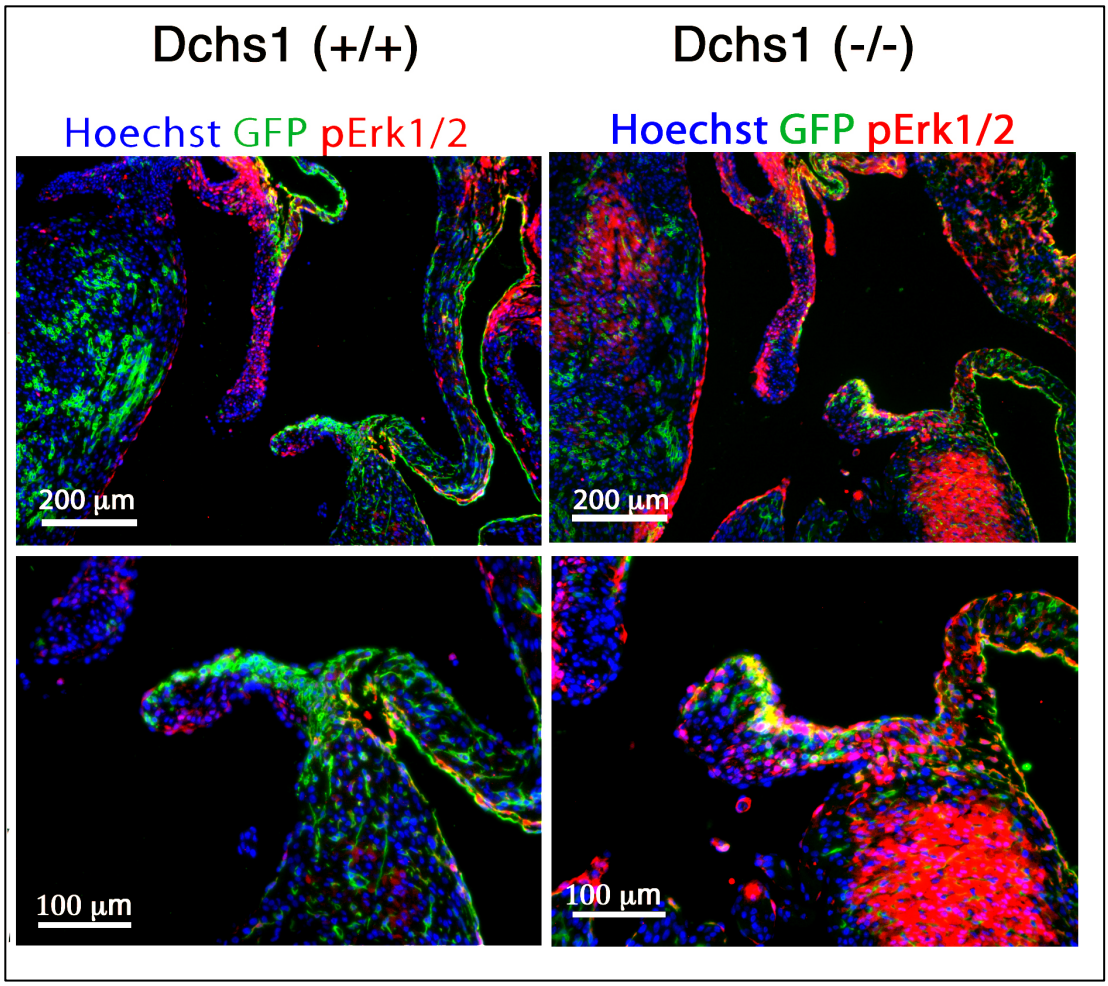

Figure 3.28. Lineage Specific Expression of pErk1/2 at P0. IHC was performed in wildtype and *Dchs1*$^{(+/-)}$ mice crossed onto the WT1-Cre/ROSA-eGFP25 background which allowed for linage tracing of the EPDCs. pErk1/2 activity (red) in EPDCs (green, GFP) was observed in the posterior leaflet of the *Dchs1*$^{(+/-)}$ (yellow, co-expression) but not in the wildtype mice.

To understand the effects of increased Erk signaling on valve disease and to determine if this pathway is pathogenic to myxomatous degeneration, transgenic mice that express a constitutively active form of MEK1 in fibroblasts (Periostin-Cre), were examined for valve defects. This mutant MEK1 contains serine-to-glutamic acid substitutions of the two phospho-acceptors at amino acids 218 and 222 in combination with an internal deletion from amino acid 32 to amino acid 51. These mutations result in high constitutive activity of MEK1, and the mutant does not need to be activated by other protein kinases (Mansour, Matten et al. 1994). This mouse was crossed onto the Periostin-Cre background to generate a fibroblast specific overexpressed MEK1 mouse by our collaborator Simon Conway, who provided heart samples for the following experiments. MEK overexpressed mice at neonatal day 0 exhibit increases in pMEK1/2 and its downstream target pERK1/2, by IHC (*Figure 3.29 a,b*). Histological analysis of the mitral valve of MEK OE mice was performed by IHC examining collagen I, HaBP, and Ki67. At neonatal day 0, enlarged misshapen leaflets are observed along with increases in proteoglycan expression (versican) and proliferating (ki67) cells, indicating increased MEK/Erk activation results in mitral valve defects similar to those observed in the *Dchs1*$^{(+/-)}$ mouse (*Figure 3.30*). In addition to these defects, I observed thickened left ventricular and septal myocardium, enlarged aortic valves, and mitral stenosis, in the MEK overexpressed mice.

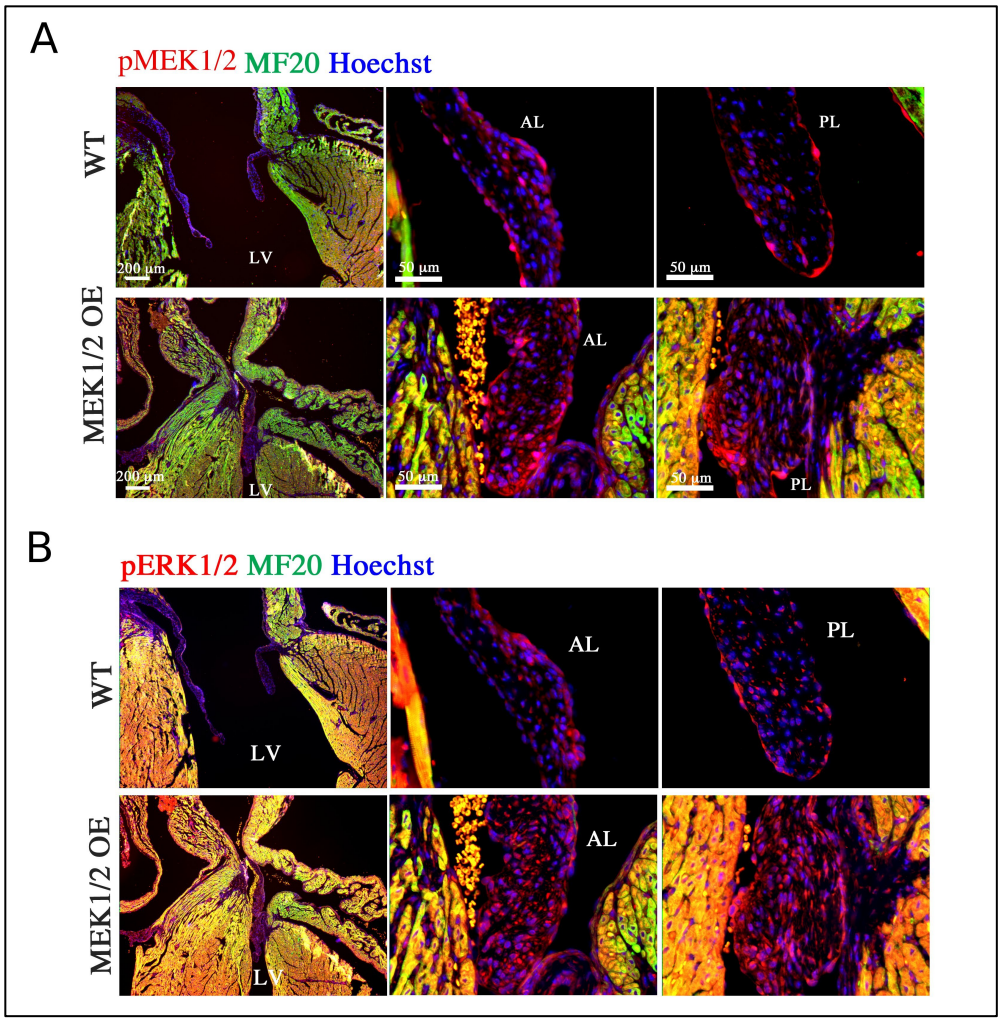

Figure 3.29. MEK Overexpression Results in Increased MEK/Erk Activity in the Mitral Valve. MEK1/2 overexpressed mice and wildtype mice (WT) were sectioned and stained by IHC for pMEK1/2 (a, red) and pErk1/2 (b, red) to compare signaling activity between genotypes. Posterior leaflet (PL), anterior leaflet (AL), left ventricle (LV).

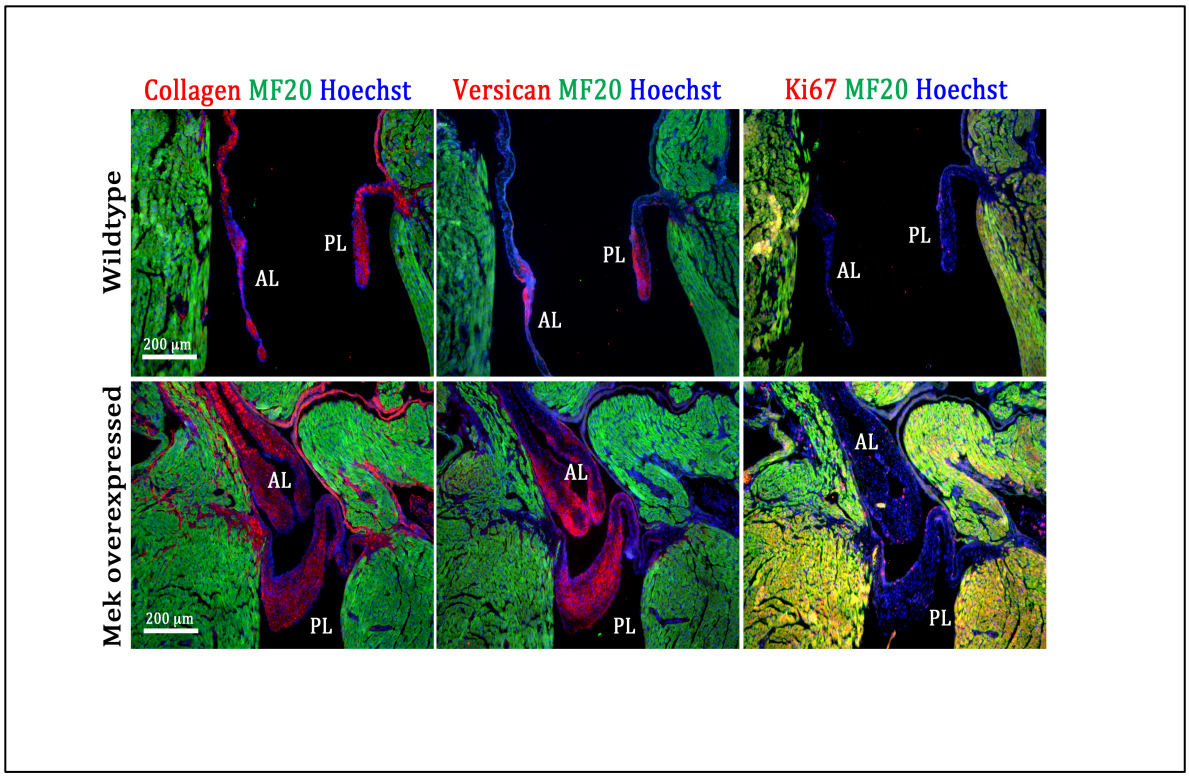

Figure 3.30. Phenotypic Analysis of The Mitral Valve in MEK Mice with MEK Overexpression. IHC for collagen I (red), versican (red), Ki67 (red), MF20 (green, myocardium) and Hoechst (blue, nuclei) was performed on wildtype and MEK overexpressed mice at neonatal day 0. Leaflet shape is altered and enlarged in the MEK overexpressed mitral leaflets concurrent with increased versican and ki67 expression.

To asses the development of mitral valve prolapse and to understand how the mitral valve in *Dchs1*$^{(+/-)}$ mice changes over time, 3D reconstructions were generated from micro-MRI slices in wildtype and *Dchs1*$^{(+/-)}$ mice at multiple timepoints, 1, 3, and 9+, and volume changes over time were quantified (*Figure 3.31*). In a wildtype mouse, leaflet volume steadily increases form 1 month to 9 months, with a significant increase in volume over this period of time in the anterior leaflet. The *Dchs1*$^{(+/-)}$ anterior leaflet displays significant increases in volume between 1 and 3 months time, as well as overall increases from 1 to 9 months. In the posterior leaflet, growth is significantly increased at every timepoint, while the wildtype displays steady growth resulting in no significant increases over time (*Figure 3.31*). Overall, loss of one Dchs1 allele results in increased leaflet growth over time, suggesting leaflet remodeling is a continuous process in MVP. This finding supports the idea that pharmacological intervention targeting leaflet remodeling may be efficacious at preventing the progression of MVP.

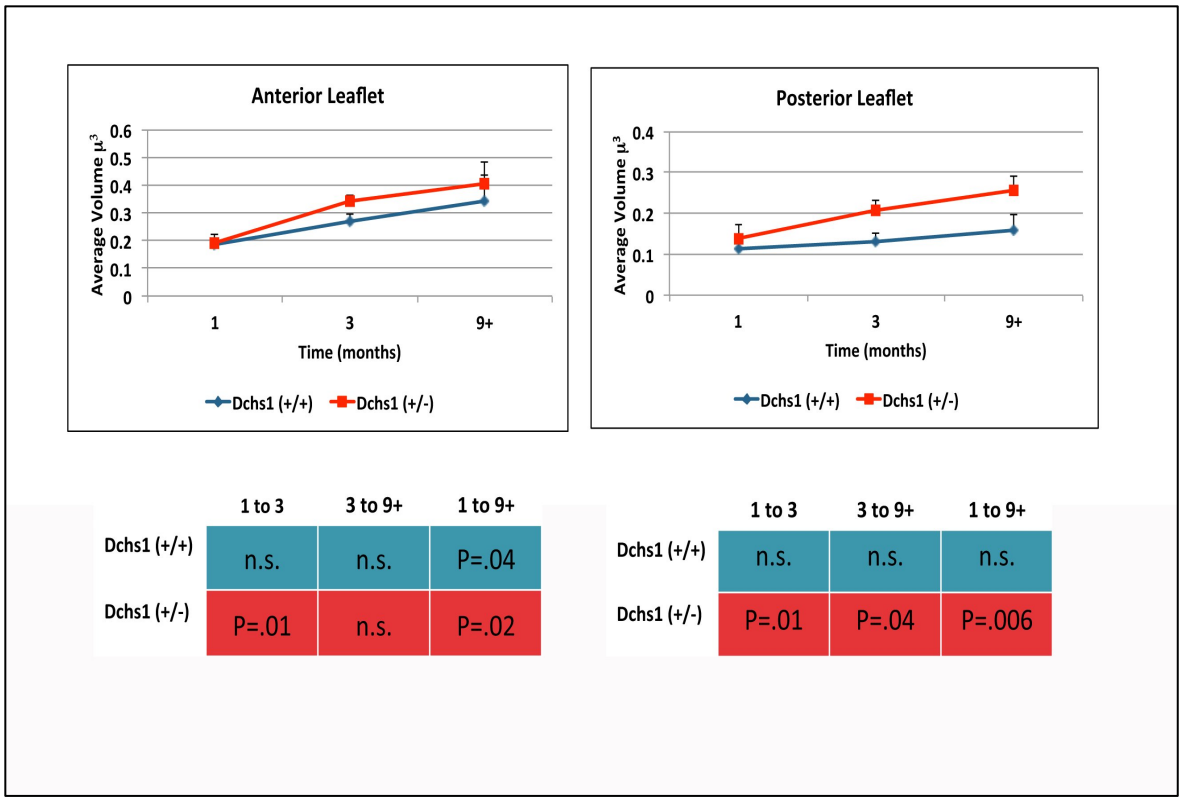

Figure 3.31. Volumetric Changes of Mitral Leaflets Over Time. Micro-MRI slices were used to generate 3D reconstructions of anterior and posterior leaflets from the mitral valve of wildtype and *Dchs1*$^{(+/-)}$ mice at 1 month, 3 months, and 9+ months of age. Volumes were quantified from these 3D reconstructions and a students T-test was used to determine significance in volume changes over time. The anterior and posterior leaflet of the *Dchs1*$^{(+/-)}$ increased significantly over time at a faster rate than wildtype leaflets, of which only the anterior showed significant increases in volume over time (1 month to 9+ months).

Discussion

The data presented in this chapter demonstrate the first identification of genetic mutations that cause mitral valve prolapse in humans. Mutations in the cadherin gene *DCHS1*, are loss of function and result in protein instability. This was shown *in vivo* by morpholino knockdown in zebrafish resulting in malformed atrioventricular canal formation and function, and by *in vitro* experiments which demonstrate a reduced mutant protein half life. Data generated in the *Dchs1*$^{(+/-)}$ mouse supports a role for Dchs1 in valve disease whereby loss of Dchs1 expression is associated with enlarged, myxomatous mitral leaflets that are functionally deficient and result in mitral valve prolapse. This murine model of disease phenocopies patients with the *DCHS1* mutation, providing a good model to study the etiology of the disease and as such is currently the only known mouse model of nonsyndromic MVP.

MVP is generally thought of as a degenerative disease since it is usually diagnosed later in life. Echocardiographic analysis of family 1, the original family linked to the MMVP2 locus, revealed the presence of mitral valve prolapse in four children under the age of 12 (Freed, Acierno et al. 2003). These children exhibited minimal to no mitral regurgitation, classifying them as clinically benign and would not have been identified as affected by MVP had they not been screened for this study. Since the presence of MVP is observed in children and genetic mutations in *DCHS1* are present at conception and throughout development, hypothesized that there may be a developmental origin for the disease.

Using the *Dchs1*$^{(+/-)}$ mouse model, the defects were traced back to development where changes in leaflet shape were visible by E17.5. Leaflet volume was unchanged between genotypes, but *Dchs1*$^{(+/-)}$ and *Dchs1*$^{(-/-)}$ exhibited significantly shortened and thickened leaflets. This phenotype persists into neonatal timepoints where thickened and enlarged leaflets are observed at postnatal day (P) 6. The Dchs1 global knockout mouse (*Dchs1*$^{(-/-)}$) exhibits shape changes similar to the mitral leaflets of the E17 *Dchs1*$^{(+/-)}$ in other organs such as kidneys, sternum, and vertebrae, where these organs become shortened and widened (Mao, Mulvaney et al. 2011). Interestingly, almost identical phenotpyes in diverse organs are observed in the Fat4 mutant mouse, suggesting both Dchs1 and Fat4 have similar biological functions and likely function in the same pathway to regulate tissue size and shape. Dchs1 and Fat4 double mutants mirror the single mutants, indicating that these cadherins likely function as a receptor and ligand pair to control organ size and shape (Mao, Mulvaney et al. 2011). The interaction between Dchs1 and Fat4 homologues (Ds, Ft) have been confirmed in *drosophila,* and function in two distinct downstream branches of signaling, one that influences Hippo signaling, and one that influences planar cell polarity signaling (PCP). Hippo signaling requires cell-to-cell contacts to initiate the phosphorylation of MST1/2 (mammalian Ste2-like kinases, Hpo orthologs) and LATS1/2 (large tumor suppressor kinase 1/2, wts orthologs) to phosphorylate and inhibit the transcription factors TAZ (transcriptional coactivator with PDZ binding motif) and YAP (Yes-associated protein, Yki ortholog), which function to promote cell proliferation and survival (Badouel

and McNeill 2011). This pathway has been shown to restrict organ size during development by suppressing cell proliferation and tissue growth in the fly and in mammals (Bando, Mito et al. 2011). Disruption of Hippo pathway components result in organ enlargement and excess cell proliferation, and is classically associated with hepatomegaly, epidermal hyperplasia, and cancer development (Dong, Feldmann et al. 2007). Neither the global Dchs1 nor the Fat4 mutant mice exhibit these classic overgrowth phenotypes. My data in the mitral valve of the Dchs1 heterozygote mouse suggest a cell polarity phenotype rather than an overgrowth phenotype. Although, it is likely Hippo signaling may play a role in the global knockout mouse, where thickened myocardium and myocardial hyperplasia are observed. This requires further analysis to determine the role of Dchs1 and Hippo signaling in myocardial growth and may provide insight into the processes of cardiac hypertrophy and growth in disease.

Defects in *Dchs1* $^{(+/-)}$ valve shape are observed during the post-EndoMT phase at E17.5, when the mitral leaflets undergo extensive remodeling to transform from globular cushions into thin stratified leaflets. Little is known about how this remodeling occurs, but it has been observed that during this process, valvular interstitial cells become aligned and make cell-to-cell contacts (de Vlaming, Sauls et al. 2012). As a corollary hypothesis to the hypothesis that MVP results from developmental defects, I proposed that Dchs1 is required for directing mitral leaflet shape and anatomy by maintaining interstitial cell alignment, oriented cell migration, and the stabilization of adherens junctions that provide cell-to-cell contacts. In agreement with this hypothesis, disruptions

in interstitial cell alignment across the proximal-distal axis in a gene-dosage dependent manner of *Dchs1*$^{(+/-)}$ and *Dchs1*$^{(-/-)}$ leaflets were observed at P0. This role for Dchs1 in regulating anatomical patterning and leaflet shape through the polarization of interstitial cells is consistent with studies in *drosophila* where loss of the Dchs1 homologue dachsous (Ds), results in non-autonomous PCP defects in the ommatidia of the eye, the abdomen, and cuticular hairs of the wing (Adler, Charlton et al. 1998, Yang, Axelrod et al. 2002, Lawrence, Casal et al. 2004, Simon 2004). Ds has been shown to play a role in left-right patterning of hindgut progenitor tissue, where asymmetric morphogenesis occurs by transferring a polarizing signal to neighboring cells by asymmetric binding of Dchs1 to Fat which serves as an upstream signal to initiate planar cell polarity signaling (PCP) (Gonzalez-Morales, Geminard et al. 2015). In addition to cell alignment, defects in the mitral valve of *Dchs1*$^{(+/-)}$ support a role for Dchs1 in VIC polarization where asymmetric localization of Dchs1 expression is observed by immunocytochemistry (ICC) in individual VICs in culture. Tissue expression of Dchs1 is presented as a gradient throughout the mitral leaflets consistent with Ds expression in the *drosophilia* wing and eye, where graded and asymmetric expression of Ds exhibits polarity-inducing effects (Zeidler, Perrimon et al. 1999, Yang, Axelrod et al. 2002, Simon 2004). It is possible a similar mechanism involving Dchs1 functions in valve development to promote the polarized orientation of VICs, but further studies examining the asymmetric localization and activation of PCP signaling components are required in addition to studies examining mitral valve defects in PCP knockouts.

One mechanism that may explain the abnormal shortened and widened shape of the mitral leaflets during development is a disruption in the process of convergent extension. This is the polarized and coordinated movement of a group of cells within a tissue, during which cells transverse to the elongating body axis to form a narrower, longer array (Keller 2002). Studies in *drosophila* demonstrate polarity genes regulate the polarized movement of cells responsible for shaping and organizing tissues (Wong and Adler 1993, Eaton 2003, Wang, Hamblet et al. 2006, Zhao, Yang et al. 2013). I observed migratory defects associated with loss of Dchs1 *in vitro* and *in vivo*, with VICs and EPDCs exhibiting increased and randomized migratory behavior. Similarly, mammalian embryos with deficient PCP signaling exhibit migratory behavior defects such as incomplete closure of the neural tube (Ybot-Gonzalez, Savery et al. 2007). PCP defects have also been linked to cilia, such as Wdpcp, a protein involved in ciliogensis that when mutated in the mouse, results in disrupted cell migration and PCP defects (Cui, Chatterjee et al. 2013). In addition, MVP and polycystic kidney disease (a well described ciliopathy resulting from defects in ciliogenesis) have a 26% comorbidity, suggesting cilia may be also be involved in valve disease (Lumiaho, Ikaheimo et al. 2001). Further supporting this, mutations in a gene required for cilia formation were recently identified by colleagues of the Norris lab in a genome-wide association study performed on a cohort of MVP patients (data unpublished). This gene has not been extensively studied in a mouse model but is currently being evaluated in our lab. Examining a link between Dchs1 and cilia formation and/or stabilization as a mechanism for the

alignment and migration defects observed in the *Dchs1*$^{(+/-)}$ mouse, is an important future direction for the lab.

The role of Dchs1 functioning as a cadherin in cell adhesion was examined by adhesion assays where patient cells harboring the *DCHS1* p.R2330C mutation displayed decreased adherent properties. VICs from *Dchs1*$^{(+/-)}$ explants migrated individually versus as a single sheet of cells in the wildtype, and displayed mis-localization of N-cadherin, a component of the adherens junctions. N-cadherin expression levels appeared to be unchanged, suggesting Dchs1 functions in the stabilization of these adherens junctions at cell-to-cell interfaces. Loss of adherens junction formation in *drosophila,* results in cells that lose polarity and become mesenchymal in phenotype (Cox, Kirkpatrick et al. 1996). The mesenchymal properties of Dchs1 deficient cells have not been extensively examined, but if loss of Dchs1 results in phenotypically mesenchymal VICs, this would likely be contribute to disease in the mitral leaflets, since cell differentiation plays a role in myxomatous degeneration (Rabkin, Aikawa et al. 2001). It is possible that loss of adherent properties in VICs and EPDCs may enable faster and more randomized migration. This would explain the faster migration observed in the *Dchs1*$^{(+/-)}$ mouse and in patient VICs with the *DCHS1* p.R2330C mutation. There is a close relationship and positioning between adherens junctions and tight junctions, and although I did not examine changes in tight junctions, it is likely these are also disrupted.

Another commonly associated result of loss of cell-to-cell contacts through adherens junctions is increased endothelial-to-mesenchymal transition

(Abdulla, Luna-Zurita et al. 2013). Since hypercellularity and expression of mesenchymal markers only present during development (α-SMA, vimentin) have been reported in diseased valve endocardial cells in animal models and human patients, re-activation of EndoMT, an embryonic pathway not present in normal adult valves, has been suggested as a potential disease inducing mechanism (Paranya, Vineberg et al. 2001, Paruchuri, Yang et al. 2006, Liu, Joag et al. 2007). A population of ovine aortic VICs have been observed to co-express CD31, an endothelial marker, along wth α-SMA. Co-expression of these factors could also be induced *in vitro* by treatment with TGFβ, suggesting a transdifferentiation event may occur in the adult (Paranya, Vineberg et al. 2001). In a tissue engineered *in vitro* model of valve endothelial cell tissue, cyclic mechanical strain can induce EMT in the adult porcine valve, where low strain induced EMT through a TGFβ dependent signaling pathway, and high strain induced EMT via increased Wnt/β-catenin signaling (Balachandran, Alford et al. 2011). While direct evidence for EndoMT processes in the diseased adult mitral valve have not been proven, evidence for the ability and plasticity of VECs to undergo transdifferentiation exists, suggesting re-activation of EndoMT as a potential mechanism by which the mitral valve undergoes myxomatous remodeling (Paruchuri, Yang et al. 2006). Lineage tracing studies where the movement of endothelial cells can be traced would provide evidence for an EndoMT event *in vivo*.

Since adherens junctions govern the permeability of endothelial and epithelial cells, loss of adhesion and adherens junction localization may result in loss of barrier function and increased permeability in the *Dchs1*$^{(+/-)}$ mouse (Tornavaca, Chia et al. 2015). EPDCs migrate from the epicardium on the outside of the heart through the AV sulcus and into the posterior leaflet (Wessels, van den Hoff et al. 2012). It is possible that the timing of this migration and the formation of these cells into a single tightly bound sheet of cells may function in providing a barrier between the posterior leaflet and the left ventricle, which is a rich source of growth factor expression (TGFβ, FGF) (Watanabe, Zaffran et al. 2012). These growth factors can stimulate many downstream signaling mechanisms that influence matrix deposition and tissue growth to promote pathogenic remodeling of the posterior leaflet. Further studies examining a role for EPDCs in providing a functional barrier at this timepoint would provide an interesting mechanism for valve development and disease.

Since the penetrance of MVP is significantly higher in the posterior leaflet (our studies show 100% penetrance in the posterior leaflet of MVP families) and EPDCs preferentially contribute to this leaflet, they may play an important role in facilitating the disease process. I examined cell proliferation in *Dchs1*$^{(+/-)}$ crossed onto the WT1-Cre/ROSA-eGFP25 background in order to determine if cell proliferation plays a role in leaflet shape, and to determine if there are differences in proliferation between cells from the epicardial origin (EPDCs) and cells from the endocardial origin. I found significant increases in cell

proliferation in the posterior leaflet of the *Dchs1*$^{(+/-)}$ and the majority of these proliferating cells were EPDCs. Additionally, the total number of EPDCs within the posterior leaflet is increased and the total number of endocardial decreased. As an explanation for this observation, it is possible EPDCs interact with endocardial derived cells to provide a signal which is responsible for turning off EndoMT. Additionally, since these cells exhibit increased migratory behavior, this could result in early infiltration into the postierior leaflet and subsequent early inhibition of EndoMT. Experiments looking at early timepoints in the WT1-Cre/ROSA-eGFP25 lineage trace mouse would confirm or refute this hypotheisis. I have not examined in detail the Dchs1 cKO Wt1-Cre, which removes Dchs1 from all epicardial and epicardial dervided cells, for valve defects. This cross would determine if epicardial-expressed Dchs1 is required for valve development and if EPDC migration defects lead to myxomatous leaflets in the adult. Additional experiments defining the role of EPDCs and the influence they have on endocardial cells would be an interesting future direction and may provide insight into the role of EPDCs in pathogenesis of MVP.

This data demonstrates a role for Dchs1 in mitral valve development, where loss of Dchs1 function results in disruptions in valvular architecture and leaflet shape during development. How the mitral leaflets become myxomatous and diseased in adulthood is unknown. Current studies examining pathogenic signaling pathways overwhelmingly support a role for TGFβ in this process. Myxomaotus thickening and elongation of the mitral valve is commonly

observed in syndromic diseases associated with increased TGfβ signaling (Ng, Cheng et al. 2004, Loeys, Chen et al. 2005, Doyle, Doyle et al. 2012). In the mouse model of Marfan's syndrome, non-canonical TGFβ signaling through Erk1/2 is directly responsible for the aortic aneurism phenotype observed in the Marfan mouse, and can be attenuated by administration of an angiotensin II receptor 1 blocker (ARB) which targets TGFβ signaling through Erk1/2 (Habashi, Doyle et al. 2011, Holm, Habashi et al. 2011). While Erk1/2 involvement has not directly been identified in the mitral valve phenotype of Marfan mice, administration of a TGFβ neutralizing antibody was able to attenuate the myxomatous phenotype, suggesting TGFβ is directly responsible for the valve phenotype observed in this mouse (Ng, Cheng et al. 2004). In human patients, circulating serum levels of TGFβ are reported to be increased in human patients with MVP and these levels correlate with posterior leaflet thickness and mitral regurgitation (Malev, Zemtsovskii et al. 2012). These data support a role for non-canonical TGFβ signaling in the pathogenesis of MVP. This data demonstrating increased pErk1/2 activation in the Dchs1 model of MVP is consistent with the literature which suggests a role for non-canonical TGFβ signaling in valve disease. Interestingly, enhanced pErk1/2 is observed during neonatal life, a timepoint that precedes myxomatous degeneration. Since myxomatous changes are not observed until adult timepoints in the mouse and the clinical presentation of MVP in human patients is commonly detected later in life, the increased Erk1/2 signaling which precedes myxomatous changes implicates this pathway in the

pathogenesis and progression of myxomatous degeneration. Since Erk1/2 is known to promote cell proliferation, MMP expression, and cellular differentiation, it is plausible that increased pErk1/2 may exert pathogenic effects in the valve tissue (Shaul and Seger 2007). In order to determine if pErk1/2 is directly responsible for myxomatous changes and associated MVP, experiments pharmocalocially targeting Erk1/2 in the *Dchs1*$^{(+/-)}$ mouse are required to determine if this treatment is sufficient to attenuate the myxomatous phenotype seen in this mouse.

While the literature supports a role for TGFβ in the pathogenesis of MVP, there are many upstream activators of Erk1/2 signaling which could be responsible for this increased signaling observed in the mitral valve including, Epidermal growth factor (EGF), Vascular endothelial growth factor (VEGF), Platelet-derived growth factor (PDGF), and Insulin-like growth factor (IGF). The source of an upstream signal responsible for initiating the increased pErk1/2 is unknown, but experiments in cultured VICs from human diseased valves suggest an autocrine/paracrine mechanism whereby angiotensin II receptor 1 blockers (ARB) are sufficient to block TGFβ-induced matrix production which contributes to abnormal valve remodeling (Geirsson, Singh et al. 2012). Alternatively, the left ventricle is a rich source of growth factors and the close proximity of the posterior leaflet to this structure in addition to a smaller surface area may provide an explanation as to why this leaflet is more commonly affected than the anterior leaflet. Contribution from circulating factors is another potential source

since levels of circulating factors have been shown to be altered in diseased states and may provide a source of aberrant signaling in the mitral valve. In support of the TGFβ hypothesis as an upstream regulator of the increased Erk signaling observed in the *Dchs1*$^{(+/-)}$ mouse, two hybrid screens performed using the intracellular domain of Dchs1 reveal Cathepsin-A as a binding partner. Cathepsin-A is a component of the elastin binding protein receptor complex responsible for elastinogenesis through export of elastin components into the extracellular matrix (Antonicelli, Bellon et al. 2009). Loss of Dchs1 likely results in loss of stabilization of thie receptor complex leading to a change in elastin deposition, which is consistent with what is seen histologically in myxomatous leaflets. Ultimately this could lead to a loss in the ability of elastin to sequester TGFβ and increase MEK/Erk signaling. This is a future direction of the work presented in this dissertation. Circulating micro-RNAs are another interesting potential contributor to disease since they have been shown to be dysregulated in canine models of MMVD. Specifically, *cfa-miR-302d,* which is responsible for inhibition of TGFβ-induced endothelial to mesenchymal transition and fibronectin production, is increased in serum of MMVD affected dogs (Faherty, Curran et al. 2012). It is likely there are multiple inputs, which together play a role in facilitating disease.

Upstream of Erk1/2 is mitogen-activated kinase kinase (MEK1/2), dual specificity kinases that preferentially phosphorylate Erk1/2 in response to growth factor stimuli. To further examine a pathogenic role for Erk1/2 in the

development of the myxomatous valve phenotype, mice with a constitutively active MEK1/2 transgene driven by periostin-Cre to target fibroblasts, were examined histologically for mitral valve defects. MEK1/2 overexpression by periostin-Cre resulted in increased pMEK1/2 and pErk1/2 signaling in the mitral valve and an enlarged mitral phenotype with increased proteoglycan deposition and cell proliferation, suggesting a direct role for this pathway in the pathogenesis of myxomatous degeneration. These findings are consistent with other disorders resulting from enhanced MEK1/2-Erk1/2 signaling. Specifically, enlarged AV valves and MVP have been reported in patients with Noonan syndrome, a genetic disorder resulting in enhanced Ras-Raf, MEK1/2-Erk1/2 signaling (Bertola, Kim et al. 2000). Mice heterozygous for a gain-of-function targeted gene modification ($D^{61}G$ in *ptpn11*, which encodes for NF1, a protein that negatively regulates Ras by maintaining it in an inactive GDP-bound state) known to cause Noonan syndrome were reported to have enlarged AV valves, enhanced cell proliferation and decreased apoptotic remodeling of the AV cushions, suggesting this pathway acts to promote cell proliferation and suppress apoptosis in the mitral valve (Hiatt, Ingram et al. 2001). Similarly, I observe increased proliferation in neonatal mice that overexpress MEK1/2 as well as in the *Dchs1*$^{(+/-)}$ mouse at P0. In addition to the mitral valve phenotype observed in the MEK1/2 overexpressed mice, I observed a thickened myocardium at P0 also similar to hypertrophic cardiomyopathy in Noonan syndrome patients with Ras mutations (Nishikawa, Ishiyama et al. 1996).

While these results support a role for MEK/Erk signaling in the

development myxomatous degeneration and progression of MVP, alternative pathways have been observed in myxomatous tissue and may also be pathogenic to MVP. Canonical TGFβ signaling through Smad2/3 has been reported in numerous studies to be increased in diseased valves (Geirsson, Singh et al. 2012, Hagler, Hadley et al. 2013, Surachetpong, Jiranantasak et al. 2013). I have not examined this pathway in detail in the *Dchs1*$^{(+/-)}$ model of MVP, but preliminary work suggests this may not be a significantly altered pathway (data not shown). It is possible there are multiple signaling pathways active in disease that act in parallel to one another to promote matrix changes. Our future studies examining direct interacting partners for the intracellular domain of Dchs1, by 2-hybrid screens, will provide insight into the role of Dchs1 and other pathways affected by Dchs1heterozygosity.

Together these data demonstrate a developmental basis for nonsyndromic mitral valve disease and mitral valve prolapse. Dchs1 is required for patterning of VICs and shaping of the mitral leaflets by promoting cellular alignment, cellular adhesion, and directing proper migration of EPDCs into the posterior leaflet. Disruptions in how the mitral valve is built during development provide the basis for valve disease and leads to secondary defects in matrix remodeling characterized by increased proteoglycan deposition, collagen fragmentation, and hypercellularity. The MEK/Erk signaling pathway may provide the initial que that initiates myxomatous degeneration since it is present before these changes occur and persist into adulthood.

Pharmocological blockage of this pathway may provide an effective therapy aimed at preventing the progression of MVP and myxomatous degeneration, and thus provide an alternative option to surgical intervention for MVP patients.

CHAPTER 4: INCREASED INFILTRATION OF EXTRA-CARDIAC CELLS IN MYXOMATOUS VALVE DISEASE

Introduction

Mitral Valve Prolapse (MVP) is a common, degenerative cardiovascular disease that occurs in 2.4% of the population. MVP occurs when enlarged and weakened mitral leaflets billow back into the left atrium and fail to properly coapt during ventricular systole, which can lead to mitral regurgitation, congestive heart failure, and even sudden cardiac death. Histologically, the valves are characterized as myxomatous due to progressive fragmentation of collagen, expansion of the proteoglycan-rich spongiosa, and increased cell proliferation. These molecular and cellular changes result in enlarged mitral leaflets that are mechanically weakened over time and become ineffective at preventing the backflow of blood. There are no known nonsurgical cures for MVP, and, as such, it is currently the most common cause of mitral valve surgery. This is likely due to poor understanding of disease etiology and progression. However, previous studies have demonstrated that mutations in the *FLNA* (*Filamin-A*) gene are causal to a rare X-linked myxomatous valvular dystrophy in humans and may provide critical clues to disease inception and pathogenetic manifestation.

The Filamin family consists of three homologous proteins: A, B and C. Filamins A and B are widely expressed, while Filamin-C expression is predominantly restricted to cardiac and skeletal muscle. Filamin exists as a homo- or hetero-dimer where it functions in crosslinking actin filaments, mechano-sensing through cell surface-bound integrins, and by means of these interactions regulates cell adhesion and migration (Kim, Sengupta et al. 2008,

Zhou, Hartwig et al. 2010). Filamin-A has been shown to directly interact with a variety of intracellular proteins and can function as a scaffold for second messengers in signal transduction. Specifically, Filamin-A has been shown to directly bind the TGFβ signaling mediators Smad and R-ras (Sasaki, Masuda et al. 2001, Griffiths, Grundl et al. 2011). Complete genetic removal of filamin-A in the mouse results in embryonic lethality by embryonic day 14 due to vascular hemorrhaging and severe cardiac malformations (Feng, Chen et al. 2006, Hart, Morgan et al. 2006). Our recent studies have shown that filamin-A is highly expressed in the mitral valve during development and is significantly diminished after birth, suggesting an important role for filamin-A during valve development (Norris, Moreno-Rodriguez et al. 2010). Our lab previously reported the developmental importance for filamin-A in the valves by generating conditional knockout mice. In these studies, filamin-A was genetically removed from endothelial-derived tissue of the atrioventricular valves, and resulted in enlarged mitral leaflets that progressed to myxomatous degeneration by two months of age. The developmental defects were attributed to alterations in valvular interstitial cell contractility and impaired ability to remodel the maturing valve matrix. These studies importantly defined a developmental etiology for myxomatous valves and have provided a clinically relevant model to study mechanisms of disease pathogenesis. Thus, in this chapter work presented builds on these previous studies and interrogates postnatal mechanisms by which myxomatous degeneration occurs using the filamin-A-deficient mouse as the model for the disease.

Results

As a model for myxomatous valvular dystrophy, the *filamin-Af/f* mouse was bred onto the *Tie2Cre*(+) background to genetically remove filamin-A from all endothelial and endothelial-derived cells (Sauls, de Vlaming et al. 2012). Since the mitral valve is largely derived from endothelium, the *Tie2Cre*(*+*); *filamin-Af/y* cKO mouse, previously described by our group, provides a model to study mechanisms that lead to the progression of myxomatous degeneration (Sauls, de Vlaming et al. 2012). Histological analysis demonstrates enlarged mitral leaflets in the cKO mouse compared to the thin and elongated leaflets of the WT by two months of age (*Figure 4.1*). Movat's, Masson's, and immunohistochemistry (IHC), for collagen I and HaBP, demonstrate characteristics of myxomatous leaflets in the cKO, with an increase in the proteoglycan-rich regions and disruption of normal matrix organization.

To determine pathogenic mechanisms that contribute to the enlarged and myxomatous mitral valve in the cKO mouse, I performed an *in vivo* analysis examining alterations in signaling. Filamin-A functions in the regulation of various growth signaling pathways, including TGFβ, through direct interactions with downstream signaling mediators (Zhou, Hartwig et al. 2010). I hypothesized that loss of filamin-A would result in the disruption of Erk1/2 signaling and that this may be pathogenic in myxomatous degeneration. By Western blot quantification of phospho/total Erk1/2 and phospho/total JNK in 2-month-old isolated anterior leaflets, and by IHC, I demonstrate that cKO mice have increased pErk1/2 and pJNK in the mitral valve (*Figure 4.2 a-c*).

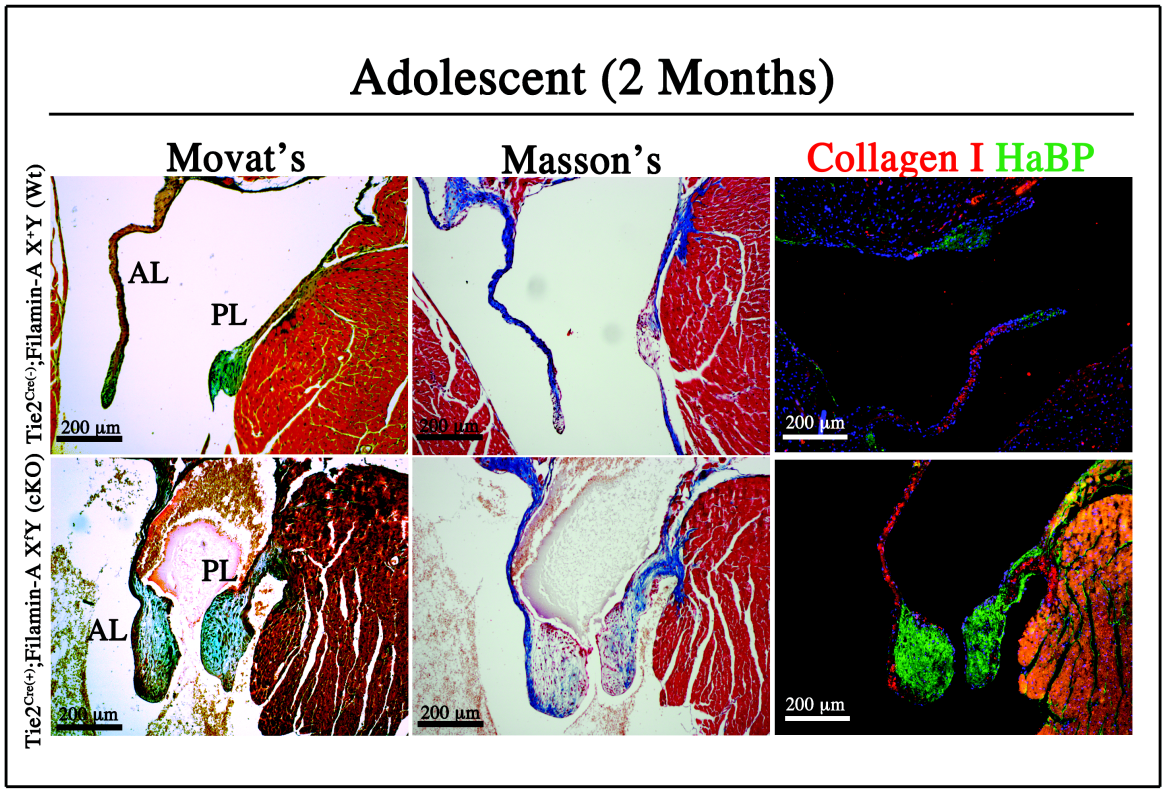

Figure 4.1. Filamin-A-deficient Mice Exhibit Myxomatous Mitral Leaflets. Adolescent 2-month-old mice were analyzed by Movat's Pentachrome, Masson's Trichrome, and Immunofluorescence for Collagen I (red) and Hyaluronan-binding protein (HaBP) (green). Movat's: Collagen (yellow), proteoglycans (blue), elastin/nuclei (black), muscle (red). Masson's: Collagen (blue), nuclei (black), muscle (red). Filamin-A-deficient mice exhibit increased proteoglycan content and disrupted matrix organization characteristic of myxomatous degeneration.

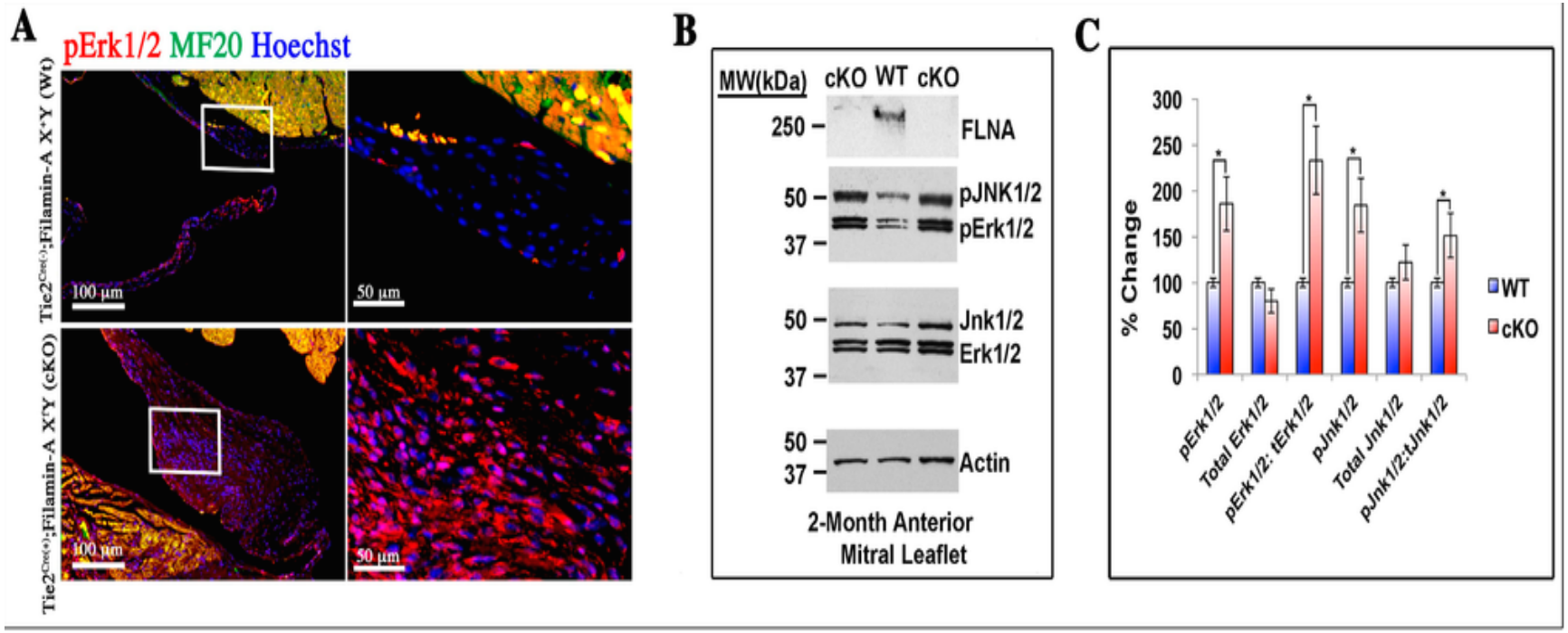
A
pErk1/2 MF20 Hoechst
Tie2Cre(-);Filamin-A X+Y (Wt)
Tie2Cre(+);Filamin-A X/Y (cKO)
100 µm
50 µm
100 µm
50 µm
B
MW(kDa)
cKO WT cKO
250
FLNA
50
37
pJNK1/2
pErk1/2
50
37
Jnk1/2
Erk1/2
50
37
Actin
2-Month Anterior
Mitral Leaflet
C
% Change
300
250
200
150
100
50
0
WT
cKO
pErk1/2
Total Erk1/2
pErk1/2: tErk1/2
pJnk1/2
Total Jnk1/2
pJnk1/2:tJnk1/2

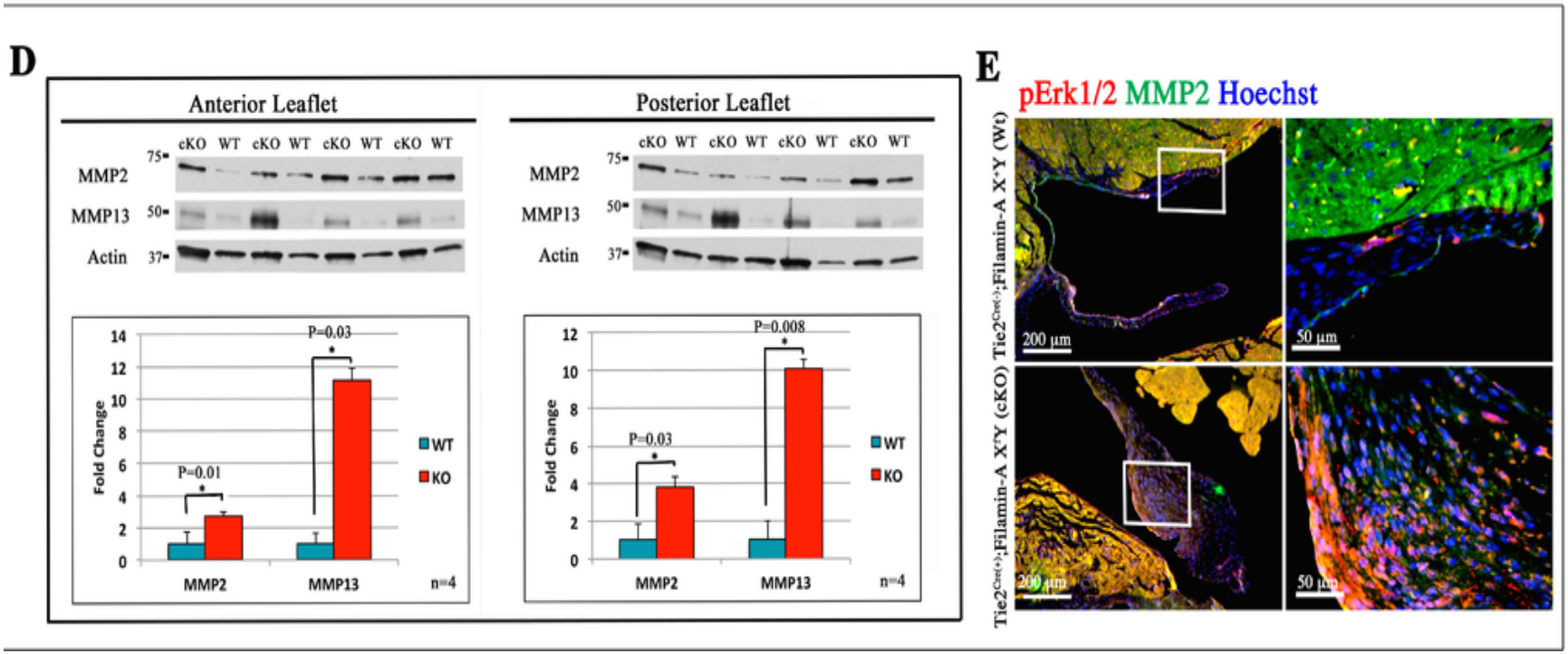
D
Anterior Leaflet
Posterior Leaflet
cKO WT cKO WT cKO WT cKO WT
MMP2
MMP13
Actin
75
50
37
Fold Change
P=0.03
P=0.01
P=0.008
WT
KO
MMP2
MMP13
n=4
E
pErk1/2 MMP2 Hoechst
Tie2Cre(+);Filamin-A X+Y (Wt)
Tie2Cre(+);Filamin-A X+Y (cKO)
200 µm
50 µm

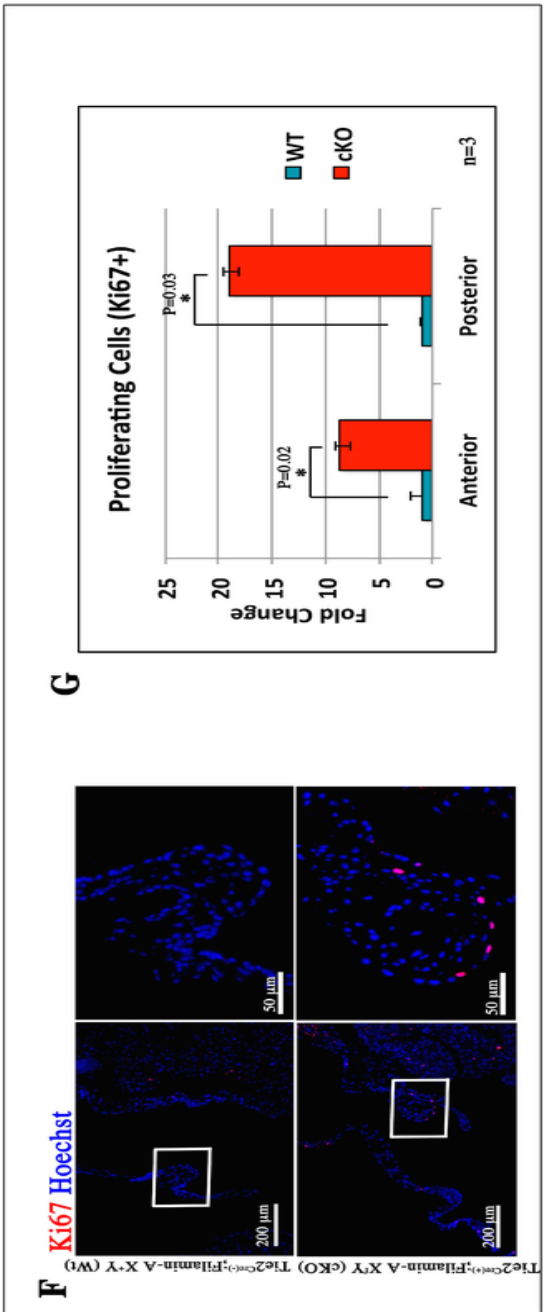

Figure 4.2. Erk1/2 Signaling, MMP expression, and Cell Proliferation are Increased in the Filamin-A cKO (A) IHC for phospho-Erk1/2 (red), MF20 (green), and nuclei (blue) demonstrate increased pErk accumulation in the 2-month-old cKO mitral valve; (B) Isolated anterior mitral leaflets from 2-month-old animals were analyzed individually by Western blot and demonstrate increased pErk1/2 and pJNK in relation to total protein, in the cKO compared to the WT; (C) Quantification of Western blot with * $p < 0.05$, $n > 4$; (D) Isolated anterior and posterior leaflets of cKO animals show increased expression of MMP2 and MMP13 compared to WT animals. All significant values are * $p < 0.05$, $n = 4$; (E) Immunofluorescence shows co-localization of pErk1/2 (red) with MMP2 expression (green); (F) Proliferating cells marked by Ki67 (red) and nuclei (blue) were quantified; (G) in both anterior and posterior leaflets. All significant values are * $p < 0.05$, $n = 3$.

Concurrent with these signaling activities, I observe increases in expression of the matrix metalloproteinases MMP2 and MMP13 in both mitral leaflets of the cKO compared to WT littermates (*Figure 4.2 d*). Additionally, pErk localizes to regions of high MMP2 expression, suggesting excessive pErk1/2 may be an upstream signal promoting MMP expression in the diseased valve (*Figure 4.2 e*), consistent with previous reports (Kuo, Chang et al. 2006). In addition to MMP expression, nuclear translocation of phospho-Erk1/2 has been reported to promote cell proliferation thorough activation of cell cycle regulatory proteins (Torii, Nakayama et al. 2004). Since there is increased Erk1/2 signaling in the cKO mouse, I examined proliferation by immunostaining for ki67, and quantified proliferating cells. As shown in *Figure 4.2 f,g*, proliferation was significantly increased in the cKO compared to the WT in both anterior and posterior leaflets.

To account for molecular changes (pErk, pJNK) and downstream consequences (MMP expression, proliferation) that contribute to disease in two-month-old cKO mice, the possibility that extra-cardiac cells may be promoting these pathogenic changes was examined. Hematopoietic cells have been shown to engraft into the murine adult mitral valve, and exhibit synthetic properties characteristic of fibroblasts as a part of normal valve homeostasis (Visconti, Ebihara et al. 2006, Hajdu, Romeo et al. 2011). I hypothesized that in the filamin-A model of myxomatous mitral valve disease, alterations in hematopoietic cell engraftment would be present in diseased valves and that these cells contribute to disease pathogenesis. Using CD45 as a marker for hematopoietic-derived cells, I observed an increase in the number of CD45-positive cells in the mitral leaflets

of the cKOs compared to WT littermates (*Figure 4.3 a*). CD45-positive cells engrafted primarily in the sub-endocardial region of the WT mouse, which is consistent with other reports in WT mice (Visconti, Ebihara et al. 2006, Hajdu, Romeo et al. 2011). The cKO mice exhibited increased engraftment of hematopoietic-derived cells not only sub-endocardially, but also in the valvular interstitum (Hajdu, Romeo et al. 2011). To determine if these cells could be contributing to the myxomatous phenotype, I examined MMP expression as it related to the CD45-positive cells. Extracellular MMP2 localized to regions surrounding CD45-positive cells, suggesting these cells may be a significant source of MMPs (*Figure 4.3 b*).

Hematopoietic-derived cells that express CD45 are highly plastic and have been shown to develop into fully differentiated macrophages (Reddy, Zhou et al. 2008, Xu and Kisseleva 2015). Since I see an increase in CD45-positive cells, I used the pan-macrophage marker F4/80 to determine if macrophage infiltration is also increased. Histologically, I observe an increase in expression of F4/80 in the cKO compared to the WT. This correlation between increased CD45 and F4/80 expressing cells suggests infiltrating CD45-positive cells may also be macrophages (*Figure 4.3 c*). To determine if there is an association between extra-cardiac cells and pathogenic mechanisms of disease, further characterization by IHC was performed. Macrophages are known to express MMPs at high levels, and have been specifically associated with MMP3 and MMP7 (Martinez and Gordon 2014).

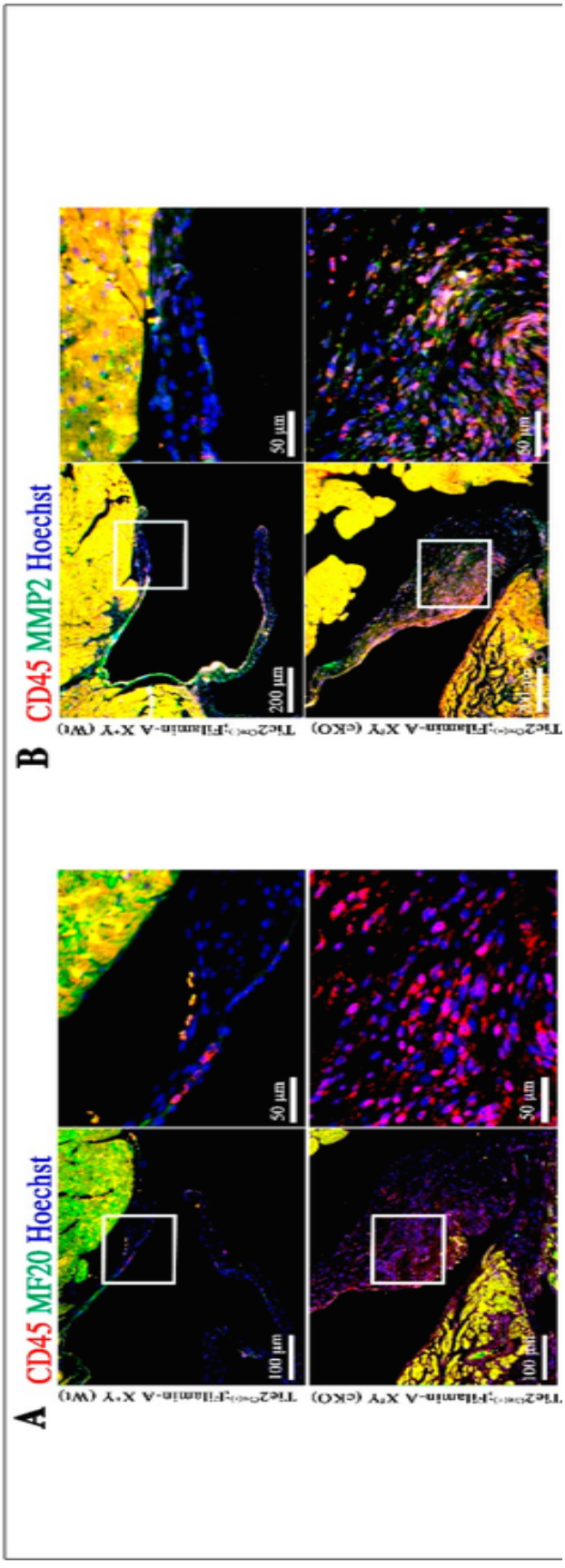
A
CD45 MF20 Hoechst
Tie2Cre(+)-Filamin-A X+Y (WT)
Tie2Cre(+)-Filamin-A X+Y (cKO)
100 μm
50 μm
B
CD45 MMP2 Hoechst
Tie2Cre(+)-Filamin-A X+Y (WT)
Tie2Cre(+)-Filamin-A X+Y (cKO)
200 μm
50 μm

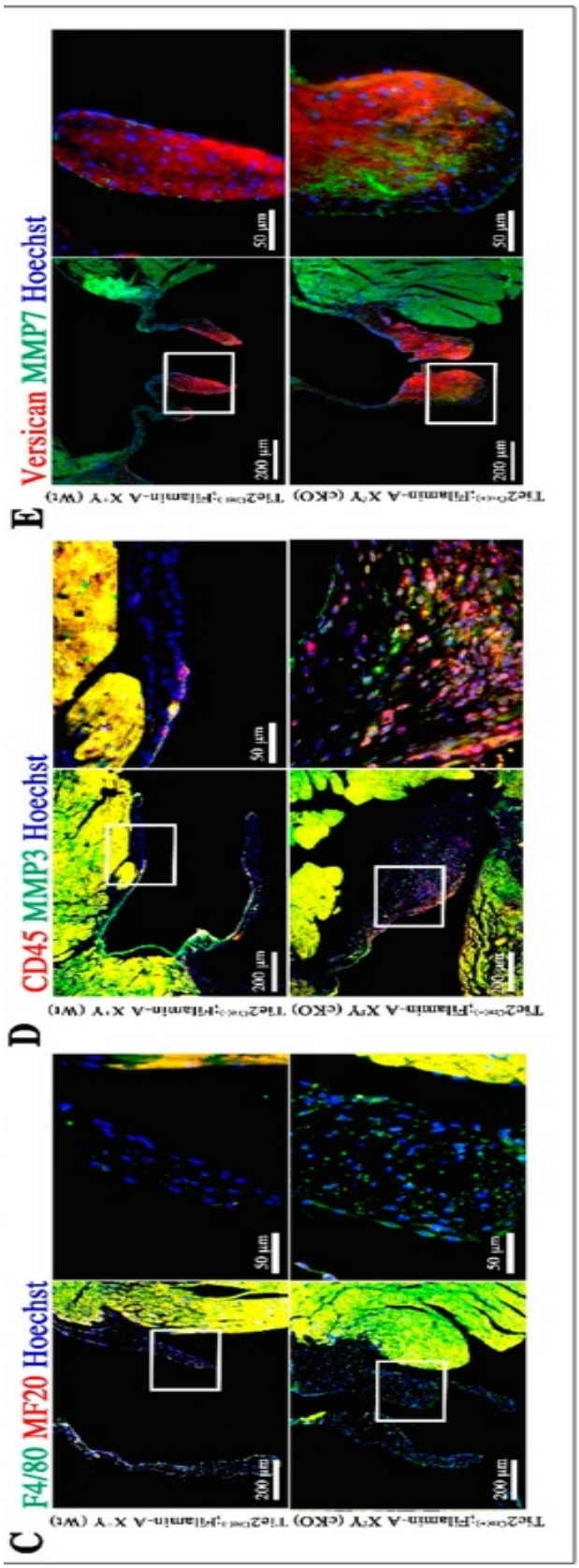
C
F4/80 MF20 Hoechst
Tie2Cre+;Filamin-A X^FY (cKO)
Tie2Cre-;Filamin-A X^FY (WT)
200 μm
50 μm
D
CD45 MMP3 Hoechst
Tie2Cre+;Filamin-A X^FY (cKO)
Tie2Cre-;Filamin-A X^FY (WT)
200 μm
50 μm
E
Versican MMP7 Hoechst
Tie2Cre+;Filamin-A X^FY (cKO)
Tie2Cre-;Filamin-A X^FY (WT)
200 μm
50 μm

Figure 4.3. CD45-positve Cells Increased in the Filamin-A cKO mouse and may Contribute to Myxomatous Degeneration. (A) CD45-positive cells (red) are increased in the cKO compared to WT littermates; (B) CD45 cells (red) localize to MMP2 (green) expression in the posterior leaflet; (C) The macrophage marker F4/80 (green) is increased in the cKO posterior leaflet compared to the WT; (D) CD45-positive cells (red) express MMP3 and are localized to regions of secreted MMP3; (E) MMP7 (green) is increased in the CKO and co-localizes with versican expression (red).

The CKO mice show increased expression of both MMP3 (*Figure 4.3 d*) and MMP7 (*Figure 4.3 e*). Additionally, elevated levels of MMP3 were found in regions enriched with CD45-positive cells in cKO valves (*Figure 4.3 d*). MMP7 distribution was primarily localized to the proteoglycan-enriched region of the leaflets, indicating a potential role in proteoglycan cleavage (*Figure 4.3 e*). This data further suggests CD45-positive cells present in the mitral valve are involved in matrix remodeling and degradation.

To determine if the cellular and molecular changes observed in the cKO mouse are relevant to human disease, pErk, CD45, and MMP expression were examined in myxomatous and normal mitral valve tissue obtained from patients who underwent mitral valve surgery or autopsy respectively. In normal mitral tissue (control), pErk1/2 was present but restricted to the ventricularis layer and localized to the sub-endocardial region (*Figure 4.4 a*). Myxomatous leaflets displayed increased pErk1/2 activity and in contrast to the control, pErk1/2 was active throughout all layers of the leaflet and was nuclear in localization compared to the primarily cytoplasmic expression in the control (*Figure 4.4 a,b*). Additionally, CD45 positive cell infiltration was present in both the control and myxomatous leaflets, and these cells also express pErk1/2. Control leaflets exhibited restricted pErk1/2 activation in the region where CD45-positive cells reside. In contrast, myxomatous leaflets exhibit pErk1/2 activation not only in CD45-positive cells themselves, but also in proximal valve interstitial cells, suggesting the extra-cardiac cells may exhibit potential paracrine effects.

MMP2 expression was also increased in the myxomatous valve compared to the control, and its localization was consistent with the pErk1/2 seen in the myxomatous valve (*Figure 4.4 c*).

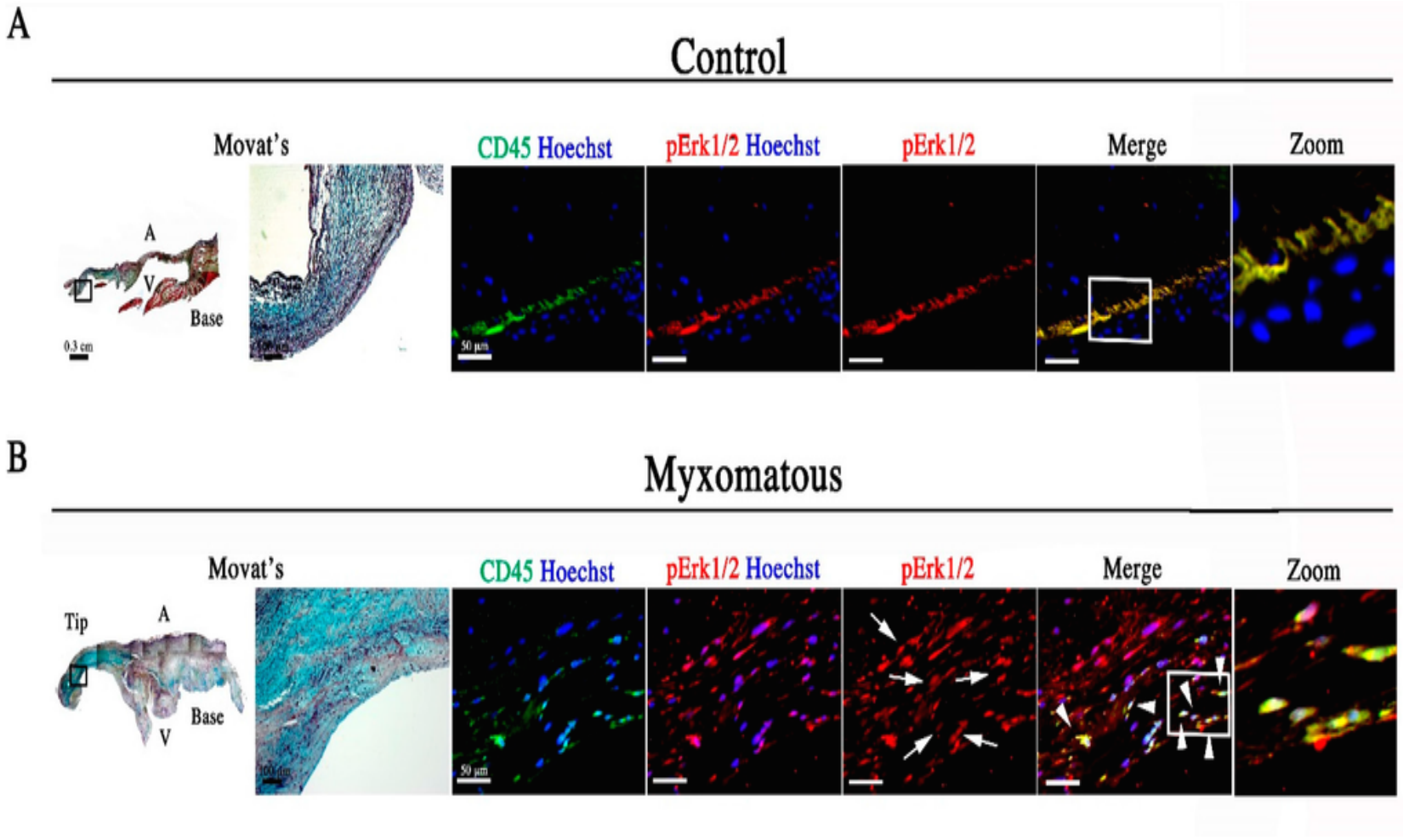
A
Control
Movat's
CD45 Hoechst
pErk1/2 Hoechst
pErk1/2
Merge
Zoom
A
V
Base
0.3 cm
50 µm
B
Myxomatous
Movat's
CD45 Hoechst
pErk1/2 Hoechst
pErk1/2
Merge
Zoom
Tip
A
Base
V
50 µm

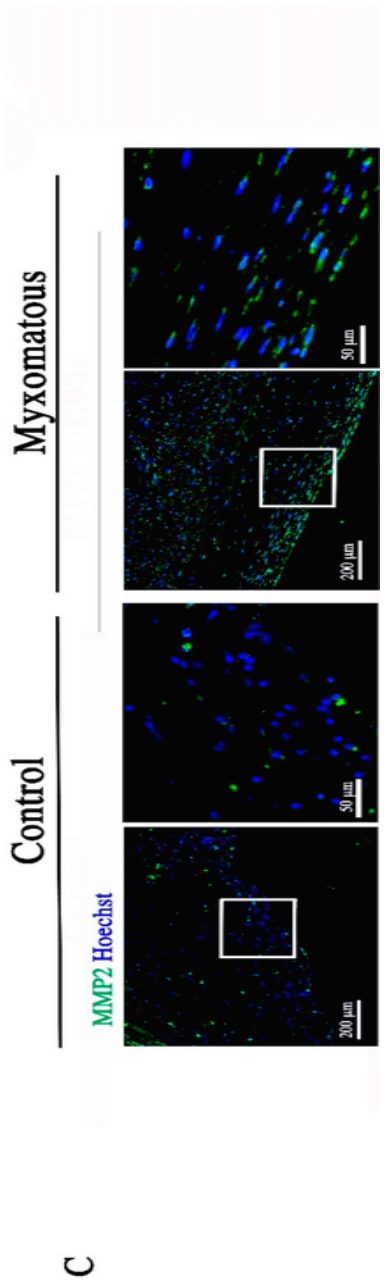

Figure 4.4. Myxomatous Human Mitral Leaflets Show Increased Infiltration of CD45-positive Cells. (A) IHC for CD45 (green) and pErk1/2 (red) and Movat's depicting elastin/nuclei (black), collagen (yellow), proteoglycans (blue), in the posterior leaflet from a normal human mitral valve; (B) Movat's and IHC in a myxomatous mitral leaflet form a human patient shows increased pErk1/2 (red) and CD45 cell (green) infiltration compared to control. CD45-positive cells also express pErk1/2 (arrowheads) and pErk1/2 is nuclear (arrows); (C) IHC for MMP2 (green) shows increased expression in the human myxomatous posterior leaflet. All images depict similar anatomical regions of the posterior leaflet.

Discussion

These results demonstrate that myxomatous changes occur by two months of age in the *Tie2*$^{Cre(+)}$; *filamin-A-XfY* conditional knockout model of myxomatous mitral valve disease. Previous studies have established a link between increased growth factor signaling and syndromic forms of myxomatous mitral valve disease. For instance, patients with Marfan syndrome, a connective tissue disease that can result in myxomatous mitral valves and MVP, have indicated increased Erk1/2 signaling as a potential pathogenic mediator of the disease (Ng, Cheng et al. 2004, Boileau, Guo et al. 2012, Doyle, Doyle et al. 2012, Malev, Zemtsovskii et al. 2012, Dugan, Temme et al. 2015). Marfan syndrome is caused by mutations in *FBN1* (*Fibrillin-1*), which result in excessive TGFβ signaling due to diminished binding of the latent form of the growth factor. This aberrant regulation of TGFβ results in alterations in pErk and pSmad2/3 activity accompanied by increased MMPs and cell proliferation (Ng, Cheng et al. 2004). As filamin-A is known to interact with TGFβ signaling components, and mutations in FLNA cause a myxomatous valve disease that is similar to the mitral valve phenotype in Marfan syndrome, I hypothesized that Erk and Jnk signaling may also be elevated in the mitral leaflets of the filamin-A deficient mouse. Indeed, the results presented here demonstrate increased Erk and Jnk activity in the mitral valve when filamin-A is lost and that this signaling correlates with regions of MMP expression. Although TGFβ can initiate Erk signaling, we cannot directly tie increased Erk activity seen in the cKO mouse to TGFβ since many growth factors are known to be upstream of Erk signaling.

These upstream signals include epidermal growth factor (EGF), fibroblast growth factor (FGF), vascular endothelial growth factor (VEGF) and in some cases reactive oxygen species can activate Erk1/2 (Roskoski 2012, Keshari, Verma et al. 2013). It is yet to be determined whether these additional factors can activate the Erk/Jnk pathway in myxomatous valves. Regardless, upon activation Erk is translocated to the nucleus where it is known to promote expression of multiple genes, including MMPs (Roskoski 2012). The gelatinase MMP2, matrilysn MMP7 and the collagenase MMP13, were both significantly increased in the filamin-A cKO valves. Increased expression of these enzymes are therefore likely candidates for contributing to myxomatous mitral valve degeneration and may contribute to the progressive deterioration of the structure and function of the valve over time. Additionally, previous studies have demonstrated that MMP-9 is also activated in cardiac and heart valve remodeling (Cheng, Huang et al. 2011, Cheng, Shi et al. 2012, Jiang, Cheng et al. 2014). Together, these findings support a putative global stimulation of MMP expression and builds additional support for this class of enzymes in aberrant matrix destruction and remodeling in valve disease.

During normal valve homeostasis, hematopoietic-derived cells that exhibit synthetic processes characteristic of fibroblasts have been shown to engraft into the mitral valve (Hajdu, Romeo et al. 2011). In human myxomatous tissue, increased CD45-positive cells and blood-derived fibrocytes with matrix-altering abilities have also been observed (Barth, Koster et al. 2005, Hajdu, Romeo et al. 2011, Geirsson, Singh et al. 2012). These data demonstrate an

increase in hematopoietic cell engraftment in the context of human and murine myxomatous valve disease, and I show these cells may contribute |to myxomatous degeneration through matrix disruption (*i.e.*, MMP expression). In the mouse, regional localization patterns of hematopoietic cells differed between genotypes, where cells in the WT are localized sub-endocardially, while cells in the cKO integrate into the interstitial region of the leaflets. Correlated with infiltrating CD45-positive cells were significant increases in MMP2 expression in myxomatous leaflets, suggesting these cells may be a source. Additionally, increased MMP expression was observed throughout the leaflets and correlated regionally with CD45-positive cell infiltration, suggesting these cells may be a source of growth factors and promote myxomatous degeneration through paracrine mechanisms that alter the behavior of valvular interstitial cells.

To further characterize the hematopoietic cell population in the myxomatous mitral valve, I examined the possibility that these cells are monocytes/macrophages. In support of the idea that an immune response is initiated in myxomatous mitral valve disease, previous studies have identified serum increases in monocyte chemoattractant protein-1 (MCP-1) and additional increases in mast cells in dogs with myxomatous mitral leaflets (Han, Black et al. 2008, Zois, Moesgaard et al. 2012). In the cKO model, I observe an increase in macrophages in diseased mitral leaflets. This increase correlates with an increase in CD45-positive cells, suggesting these cells may also be macrophages. Expression of MMP3 by hematopoietic-derived cells further suggests these cells are TH-1 polarized M1 macrophages, which are classically associated with a pro-

inflammatory phenotype and MMP expression (Martinez and Gordon 2014). To further support this, I show increased expression of MMP7, another macrophage-expressed metalloproteinase in M1 polarized macrophages. Expression of MMP7 preferentially corresponds to proteoglycan-rich regions of the mitral leaflets and is largely absent in the WT. Since MMP7 can cleave proteoglycans, this may be a mechanism by which proteoglycans are disrupted during disease. Both MMP-3 and MMP-7 degrade a number of ECM components including adhesive glycoproteins such as, laminin, fibronectin, tenascin, and some types of collagen (Stamenkovic 2003). Additionally, macrophages secrete factors that can have paracrine effects on the surrounding tissue. Previous studies have demonstrated this effect in dermal fibroblasts subjected to factors produced by M1 macrophages, where these cells show enhanced degradation properties in response to conditioned media (Ploeger, Hosper et al. 2013). Macrophages up-regulate MMPs in response to contact with different ECM components including collagen, laminin and fibronectin (Khan, Howe et al. 2004). The mitral valve, which is composed of different matrix components, is an environment that would likely trigger up-regulation of MMPs in macrophages.

To determine if the molecular and cellular changes observed in the filamin-A model of myxomatous valvular dystrophy are relevant to nonsyndromic myxomatous disease in humans, I examined human resected mitral leaflets by IHC. Consistent with the murine studies, increases in pErk signaling were observed in human myxomatous posterior leaflets compared to normal tissue. Localization of pErk1/2 was confined to the ventricularis, sub-

endocardial region of control leaflets and was primarily cytoplasmic, in contrast to the myxomatous leaflets, which displayed nuclear pErk1/2 activation throughout the entirety of the leaflet. Cellular populations of hematopoietic cells were increased in the human myxomatous leaflets and displayed co-expression of nuclear pErk1/2. MMP2 expression was also increased in myxomatous leaflets and observed in regions that encompass CD45 positive cells. These results are consistent with previous reports that show increases in MMP2 activity in human mitral leaflets with myxomatous, floppy valves (Togashi, Tamura et al. 2007). Taken together, the mouse and human data support the hypothesis that increased hematopoietic cell infiltration contributes to disease pathogenesis in myxomatous mitral valve disease.

CHAPTER 5: OVERALL DISCUSSION

Myxomatous dystrophy of the cardiac valves is a heterogeneous group of disorders that can manifest in syndromes such as Marfan's Disease, or isolated events affecting only the mitral valve, such as mitral valve prolapse. Mitral valve prolapse is the most common form of myxomatous valve disease and is the leading cause of mitral valve surgery (Levy and Savage 1987). During myxomatous degeneration, the valve tissue becomes enlarged and weakened, resulting in floppy tissue unable to prevent the backflow of blood. Histologically, this is characterized by extracellular matrix disruption (i.e. MMP expression), collagen fragmentation, increased proteoglycan deposition, and hypercelluarity (Pellerin, Brecker et al. 2002). Despite being a common disorder, little is known about the etiology of the non-sydromic form of this disease, and this is likely due to a lack of genetic information identifying the origins of the disease. The work presented here focuses on two genetic mouse models: the filamin-A cKO mouse (*filamin-A $X^{f}Y$/Tie2-Cre*), which targets the genetic removal of filamin-A in the endothelium and cells derived from the endothelium, and the Dchs1 haploinsufficient mouse (*Dchs1$^{(+/-)}$*), both of which exhibit myxomatous mitral valves. These models were generated based on genetic data implicating *FLNA* and *DCHS1* genes in myxomatous valvular dystrophy and mitral valve prolapse, respectively (Freed, Acierno et al. 2003, Kyndt, Gueffet et al. 2007). The study of two different genetic mouse models of myxomatous valve disease in addition to human tissue from MVP patients provides a unique opportunity to identify

common mechanisms of disease between these models in order to selectively identify therapeutic targets that are relevant to all myxomatous patients, including those whose genetic origin of the disease is unknown.

This work presents the first genetic identification of mutations that cause non-sydromic MVP in human patients and thus provides an avenue to study the disease in an animal model system. Mutations in the gene *DCHS1* were identified by linkage analysis and subsequent deep sequencing in a large family with inherited MVP. The mutation was experimentally determined to be loss-of-function, resulting in protein instability. The *Dchs1*$^{(+/-)}$ mouse was characterized as a model of nonsyndromic MVP, and phenocopies the MVP patients functionally (prolapse by echo), structurally (MRI, 3D reconstructions), and histologically (myxomatous characteristics). The origins of the disease in the *Dchs1*$^{(+/-)}$ mouse were traced back to development, where disruptions in valve shape lead to a myxomatous mitral valve in the adult. This process, regulated by the cadherin Dchs1, is related to defects in cell adhesion, migration, and orientation, which have been recapitulated in human VICs harboring the *DCHS1* p.R2330C mutation. Mutations in the gene *FLNA* (filamin-A) have been attributed to myxomatous valvular dystrophy, a pan valvulopathy affecting all cardiac valves, and associated MVP. Similar to the *Dchs1*$^{(+/-)}$ model, the filamin-A mouse model of myxomatous valvular dystrophy (*filamin-A X*^{f}*Y/Tie2-Cre*) displays developmental defects which precede myxomatous disease in the adult. Filamin-A functions to regulate leaflet size and shape during development through a novel mechanism involving the cooperation between serotonin,

filamin-A, and transglutaminase (TG2). This mechanism is required to direct interstitial cell driven matrix remodeling and compaction during the post-EndoMT phase of valve development. Both the *Dchs1*$^{(+/-)}$ and *filamin-A XfY/Tie2-Cre* models of myxomatous valve disease demonstrate a previously unrecognized developmental origin for myxomatous mitral valve disease that is not clinically detected until adulthood. Valve defects are initially observed in both models during the post-EndoMT stage of valve development, placing an emphasis on leaflet remodeling driven by interstitial cells. During this phase of development, mesenchymal cells differentiate into valvular interstitial cells (VIC), make cell-to-cell contacts, become aligned, and remodel the surrounding ECM in order to form the thin, elongated leaflets of the mature mitral valve (de Vlaming, Sauls et al. 2012). Importantly, defects in both models of disease are observed prior to myxomatous degeneration suggesting processes that control valve shape and maturation are critical for maintaining the valve in a non-degenerative state. These studies demonstrate matrix compaction, cell migration, alignment and polarity are critical to direct leaflet size and shape during the post-EndoMT stage of valve development. To better understand the link between Dchs1 and Filamin-A in valve development and disease, crosses between the two models to generate mice deficient in both genes would provide a future study that would link the two models.

As a secondary consequence to altered leaflet anatomy during development, *in vivo* and *in vitro* data discussed in previous chapters, demonstrate increased pErk1/2 signaling present in both the *Dchs1*$^{(+/-)}$ and

filamin-A XfY/Tie2-Cre adult mice, human patient cells harboring the *DCHS1* p.R2330C mutation, and mitral valve tissue from human patients with an unknown genetic origin of MVP. Similarly, increased Erk activation has also been reported in canine myxomatous valves (Disatian and Orton 2009). These data suggest increased pErk1/2 is a potential pathogenic signal that is relevant to the development of myxomatous degeneration in patients with multiple genetic backgrounds. Furthermore, analysis of the *Dchs1*$^{(+/-)}$ mice indicate this signaling precedes myxomatous degeneration at neonatal day 0, suggesting Erk activity drives myxomatous degeneration and can be therapeutically targeted before myxomatous changes occur and thus prevent MVP. Determining if Erk activation is pathogenic to the development of mitral valve disease requires *in vivo* experiments to determine if abrogation of Erk activation is sufficient to prevent myxomatous changes and MVP. Administration of drugs such as RDEA119, a potent allosteric inhibitor of MEK currently undergoing clinical trials for cancer patients, and/or drugs which target Erk signaling through an indirect mechanism such as angiotensin receptor blockers (ARBs), would be ideal candidates for these experiments. Administration of these drugs to genetically susceptible juvenile mice that do not exhibit a myxomatous phenotype and have not yet developed MVP, would determine the pathogenesis of Erk signaling in the progression of the disease.

Why loss-of-function mutations in filamin-A or Dchs1result in increased Erk activation is unknown. There are a myriad of signals which can initiate the phosphorylation of Erk1/2. In particular, transforming growth factor (TGF)-β is

of interest, since genetic mutations that cause syndromic forms of MVP, are directly related to increased TGFβ signaling (Brown, DeMots et al. 1975, Boileau, Guo et al. 2012, Doyle, Doyle et al. 2012, Dugan, Temme et al. 2015). Well-established TGFβ responsive genes, such as collagen and elastin, are present in significant excess in diseased valve tissue and their production is shown to be dependent on the presence of TGFβ (Geirsson, Singh et al. 2012). Additionally, TGFβ levels are increased in human MVP patient cell cultures and in the circulation of MVP patients where levels correlate with posterior leaflet thickness (Brown, DeMots et al. 1975, Loeys, Chen et al. 2005, Doyle, Doyle et al. 2012, Malev, Zemtsovskii et al. 2012, Hagler, Hadley et al. 2013). These studies support the possibility that TGFβ may be misregulated in nonsyndromic myxomatous mitral valve disease and as a result, signaling through Erk1/2 to promote myxomatous changes. In the filamin-A cKO mouse, serotonin may provide the link between loss of filamin-A and increased Erk signaling. Other studies have shown serotonin can increase TGFβ1 signaling in mesangial cells and in aortic valve cells via Erk1/2 signal transduction to induce proliferation and matrix deposition, including sulfated glycan and hyaluronic acid (Grewal, Mukhin et al. 1999, Jian, Xu et al. 2002). Studies done in canine models of myxomatous valve disease have found a downregulation of the serotonin transporter (SERT), which is responsible for the internalization of 5HT, and increased levels of the serotonin receptor, further suggesting these components play a role in valve disease (Oyama and Levy 2010). Serotonin has also been

directly linked to myxomatous valve disease in those patients who received the ergot deriviative drug, FenPhen a SERT inhibitor and serotonin receptor agonist, since these patients present with myxomatous valve disease (Connolly, Crary et al. 1997, Connolly, Bakay et al. 2009). Thus, these studies present a potential link between 5HT, TGFβ, and the pathogenesis of myxomatous degeneration. Since the filamin-A cKO mouse is unable to bind serotonin to filamin-A *in vivo*, it is possible that an excess of serotonin is present due to the inability of filamin-A to sequester it. This is observed in patients with the filamin-A mutations, who exhibit increased circulating serotonin levels. Thus it is possible excess serotonin may be responsible for TGFβ activation and subsequent signaling through Erk1/2 in the filamin-A model of disease.

Another consequence secondary to developmental defects identified in the filamin-A cKO mouse and human MVP patient samples, is the increased infiltration of hematopoietic-derived cells (CD45+ cells). In normal mice, these cells have been shown to exhibit phenotypic characteristics of fibroblasts that express collagen I, indicating these cells have the ability to incorporate into valve tissue and alter the ECM (Hajdu, Romeo et al. 2011). In the filamin-A cKO, these cells express pErk1/2 in the mitral valve and correlate with increased MMP expression and increased cell proliferation, suggesting these cells may play a role in facilitating myxomatous degeneration. Furthermore, the increased presence of macrophages in diseased valves suggests the infiltrating hematopoietic-derived cells may also be immune cells. Since these infiltrating

hematopoietic-derived cells are present in the filamin-A cKO mouse and in mitral valve tissue from patients with an unknown genetic origin of MVP, the influx of hematopoietic cells may be a widespread event relevant to all myxomatous patients. Furthermore, studies determining the direct effect hematopoietic cells have on the surrounding ECM and influence they have on the cells around them would determine if these cells are indeed pathogenic to myxomatous mitral valve disease.

Overall, the data in this dissertation identify a genetic origin for nonsyndromic MVP, define disruptions in cellular processes which lead to developmental defects in how the valve is built (compaction, migration, adhesion, alignment) and present secondary consequences (pErk1/2 signaling/infiltrating CD45-positive cells and macrophages) which lead to myxomatous degeneration and MVP. An overall view of these findings is presented in *Figure 5.1*, whereby these studies begin at the genomic level, progress into the cellular and tissue levels, and finally, identify the functional consequences of the developmental defects that ultimately lead to disease. From these studies, pharmacological targeting of the Erk1/2 signaling pathway and/or immune cell infiltration provides a potential therapeutic aimed at preventing the progression of myxomatous mitral valve disease and associated mitral valve prolapse.

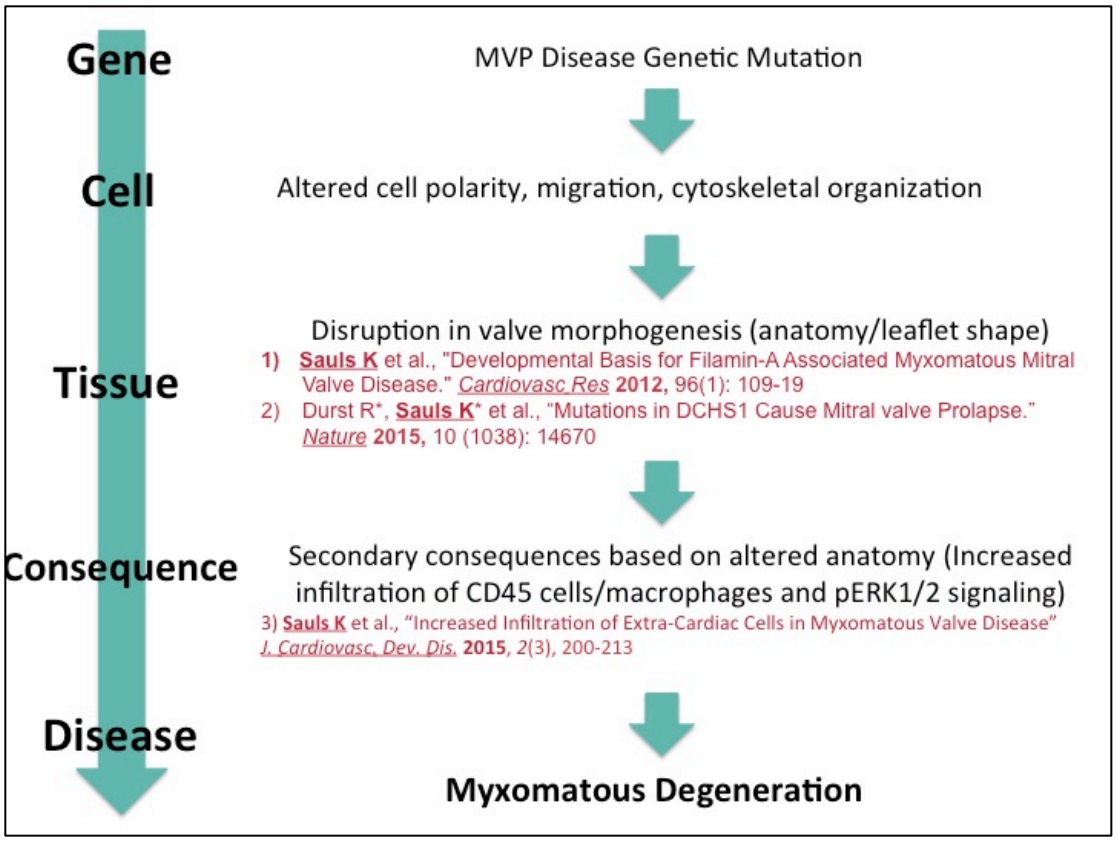

Figure 5.1 Flow Chart Summarizing Overall Findings. These studies began with the identification of a disease causing genetic mutation, identified defects on the cellular level, characterized changes in valve anatomy which begin during development, and identified secondary consequences that are observed postnatally and in adult life, ultimately leading to myxomatous degeneration. The blue arrow in the far left depicts the hierarchy of components studied. The red text indicates publications linked to the overall findings found in each component. Together these events in a temporal manner lead to myxomatous valve disease and MVP.

CHAPTER 6: MATERIALS AND METHODS

CHAPTER 1: INTRODUCTION:

Histological Analysis of Human Tissue

Human tissues were obtained from surgical specimens as part of a Leducq transatlantic network. Control valve biopsies were obtained from patients who perished as a result of either subarachnoid hemorrhage or intracranial bleeds. Myxomatous valves were surgical cases obtained from patients who fit diagnostic criteria of myxomatous degeneration and mitral valve prolapse. This was defined by >2 mm atrial leaflet displacement in a parasternal long-axis view as well as >5 mm valve thickness.. All samples were harvested by offsite partners and were fixed, embedded and sectioned in their various laboratories. Sections were sent to our group at the Medical University of South Carolina (MUSC) for histological assessment. Consent and Institutional Review Board (IRB) approval for these studies is in place at partnering institutions. Slides with tissue sections were deparafinized in xylene and rehydrated through a series of ethanols. Slides were then incubated in Bouin's solution (Electron Microscopy Sciences) for 1 hour at 50°C and then rinsed in distilled water for 5 mins to remove picric acid deposits. A modified Movat's Penachrome stain was performed.

CHAPTER 2: DEVELOPMENTAL BASIS FOR FILAMIN-A-ASSOCIATED MYXOMATOUS MITRAL VALVE DISEASE

Gene Targeted Mice

All mouse experiments were performed under protocols previously approved by the Institutional Animal Care and Use Committee (IACUC) at the Medical University of South Carolina. Female mice homozygous for a conditional "floxed" allele of *FLNA* (*Filamin-Af/f*) were bred with male transgenic mice expressing Cre under control of the *Tie2* promoter (*Tie2Cre(+)*), which will target valve endocardium and endocardial-derived mesenchyme, resulting in a (*Tie2Cre(+); Filamin-Af/y*) conditional knockout (cKO) mouse. As Filamin-A is X-linked in both mouse and humans, these analyses were primarily focused on male mice, although some female mice have been characterized for phenotypic differences. No difference in phenotype is observed between male and female animals.

Western Analyses

HH40 chick mitral valve fibroblasts were grown in culture following isolation and harvested at passage numbers 1-3. Cells were lysed in 1X RIPA and equal amounts of protein were subjected to Western Analyses using antibodies described above (1:1000 dilution for each). Equal amounts of growth medium were loaded in each of their respective lanes (15 μL each).

Volumetric Quantification by Reconstruction

Three-dimensional reconstructions were performed using Amira 5.3.3 software (Visage Imaging, Andover, MA). 80-100 5 mm thick sections were used to generate each E17.5 or P1 reconstruction. Hematoxylin and Eosin stained slides were used in the analyses. Volumetric measurements were generated from >3 hearts from each genotype. Final data are presented as average volumes obtained from Amira 3D reconstructions of the cKO valves compared to WT.

TG2/Serotonylation Assays

Mitral valve fibroblasts were obtained from fetal chick (HH40) and solubilized using standard 1X RIPA buffer. Samples were incubated in the presence or absence of TG2 antagonist, Cystamine (10mM) in a calcium rich buffer (250mM Tris–Cl, pH 7.4; 33 mM NaCl, 250 mM CaCl2, 1X protease inhibitor-Sigma), for 30 min at 37°C. Co-IP reactions were performed using a serotonin antibody (Pierce, 1:100). Immunocomplexes were recovered using protein-A/G agarose beads (Roche), spun, and washed 3 times in 1X TBST. Proteins were solubilized in 2X SDS-PAGE buffer and subjected to Western analyses and probed for Filamin-A. Confirmatory Co-IP's were performed using lysate from cultured chick fetal mitral valve fibroblasts. Cultures were obtained by trypsinizing 120 fetal chick MV's and plated in 1X M199, 1% chick serum, 1% ITS, pen/strep. Cells were passaged a maximum of 3 times after which they were used for TG2/Serotonylation assays in which we incorporate biotinylated serotonin (100 mM) into the reaction cocktail. For synthesis of the biotinylated serotonin,

serotonin hydrochloride (Tocris, Inc.) and EZ-Link Sulfo-NHS- LC-LC-Biotin (Thermo Scientific) were used. Equimolar amounts of serotonin and Sulfo-NHS-LC-LC-Biotin were reacted at room temperature using pyridine as the solvent system. The reaction mixture was frozen, lyophilized, and purified by reverse-phase HPLC; product was validated via mass spectroscopy and stored at -20°C before use. Filamin-A antibody (Epitomics, 1:100) was used to IP immunocomplexes followed by Western blotting and detection using a streptavidin-HRP antibody. All co-IP experiments were performed a minimum of 3 times, each providing consistent results.

Matrix Compaction Assays

Collagen compaction Assay: Assays were performed with cultured fetal chick mitral valve fibroblasts (5x10/ml) at passage 3 or less. Rat tail collagen (2mg/ml-BD biosciences) was neutralized with 10N NaOH and cells were added. Collagen/Cell mixture was quickly added to 4-well nunc cultured dishes and placed in incubator for polymerization. Polymerized gels were released from the wells and allowed to be free-floating in low serum containing chick media (1X M199, 1%ITS, 0.1% Chick Serum) for 5 days. Each day area measurements were scored and % compaction was calculated based on (Ao/A). The following day chemicals were added (serotonin, clomipramine, cystamine, fluoxetine—Tocris, Inc.) at appropriate doses as described in results. Data represent a minimum of 4 individual experiments for each pharmacological intervention and were repeated a minimum of 3 times. Fibrin Compaction Assays: Primary E17.5

anterior mitral leaflet cultures were established by microdissecting out the anterior leaflets on filamin-A cKO and WT valves and placing the entire valve in culture (48-well for each leaflet). Cells were grown in culture for ~2 weeks to generate enough cells to perform compaction assays. Media used for growth: 1X MEM, 10% FBS, 1X Pen/Strep, 1X L-glutamine, 1X Na-pyruvate, 1X Vitamin-mix (Invitrogen), 1X non-essential amino acids, 5mM HEPES, 10 mM Glucose, 1mM ascorbate. 50,000 cells were resuspended in fibrinogen (5mg/ml—Sigma), 1 unit/mL thrombin and added to each well of a BSA treated 96-well dish. Gels contracted over 24 hour period and scored for area changes as described above. Data represent a minimum of 5 experiments from 4 cKO and 5 WT littermate cells and were repeated in quadruplicate.

Statistics

Statistical significance was determined using a student's *t*-test (two-tailed, type 2), with significance ($p < 0.05$). Statistical data are presented as standard deviations from the mean.

Study participants

Family 1 was originally recruited through the Echocardiography Laboratory at Massachusetts General Hospital as part of a phenotype-driven genetic study of MVP. MVP was diagnosed by specific criteria (>2 mm atrial leaflet displacement in a parasternal long-axis view). The study was approved by the Institutional Review Board of Partners Healthcare, Boston, Massachusetts, and all participants provided written informed consent. Complete details of the linkage analysis on this large, multigenerational family have been previously published (Freed, Acierno et al. 2003). In brief, the family contains 41 individuals in five generations. Echocardiograms and DNA were obtained on 28 subjects, of whom 12 were diagnosed with MVP, three were classified as having nondiagnostic minimal leaflet displacement, and 13 were unaffected. Three patients had non-diagnostic valve leaflet displacement and were considered unknown for the original linkage analysis. The proband had prominent MVP with thickened leaflets, severe mitral regurgitation, and heart failure ultimately requiring surgical valve repair. Other affected members also showed diffuse leaflet thickening, prolapse, and mitral regurgitation of varying severity; one required surgical repair. No extracardiac manifestations of connective-tissue abnormalities or Marfan syndrome were present in any family members. Following a complete genome scan, parametric and non-parametric analyses confirmed linkage of this family to a 4.3 cM region of chromosome 11p15.4.

Consistent with the model of sex- and age-dependent penetrance, several of the unaffected members who carried the MVP allele were less than 15 years old at the time of evaluation. Importantly, an analysis using only affected individuals confirmed the linkage result.

DNA sequencing and variant calling in family 1

In order to identify the mutation, four affected individuals who shared the disease haplotype were chosen for sequencing. To reduce the likelihood of random haplotype sharing, we selected individuals with four distinct haplotypes on the non-MVP allele. A 2.1 Mb region of human chromosome 11 (5094774–7248926; NCBI36 coordinates) was targeted and screened for repetitive regions using the SureSelect system (Agilent). DNA extraction was performed using the AutoGenFlex STAR automated system (Autogen) and FlexiGen DNA purification reagents (Qiagen) according to the manufacturers' instructions. Bait oligonucleotides were designed to the non-repetitive regions of the targeted linkage peak, resulting in 1.03 Mb of target sequence using the SureSelect in-solution long RNA baits (Agilent). Captured DNA was amplified and quantified using the Agilent High Sensitivity DNA Kit for the Agilent 2100 Bioanalyzer, and sequenced using Illumina sequencing chemistry (paired-end, 100 cycles) at the Venter Institute supported by the NHLBI Resequencing and Genotyping Program. One hundred bases were sequenced from each end of the captured DNA fragments. Image analysis and base calling were performed using Illumina's GA Pipeline version 1.6.0. Sequence reads were mapped to the human genome

(ncbi36) and variants identified using clc-ngs-cell-2.0.5-linux_64 (clc_ref_assemble_long -q -p fb ss 180 360 –I –r, and find_variations -c 8 -v -f 0.2). Variants were classified using VariantClassifier. 4,891 SNVs were identified in the four subjects, 1,951 were shared by all four subjects. We classified all rare SNVs or those of unknown frequency based on conservation data, population genetic data, and predictive functional impact from public resources. We performed analyses of conservation of the variant locus using PhyloP, PhastCONS and GERP, and assessed the population frequency initially using the Exome Variant Server, NHLBI GO Exome Sequencing Project (ESP), Seattle, Washington (http://evs.gs.washington.edu/EVS/) as an initial filter and the 1000 Genomes Project as a secondary filter, cognizant of the limitations of the low-depth coverage of the 1000 Genomes Project to characterize rare mutations, which were available during the initial analyses.

Sporadic MVP patient cohort

As part of an international consortium on mitral valve disease, we initiated collection of MVP patients with the eventual goal of performing GWAS studies in MVP. To date, 1,896 patients have been collected in the United States, France, and Spain. MVP was defined as systolic displacement of one or both mitral leaflets ≥ 2mm beyond the annulus in parasternal or apical long-axis views, asymmetric posterior leaflet prolapse was also included in any view, including apical 4-chamber, when confirmed by side-to-side long-axis scanning.

Patients were required to have no evidence by history, physical examination, or imaging for Marfan syndrome or other connective tissue disorders associated with MVP.

Exome sequencing, genotyping, and variant evaluation

As part of an MVP exome sequencing pilot project conducted by the Leducq Mitral Network, exome data were generated on twenty-one severe, early onset MVP patients and made available to identify variants in *DCHS1.* Fifteen patients were collected in Paris and had severe bileaflet mitral valve prolapse with myxomatous leaflets and an average age of onset of 15 years. Six patients were collected in Nantes, France, and had similar clinical characteristics with an average age at onset of 42. Exome capture was carried out using the SureSelect Human All Exon System using the manufacturer's protocol version 1.0 that is compatible with Illumina paired-end sequencing. Exome-enriched genomes were multiplexed by flow cell for 101-bp paired-end read sequencing according to the protocol for the Hiseq 2000 sequencer (version 1.7.0; Illumina) to allow a minimum coverage of 30×. Reads were aligned to the human reference genome (UCSC NCBI36/hg19) using the Burrows-Wheeler Aligner (version 0.5.9). Evaluation of the *DCHS1* gene yielded 4 novel coding sequence variants that confirmed following repeat Sanger sequencing: 6646587 G/A (p.R2330C) 6646709 G/A (p.A2289V), 6648584 C/T (p.A1896T), 6648820 A/G (p.V1817A), base pair positions are NCBI36 coordinates. These four variants, in addition to the variants identified in family 1, were genotyped using Sequenom technology

in the sporadic cohort. The major steps included primer and multiplex assay design using Sequenom's MassARRAY Designer software, DNA amplification by PCR, post-PCR nucleotide deactivation using shrimp alkaline phosphatase (SAP) to remove phosphate groups from unincorporated dNTPs, single-base extension reaction for allele differentiation, salt removal using ion-exchange resin, and mass correlated genotype calling using SpectroCHIP array and MALDI-TOF mass spectrometry. Quality control to determine sample and genotyping quality and to potentially remove poor SNPs and/or samples was performed in PLINK, a whole genome association analysis toolset. We predicted the impact on gene function using PolyPhen2, Mutation Taster and LRT.

Identification of family 2 and 3

In order to identify other mutations in *DCHS1*, we first evaluated *DCHS1* in the exome sequence data described above, reasoning that early onset forms may be more likely to have strong genetic aetiologies. Rare variants causing amino acid substitutions in *DCHS1* were identified in four individuals (p.V1817A, p.A1896T, p.A2289V, and p.R2330C) and genotyped in a cohort of 1,864 sporadic MVP patients that included the 21 individuals with exome data; two of these variants, both localized to exon 19, were observed in the MVP cohort (p.A2289V in two cases and p.R2330C in three cases). The proband in family 2 carried the p.R2330C variant and underwent surgery for MVP in Paris. We were able to collect DNA and echocardiograms on first-degree relatives at that time. Additional clinical characteristics of the proband in family 2 included congestive

heart failure (NYHA II/III) with left ventricular dilatation (70/50 mm end-diastolic/end-systolic dimensions), impaired left ventricular systolic function (ejection fraction 53%, low for this volume overload), recurrent symptomatic atrial fibrillation, non-sustained ventricular tachycardia, and exercise-induced pulmonary hypertension (70 mm Hg systolic). The proband in family 3 was originally collected in Amiens, France. All echocardiograms were read in both Boston and Paris and readers were blind to genotype data.

D. rerio studies

Husbandry, knockdown and expression analyses were performed in the wild-type *D. rerio* (zebrafish) strain Tubingen AB. Morpholinos were injected at a dose of 1.5 ng (after dose optimization) into single-cell embryos to achieve gene knockdown, and phenotypes were examined at 48 and 72 h post-fertilization in three separate experiments of 50–75 embryos and compared to controls using Fisher's exact test. Morpholino GeneTools LLC (Philomath, OR) sequences were as follows: *apbb1* A A C A A A G C G T A C C A C T C A G A T T A G C , *dchs1a* T A A A G A A A T G A C A G T C C T A C C T C C A , and *dchs1b* C A T A A C T G T T A A G A G T T C C G C T A C A . Knockdown was confirmed by quantitative polymerase chain reaction. qPCR was performed as previously described[33]. In brief, 20–30 morpholino-injected embryos were collected at 72 hpf, and snap frozen in liquid nitrogen. TRIzol (Sigma) was added, RNA was purified according to the manufacturer's instructions, and cDNA was prepared using a Superscript III Kit (Invitrogen). Primer sets were as follows: *apbb1*, 5′ - G T G G A G G C G A G A A C

A G A G , 5 ′ - C C A G C A G G A A G A T C C G T G T C ; *dchs1a*, 5 ′ - G T T T C A T G G A G G T T A C A G C , 5 ′ - C T T A A T C C A C C C C C A T C C A C ; *dchs1b*, 5 ′ - G T T T C C T T G A G G T A A A G G C G G , 5 ′ - G G C C A C C C C C A T C G G A C G . qPCR was performed using SYBR Green (Applied Biosystems) in triplicate on an Applied Biosystems 7500 Fast Real-Time PCR instrument and normalized against β-actin. All zebrafish experiments were performed under protocols approved by the Institutional Animal Care and Use Committee at Massachusetts General Hospital.

D. rerio in situ hybridizations

In situ hybridizations were performed as previously described using a partial clone of *dchs1b* (Open Biosystems, Clone ID 7136458) amplified with primers containing a T7 RNA polymerase site engineered onto the 3′ end of the reverse primer (Forward 5 ′ - G G C A G T T C A A G T G G T G G T . Reverse: T A A T A C G A C T C A C T A T A G G G T T A A A T C C T C A T C T C A G C C T C A , T7 site underlined.) The *dchs1b* probe was produced using a T7 RNA polymerase (Ambion) and digoxigenin-labelled dNTPs (Roche). Other riboprobes used in the study have been previously described.

Generation of *DCHS1* expression constructs

Human *DCHS1* and the mutant containing the c.590C>T and c.7538G>A sequence changes were synthesized by Integrated DNA Technologies. A unique EcoRI site, a T7 polymerase site, and a Kozak sequence were added to the 5′ end of each

gene, while a V5 tag and unique Xho1 site were added to the 3′ end. Each gene was then subcloned into the expression vector pcDNA3.1. Additional expression constructs were generated that contained only the c.590C>T (p.P197L) mutation or only the c.7538G>A (p.R2513H) mutation. These constructs were made using the QuikChange II XL Site-Directed Mutagenesis Kit (Agilent Technologies) as per the manufacturer's instructions. The P197L construct was generated from the double mutant construct by changing the R2513H (c.7538G>A) mutation back into the wild type sequence using the following primers: 5′-gctgatggaagccgcagccatgccgct, 3′-agcggcatggctgcggcttccatcagc. (The underlined bold base indicates the base pair changed.) The R2513H construct was generated by introducing the (c.7538G>A) mutation into the wild type *DCHS1* construct using the following primers: 5′-gctgatggaagccacagccatgccgct, 3′-agcggcatggctgtggcttccatcagc.

Preparation and injection of *DCHS1* mRNA

mRNA was prepared from the wild-type *DCHS1* and *DCHS1* mutant expression vectors using a T7 mMessage mMachine Kit (Ambion) according to the manufacturer's instructions. Injection mixtures containing 0.75 ng *dchs1b* MO alone, or 0.75 ng *dchs1b* MO plus 7 fg μl^{-1} of human *DCHS1* mRNA (either wild type or mutant) were injected into one-cell embryos, and fish were scored for atrioventricular canal defects (failure to loop, and presence of regurgitation) 72 h later. Data were collected from three independent experiments performed with 20–30 embryos each and comparisons made using Fisher's Exact test.

Isolation of *DCHS1* p.R2330C MVP and control patient mitral valve tissue and valvular interstitial cells

Resected posterior mitral valve tissue was used for culture and histology. For culture, valve pieces were minced in phosphate buffered saline (PBS) and washed in DMEM with antibiotics (penicillin/streptomycin (P/S) and fungizone) and incubated in DMEM with collagenase type II (Worthington) (1 mg ml^{-1}) at 37 °C for 12 h. Following mechanical dissociation in DMEM, the cell suspension was filtered through a 40-μm cell strainer and cells were cultured in DMEM with 15% fetal calf serum and antibiotics (P/S, fungizone). Although rare valve endothelial cells were present at P0, only cells with a fibroblastic phenotype (VICs) remained following P1-2. For all experiments, these valvular interstitial cells were used before passage 5. For histology: valves were fixed in formalin, embedded in paraffin and sectioned at 5 μm. Movat's Pentachrome histological stain was performed using standard procedures.

Cell culture studies

Wild type, p.P197L, p.R2513H and p.P197L/R2513H *DCHS1* constructs were either synthesized by Integrated DNA Technologies or generated by site-directed mutagenesis (as described above), with an amino-terminal V5 epitope tag. Except where indicated, "mutant *DCHS1"* indicates the double mutant p.P197L/p.R2513H haplotype in family 1. These constructs were expressed in mycoplasma-free HEK293 cells (ATCC, not independently authenticated) using cationic lipid-mediated transient transfection (Lipofectamine LTX, Invitrogen).

Protein expression of transfected HEK cells was measured by quantifying western blots using an antibody to the V5 epitope tag (Invitrogen). Patient cells: for patient cells, control and p.R2330C valvular interstitial fibroblasts from posterior leaflets were plated at 2.5×10^4 cells in a 24-well dish. 24 h later, protein stability experiments were performed. Protein stability experiments involved addition of cycloheximide 24 h after transfection (WT and p.R2513H transfectants) or plating (control or p.R2330C patient cells). For the cycloheximide experiments, media containing 100 ng ml^{-1} of cycloheximide was added at 24 h post-transfection and each well was harvested as above at the indicated time points. Western blots were probed with either a mouse anti-V5 primary antibody (1:4,000 dilution Invitrogen) or a rabbit anti-*Dchs1* antibody(1:1,500 dilution), and an HRP-linked secondary at the same dilution (Thermo Scientific). Blots were also probed with a mouse anti-tubulin primary (Millipore) at a 1:4,000 dilution, and the same secondary antibody as above. Blots were treated with Pierce ECL Substrate and visualized on film. For quantitation, blot pixel intensity was measured by ImageJ (NIH), and normalized to tubulin. Each sample was run in triplicate, and a regression curve was fit and half-lives calculated using SigmaPlot 12.

Mouse studies

Dchs1 mice and genotyping were previously described[22]. All mice were blinded for genotype. Following phenotypic analyses, the genotypes of each sample were matched with the experimentally determined data sets. Histology, mitral valve

analyses (echocardiography, MRI, and morphometric determination), and expression studies were performed on embryonic and adult (9-month male) wild-type (*Dchs1*$^{+/+}$), heterozygote (*Dchs1*$^{+/-}$), and knockout (*Dchs1*$^{-/-}$) hearts (C57/Bl6;Sv129 mixed background). For histology: fetal (E17.5) and adult (9-month) hearts were processed for haematoxylin and eosin stainings and immunohistochemistry (IHC) as previously described. For fetal analyses, *Dchs1*$^{(+/+)}$, *Dchs1*$^{(+/-)}$, and *Dchs1*$^{(-/-)}$ mice were analysed (n = 5 per genotype). Due to neonatal lethality of the *Dchs1*$^{(-/-)}$ mice and loss-of-function *Dchs1* mutations in humans, adult analyses were restricted to *Dchs1*$^{(+/+)}$ (n = 7) and *Dchs1*$^{(+/-)}$ (n = 5). For all analyses male mice were used. Antibodies used for IHC were: hyaluronan binding protein (HABP) to stain proteoglycans (1:100) (Calbiochem), collagen I (1:100) (MDbio), and Hoescht to stain nuclei (1:10,000) (Invitrogen). AMIRA 3D reconstructions were performed to generate volumetric measurements of fetal (E17.5) anterior and posterior mitral leaflets (n = 5 for each genotype). Length and width measurements of the mitral leaflets were obtained from histological sections. 25 consecutive 5 μm sections from anterior and posterior mitral leaflets of each genotype were used for measurements (*Dchs1*$^{(+/+)}$, n = 4, *Dchs1*$^{(+/-)}$, n = 7, *Dchs1*$^{(-/-)}$, n = 5). ImageJ software was used to measure the length of anterior and posterior leaflets from annulus to tip and the perpendicular width at the base, mid-region and tip. Measurements were compared to wild-type data to generate fold change and statistical significance ($P < 0.01$) was calculated using a Student's t-test. For quantification of mitral valve interstitial cell alignment: hearts were initially dissected from E17.5

fetuses. The apex of the heart was dissected and discarded followed by removal of the left atrium. A cut was made cranial to caudal along the anterior aspect of the myocardium. The left ventricle was reflected to gain visualization of the leaflets. The left ventricle and interventricular septum were pinned such to stretch the papillary muscle and the chords. This resulted in obtainment of the leaflet as a planar sheet of tissue. The tissue was fixed in this position to ensure the leaflet was maintained in this orientation, as failure to do so results in curling of the leaflet making measurements and plane of orientation inconsistent between animals. Once the planar leaflet tissue was fixed in 4% PFA for 5 min, the leaflet was released from the heart by cutting the chords and dissecting along the annulus fibrosae. The tissue was then processed through normal protocols and placed en-face on paraffin. This technique was performed blinded to genotype and performed in exactly the same manner for all valve isolates. Performing this type of dissection and tissue processing ensures that all leaflets are placed in nearly identically oriented planes. The vector maps and quantification of cell alignment were performed blinded by two independent researchers. Only after the data was generated did a third researcher perform the PCR genotyping. Vector maps were manually generated.. Cells that deviated >10 degrees from an average alignment plane were counted as misaligned. Interstitial cells within anterior leaflets from each genotype were measured. Total number of cells measured were: WT = 1,083, (n = 4); Het = 1,118, (n = 4); KO = 1,953, (n = 4). Statistical significance was calculated using a *Students t*-test with a P value < 0.05 being significant. Very little variation existed between the

independent valves of each genotype as is graphically depicted. For mouse echocardiography the Vevo2100 imaging system (VisualSonics, Toronto, Canada) was used with 22–55 MHz linear transducer probe (MS550D) and used for 2-D B-mode and M-mode analysis. Heart rate was maintained at 400–500 bpm via isoflurane anaesthesia. The mitral valve leaflet was visualized and its function was assessed in parasternal long-axis B-mode view by placing the transducer on the left lateral chest wall. End-systolic and end-diastolic left ventricular dimensions and wall thicknesses were measured according to the American Society of Echocardiography guidelines as applied to mice. Left ventricular wall thickness was measured at the level of interventricular septum and the posterior wall. Left ventricular volume was calculated from Simpson's method of disks and ejection fraction determined from the formula (left ventricular end-diastolic-end-systolic volume)/(left ventricular end-diastolic volume). Offline image analyses were performed using dedicated VisualSonics Vevo2100 1.2.0 software. Mitral valve prolapse was determined based on superior systolic displacement of one or more leaflets above the line connecting the annular hinge points in the long-axis view (n = 6 per genotype). For MRI experiments: 9-month-old male *Dchs1*$^{(+/+)}$ and *Dchs1*$^{(+/-)}$ mice (n = 4) were sacrificed and the hearts were perfusion fixed and immersed 1:40 (12.5 mmol) Gadolinium (ProHance) in 10% formalin overnight before imaging. MRI was undertaken at 7T using a Bruker Biospin console (Pavavision 5.1) with a volume transmitter coil and a phased array surface coil. Gradient echo FLASH 3D images were collected with repetition time/echo time = 50 ms/5.4 ms, flip angle = 30°,

number of excitations = 3, matrix = 256 × 256 × 256 and pixel resolution = 55 × 55 × 59 μm. Images in DICOM format were imported into AMIRA 3D reconstruction software and volume quantification were performed. Pairwise comparison of littermates were performed and statistical significance was determined (Student's *t*-test) with $P < 0.01$. All mouse experiments were performed under protocols approved by the Institutional Animal Care and Use Committee, Medical University of South Carolina. Prior to cardiac resection, mice were euthanized in accordance with the Guide for the Care and Use of Laboratory Animals (NIH Publication No. 85-23, revised 1996).

RNA expression analyses of *Dchs1* and *Apbb1*

Section *in situ* hybridization was performed on 4 embryos at each time point to localize *Dchs1* expressing cells throughout cardiac development. A *Dchs1* digoxigenin-labelled riboprobe (Roche) was generated against region 9222–10180 of accession number NM_00162943 and used for *in situ* hybridization at E11.5, E13.5, and E15.5. RNA *in situ* hybridization for *Apbb1* at E14.5 was performed through GenePaint. Two separate riboprobes were used to analyse *Apbb1* RNA expression at E14.5. These probes were generated against regions 1676–2506 and 370–1967 of accession number NM_001253885.1. These probes span all known isoforms for *Apbb1* and provide similar spatial RNA expression patterns.

Protein expression

Dchs1 antibodies were generated by immunizing rabbits with a synthetic peptide corresponding to rat Dchs1 protein sequence: C S T Y M V E S P D L V E A D S A A (region 1308–1324 of accession number NP_001101014). Immunohistochemistry was performed using a 1:100 dilution of primary antibody.

In vivo lineage trace

To trace the fate of epicardially derived cells in *Dchs1*$^{(+/+)}$ and *Dchs1*$^{(+/-)}$ mitral leaflets, the Wt1/IRES/GFP-Cre mouse was bred with the *Dchs1*$^{(+/+)}$ and *Dchs1*$^{(+/-)}$ mice (n = 4 per genotype). Mice were euthanized at neonatal day 0 (P0), hearts were isolated and fixed overnight at 4 °C in 4% paraformaldehyde dissolved in PBS. Hearts were processed through a series of graded ethanol, cleared in toluene, and embedded in Paraplast Plus (Fisherbrand, 23-021-400). Hearts were sectioned at 5 μm and slides were treated with 15 ml of antigen unmasking solution (Vector Biolabs, H-3300) in 1,600 ml of distilled water for 10 min in a pressure cooker (Cuisinart) followed by incubation for 1 h at room temperature with 1% BSA (Sigma, B4287) in PBS. Expression of EGFP after Cre recombination was detected by immunofluorescence using antibodies against GFP (Abcam, 13970) and myosin heavy chain (MF20; DSHB). 5 μm sections throughout the entire valve were used for 3D reconstructions using Amira software. The volume of GFP positive cells and the volume of each mitral leaflet were measured using this software. Cell counting was done on GFP positive and

GFP negative cells every 15 μm throughout the entire valve. Pairwise comparison of littermates were performed and statistical significance was determined (Student's *t*-test) with $P = 0.04$ for posterior leaflet and $P = 0.86$ for anterior leaflet.

In vitro migration

Human mitral valve interstitial cells were isolated from a control and the patient with the *DCHS1* mutation (p.R2230C) (proband family 2) and seeded into the Radius 24-well Cell Migration Assay plate containing hydrogels (Cell Biolabs, CBA-125). Cells were allowed to adhere overnight and then gels were dissolved. Wells were imaged over a period of 24 h and area of the cell free region was measured in Photoshop v.10.0.01 and subtracted from the initial area of the hydrogel to generate area migrated over time. Migration in the *Dchs1*$^{(+/+)}$ and *Dchs1*$^{(+/-)}$ mice was assessed by explanting P0 neonatal posterior mitral leaflets onto plastic. Images of the explants and migrating cells were captured at multiple time points. Distance migrated was measured as the distance from the explant to the farthest migrating cell. Measurements were taken at 5 points around the explant and averaged to calculate distance migrated. After 24 h, cells were fixed in ice-cold 100% methanol for 10 min and immunofluorescence was performed using an antibody against N-cadherin (1:1,000 dilution, BD Transduction Labs, 610920). Pairwise comparisons were performed and statistical significance was determined (Student's *t*-test) with $P < 0.05$.

CHAPTER 4: INCREASED INFILTRATION OF EXTRA-CARDIAC CELLS IN MYXOMATOUS VALVE DISEASE

Gene Targeted Mice

All mouse experiments were performed under protocols previously approved by the Institutional Animal Care and Use Committee (IACUC) at the Medical University of South Carolina. Female mice homozygous for a conditional "floxed" allele of *FLNA* (*Filamin-Af/f*) were bred with male transgenic mice expressing Cre under control of the *Tie2* promoter (*Tie2Cre(+)*), which will target valve endocardium and endocardial-derived mesenchyme, resulting in a (*Tie2Cre(+); Filamin-Af/y*) conditional knockout (cKO) mouse. As Filamin-A is X-linked in both mouse and humans, these analyses were primarily focused on male mice, although some female mice have been characterized for phenotypic differences. No difference in phenotype is observed between male and female animals.

Histology, Immunohistochemistry/Immunofluorescence

Hearts from 2-month-old mice were isolated and fixed overnight in 10% Formalin (Sigma) overnight at room temperature. Human immunofluorescence was performed on 5-micron sections of posterior leaflet from the mitral valve of normal (control) and diseased (myxomatous) tissue. Human tissues were obtained from surgical specimens as part of a Leducq transatlantic network. All samples were harvested by offsite partners and were fixed, embedded and sectioned in their various laboratories. Sections were sent to our group at the Medical University of South Carolina (MUSC) for histological assessment.

Consent and Institutional Review Board (IRB) approval for these studies is in place at partnering institutions. For human tissue analyses, 3 control and 5 myxomatous valves were analyzed. Control valve biopsies were obtained from patients who perished as a result of either subarachnoid hemorrhage or intracranial bleeds. Myxomatous valves were surgical cases obtained from patients who fit diagnostic criteria of myxomatous degeneration and mitral valve prolapse. This was defined by >2 mm atrial leaflet displacement in a parasternal long-axis view as well as >5 mm valve thickness. All patient samples involved in the study were men greater than 50 years of age. For immunohistochemistry (IHC): Antigen retrieval was performed for 10 min using antigen unmasking solution (Vector Laboratories, Burlingame, CA, USA, Cat#H-3300) by pressure cooker (Cuisinart, Stamford, CT, USA). Antibodies and their dilutions used for immunological experiments include: Collagen I (MD Biosciences, St. Paul, MN, USA, Cat#203002, 1:200), HaBP (EMD Millipore, Billerica, MA, USA, Cat#385911, 1:200), pERK1/2 (Cell Signaling Technology, Danvers, MA, USA, Cat#4370, 1:50), MMP2 (Abcam, Cambridge, MA, USA, Cat#ab37150, 1:250), MF20 (DSHB, Iowa City, IA, USA, Concentrate, 1:50), Ki67 (Abcam, Cat#ab16667, 1:250), Filamin-A (Abcam, Cat#ab76289, 1:250), MMP3 (Abcam, Cat#ab38907, 1:250), Versican (gift from Stan Hoffman, Medical University of South Carolina, 1:250), MMP7 (Abcam, Cat#ab38996, 1:500), CD45 (Abcam, Cat#ab10558, 1:100, for mouse), and CD45 (EMD Millipore, Cat#05-1410, 1:100, for human). For fluorescent detection of the primary antibodies, Alexa fluor 568 and Alexa fluor 488 secondary antibodies were used (Life Technologies, Rockville, MD, USA).

Hyaluronan-binding protein (HaBP) was visualized by streptavidin-fluorescein (Life Technologies, Cat#S-32354, 1:100). Nuclei were counterstained with Hoechst (Life Technologies, Cat#H3569, 1:10,000) for 10 min and slides were coverslipped with SlowFade mounting medium (Life Technologies, Cat#S36937). Images were acquired with a Leica fluorescent microscope (Leica Biosystems, Buffalo Grove, IL, USA); $n > 3$ for each experiment.

Western Blotting

Isolated mitral leaflets from 2-month old mice were placed in SDS-PAGE buffer and boiled at 95 °C for 7 min before being run on a 4%–20% gradient polyacrylamide gel by electrophoresis (Biorad, , Cat#456-1094). A single leaflet per lane was used for Western blot experiments. Gels were transferred to a nitrocellulose membrane (Biorad, Cat#170-4158) and blocked for 1 h in 5% block (Biorad, Cat#170-6404) dissolved in 1X tris-buffered saline with Tween20 (BDH Chemicals, Poole Dorset, UK). Primary antibodies were incubated at (1:1000) dilution overnight at 4 °C. Primary antibodies used were pERK1/2 (Cell signaling, Cat#4370), pJNK1/2 (Cell Signaling, Cat#9255S), Erk (Cell Signaling, Cat#4695), JNK (Cell Signaling, Cat#9258S), MMP2 (Abcam, Cat#ab51125), MMP13 (Abcam, Cat#ab51072), and Actin (EMD Millipore, Cat#mab1501). Appropriate HRP-conjugated secondary antibodies were used at (1:10,000) in 5% block and incubated for 1 h at room temperature. Protein was detected using a chemiluminescent substrate (Life Technologies, Cat#34095). The entire process of tissue extraction to detection occurs within 18 hours. We have

determined that the rapidity of these experiments is critical in obtaining reproducible Western blots from single murine leaflets due to the small size and relative amounts of protein present in the extracts. Exact numbers of replicates are denoted in Figure legends.

Statistics

Statistical significance was determined using a student's *t*-test (two-tailed, type 2), with significance ($p < 0.05$). Statistical data are presented as standard deviations from the mean.

REFERENCES

Abdulla, T., L. Luna-Zurita, J. L. de la Pompa, J. M. Schleich and R. Summers (2013). "Epithelial to mesenchymal transition-the roles of cell morphology, labile adhesion and junctional coupling." Comput Methods Programs Biomed **111**(2): 435-446.

Adler, P. N., J. Charlton and J. Liu (1998). "Mutations in the cadherin superfamily member gene dachsous cause a tissue polarity phenotype by altering frizzled signaling." Development **125**(5): 959-968.

Adzhubei, I. A., S. Schmidt, L. Peshkin, V. E. Ramensky, A. Gerasimova, P. Bork, A. S. Kondrashov and S. R. Sunyaev (2010). "A method and server for predicting damaging missense mutations." Nat Methods **7**(4): 248-249.

Antonicelli, F., G. Bellon, S. Lorimier and W. Hornebeck (2009). "Role of the elastin receptor complex (S-Gal/Cath-A/Neu-1) in skin repair and regeneration." Wound Repair Regen **17**(5): 631-638.

Armstrong, E. J. and J. Bischoff (2004). "Heart valve development: endothelial cell signaling and differentiation." Circ Res **95**(5): 459-470.

Arndt, J. W., C. A. Reynolds, G. E. Singletary, J. M. Connolly, R. J. Levy and M. A. Oyama (2009). "Serum serotonin concentrations in dogs with degenerative mitral valve disease." J Vet Intern Med **23**(6): 1208-1213.

Badouel, C. and H. McNeill (2011). "SnapShot: The hippo signaling pathway." Cell **145**(3): 484-484 e481.

Balachandran, K., P. W. Alford, J. Wylie-Sears, J. A. Goss, A. Grosberg, J. Bischoff, E. Aikawa, R. A. Levine and K. K. Parker (2011). "Cyclic strain induces dual-mode endothelial-mesenchymal transformation of the cardiac valve." Proc Natl Acad Sci U S A **108**(50): 19943-19948.

Bando, T., T. Mito, T. Nakamura, H. Ohuchi and S. Noji (2011). "Regulation of leg size and shape: involvement of the Dachsous-fat signaling pathway." Dev Dyn **240**(5): 1028-1041.

Banerjee, I., K. Yekkala, T. K. Borg and T. A. Baudino (2006). "Dynamic interactions between myocytes, fibroblasts, and extracellular matrix." Ann N Y Acad Sci **1080**: 76-84.

Barnette, D. N., A. Hulin, A. S. Ahmed, A. C. Colige, M. Azhar and J. Lincoln (2013). "Tgfbeta-Smad and MAPK signaling mediate scleraxis and proteoglycan expression in heart valves." J Mol Cell Cardiol **65**: 137-146.

Barth, P. J., H. Koster and R. Moosdorf (2005). "CD34+ fibrocytes in normal mitral valves and myxomatous mitral valve degeneration." Pathol Res Pract **201**(4): 301-304.

Bertola, D. R., C. A. Kim, S. M. Sugayama, L. M. Albano, J. Wagenfuhr, R. L. Moyses and C. H. Gonzalez (2000). "Cardiac findings in 31 patients with Noonan's syndrome." Arq Bras Cardiol **75**(5): 409-412.

Boileau, C., D. C. Guo, N. Hanna, E. S. Regalado, D. Detaint, L. Gong, M. Varret, S. K. Prakash, A. H. Li, H. d'Indy, A. C. Braverman, B. Grandchamp, C. S. Kwartler, L. Gouya, R. L. Santos-Cortez, M. Abifadel, S. M. Leal, C. Muti, J. Shendure, M. S.

Gross, M. J. Rieder, A. Vahanian, D. A. Nickerson, J. B. Michel, L. National Heart, P. Blood Institute Go Exome Sequencing, G. Jondeau and D. M. Milewicz (2012). "TGFB2 mutations cause familial thoracic aortic aneurysms and dissections associated with mild systemic features of Marfan syndrome." Nat Genet **44**(8): 916-921.
Brown, C. B., A. S. Boyer, R. B. Runyan and J. V. Barnett (1996). "Antibodies to the Type II TGFbeta receptor block cell activation and migration during atrioventricular cushion transformation in the heart." Dev Biol **174**(2): 248-257.
Brown, O. R., H. DeMots, F. E. Kloster, A. Roberts, V. D. Menashe and R. K. Beals (1975). "Aortic root dilatation and mitral valve prolapse in Marfan's syndrome: an ECHOCARDIOgraphic study." Circulation **52**(4): 651-657.
Butcher, J. T., T. C. McQuinn, D. Sedmera, D. Turner and R. R. Markwald (2007). "Transitions in early embryonic atrioventricular valvular function correspond with changes in cushion biomechanics that are predictable by tissue composition." Circ Res **100**(10): 1503-1511.
Butcher, J. T. and R. M. Nerem (2007). "Valvular endothelial cells and the mechanoregulation of valvular pathology." Philos Trans R Soc Lond B Biol Sci **362**(1484): 1445-1457.
Butcher, J. T., R. A. Norris, S. Hoffman, C. H. Mjaatvedt and R. R. Markwald (2007). "Periostin promotes atrioventricular mesenchyme matrix invasion and remodeling mediated by integrin signaling through Rho/PI 3-kinase." Dev Biol **302**(1): 256-266.
Camenisch, T. D., A. P. Spicer, T. Brehm-Gibson, J. Biesterfeldt, M. L. Augustine, A. Calabro, Jr., S. Kubalak, S. E. Klewer and J. A. McDonald (2000). "Disruption of hyaluronan synthase-2 abrogates normal cardiac morphogenesis and hyaluronan-mediated transformation of epithelium to mesenchyme." J Clin Invest **106**(3): 349-360.
Canty, E. G., Y. Lu, R. S. Meadows, M. K. Shaw, D. F. Holmes and K. E. Kadler (2004). "Coalignment of plasma membrane channels and protrusions (fibripositors) specifies the parallelism of tendon." J Cell Biol **165**(4): 553-563.
Canty, E. G., T. Starborg, Y. Lu, S. M. Humphries, D. F. Holmes, R. S. Meadows, A. Huffman, E. T. O'Toole and K. E. Kadler (2006). "Actin filaments are required for fibripositor-mediated collagen fibril alignment in tendon." J Biol Chem **281**(50): 38592-38598.
Chaki, M., R. Airik, A. K. Ghosh, R. H. Giles, R. Chen, G. G. Slaats, H. Wang, T. W. Hurd, W. Zhou, A. Cluckey, H. Y. Gee, G. Ramaswami, C. J. Hong, B. A. Hamilton, I. Cervenka, R. S. Ganji, V. Bryja, H. H. Arts, J. van Reeuwijk, M. M. Oud, S. J. Letteboer, R. Roepman, H. Husson, O. Ibraghimov-Beskrovnaya, T. Yasunaga, G. Walz, L. Eley, J. A. Sayer, B. Schermer, M. C. Liebau, T. Benzing, S. Le Corre, I. Drummond, S. Janssen, S. J. Allen, S. Natarajan, J. F. O'Toole, M. Attanasio, S. Saunier, C. Antignac, R. K. Koenekoop, H. Ren, I. Lopez, A. Nayir, C. Stoetzel, H. Dollfus, R. Massoudi, J. G. Gleeson, S. P. Andreoli, D. G. Doherty, A. Lindstrad, C. Golzio, N. Katsanis, L. Pape, E. B. Abboud, A. A. Al-Rajhi, R. A. Lewis, H. Omran, E. Y. Lee, S. Wang, J. M. Sekiguchi, R. Saunders, C. A. Johnson, E. Garner, K. Vanselow, J. S. Andersen, J. Shlomai, G. Nurnberg, P. Nurnberg, S. Levy, A. Smogorzewska, E.

A. Otto and F. Hildebrandt (2012). "Exome capture reveals ZNF423 and CEP164 mutations, linking renal ciliopathies to DNA damage response signaling." Cell **150**(3): 533-548.
Chakraborty, S., E. E. Wirrig, R. B. Hinton, W. H. Merrill, D. B. Spicer and K. E. Yutzey (2010). "Twist1 promotes heart valve cell proliferation and extracellular matrix gene expression during development in vivo and is expressed in human diseased aortic valves." Dev Biol **347**(1): 167-179.
Chen, B., R. T. Bronson, L. D. Klaman, T. G. Hampton, J. F. Wang, P. J. Green, T. Magnuson, P. S. Douglas, J. P. Morgan and B. G. Neel (2000). "Mice mutant for Egfr and Shp2 have defective cardiac semilunar valvulogenesis." Nat Genet **24**(3): 296-299.
Cheng, X. W., Z. Huang, M. Kuzuya, K. Okumura and T. Murohara (2011). "Cysteine protease cathepsins in atherosclerosis-based vascular disease and its complications." Hypertension **58**(6): 978-986.
Cheng, X. W., G. P. Shi, M. Kuzuya, T. Sasaki, K. Okumura and T. Murohara (2012). "Role for cysteine protease cathepsins in heart disease: focus on biology and mechanisms with clinical implication." Circulation **125**(12): 1551-1562.
Chester, A. H., M. Misfeld, H. H. Sievers and M. H. Yacoub (2001). "Influence of 5-hydroxytryptamine on aortic valve competence in vitro." J Heart Valve Dis **10**(6): 822-825; discussion 825-826.
Cho, E. and K. D. Irvine (2004). "Action of fat, four-jointed, dachsous and dachs in distal-to-proximal wing signaling." Development **131**(18): 4489-4500.
Clark, H. F., D. Brentrup, K. Schneitz, A. Bieber, C. Goodman and M. Noll (1995). "Dachsous encodes a member of the cadherin superfamily that controls imaginal disc morphogenesis in Drosophila." Genes Dev **9**(12): 1530-1542.
Connolly, H. M., J. L. Crary, M. D. McGoon, D. D. Hensrud, B. S. Edwards, W. D. Edwards and H. V. Schaff (1997). "Valvular heart disease associated with fenfluramine-phentermine." N Engl J Med **337**(9): 581-588.
Connolly, J. M., M. A. Bakay, J. T. Fulmer, R. C. Gorman, J. H. Gorman, 3rd, M. A. Oyama and R. J. Levy (2009). "Fenfluramine disrupts the mitral valve interstitial cell response to serotonin." Am J Pathol **175**(3): 988-997.
Cox, R. T., C. Kirkpatrick and M. Peifer (1996). "Armadillo is required for adherens junction assembly, cell polarity, and morphogenesis during Drosophila embryogenesis." J Cell Biol **134**(1): 133-148.
Cui, C., B. Chatterjee, T. P. Lozito, Z. Zhang, R. J. Francis, H. Yagi, L. M. Swanhart, S. Sanker, D. Francis, Q. Yu, J. T. San Agustin, C. Puligilla, T. Chatterjee, T. Tansey, X. Liu, M. W. Kelley, E. T. Spiliotis, A. V. Kwiatkowski, R. Tuan, G. J. Pazour, N. A. Hukriede and C. W. Lo (2013). "Wdpcp, a PCP protein required for ciliogenesis, regulates directional cell migration and cell polarity by direct modulation of the actin cytoskeleton." PLoS Biol **11**(11): e1001720.
D'Addario, M., P. D. Arora, J. Fan, B. Ganss, R. P. Ellen and C. A. McCulloch (2001). "Cytoprotection against mechanical forces delivered through beta 1 integrins requires induction of filamin A." J Biol Chem **276**(34): 31969-31977.
de la Pompa, J. L., L. A. Timmerman, H. Takimoto, H. Yoshida, A. J. Elia, E. Samper, J. Potter, A. Wakeham, L. Marengere, B. L. Langille, G. R. Crabtree and T. W. Mak

(1998). "Role of the NF-ATc transcription factor in morphogenesis of cardiac valves and septum." Nature **392**(6672): 182-186.
de Lange, F. J., A. F. Moorman, R. H. Anderson, J. Manner, A. T. Soufan, C. de Gier-de Vries, M. D. Schneider, S. Webb, M. J. van den Hoff and V. M. Christoffels (2004). "Lineage and morphogenetic analysis of the cardiac valves." Circ Res **95**(6): 645-654.
de Vlaming, A., K. Sauls, Z. Hajdu, R. P. Visconti, A. N. Mehesz, R. A. Levine, S. A. Slaugenhaupt, A. Hagege, A. H. Chester, R. R. Markwald and R. A. Norris (2012). "Atrioventricular valve development: new perspectives on an old theme." Differentiation **84**(1): 103-116.
Dietz, H. C., G. R. Cutting, R. E. Pyeritz, C. L. Maslen, L. Y. Sakai, G. M. Corson, E. G. Puffenberger, A. Hamosh, E. J. Nanthakumar, S. M. Curristin and et al. (1991). "Marfan syndrome caused by a recurrent de novo missense mutation in the fibrillin gene." Nature **352**(6333): 337-339.
Dina, C., N. Bouatia-Naji, N. Tucker, F. N. Delling, K. Toomer, R. Durst, M. Perrocheau, L. Fernandez-Friera, J. Solis, P. investigators, T. Le Tourneau, M. H. Chen, V. Probst, Y. Bosse, P. Pibarot, D. Zelenika, M. Lathrop, S. Hercberg, R. Roussel, E. J. Benjamin, F. Bonnet, S. H. Lo, E. Dolmatova, F. Simonet, S. Lecointe, F. Kyndt, R. Redon, H. Le Marec, P. Froguel, P. T. Ellinor, R. S. Vasan, P. Bruneval, R. R. Markwald, R. A. Norris, D. J. Milan, S. A. Slaugenhaupt, R. A. Levine, J. J. Schott, A. A. Hagege, F. Mvp, X. Jeunemaitre and M. N. Leducq Transatlantic (2015). "Genetic association analyses highlight biological pathways underlying mitral valve prolapse." Nat Genet **47**(10): 1206-1211.
Disatian, S. and E. C. Orton (2009). "Autocrine serotonin and transforming growth factor beta 1 signaling mediates spontaneous myxomatous mitral valve disease." J Heart Valve Dis **18**(1): 44-51.
Dong, J., G. Feldmann, J. Huang, S. Wu, N. Zhang, S. A. Comerford, M. F. Gayyed, R. A. Anders, A. Maitra and D. Pan (2007). "Elucidation of a universal size-control mechanism in Drosophila and mammals." Cell **130**(6): 1120-1133.
Doyle, A. J., J. J. Doyle, S. L. Bessling, S. Maragh, M. E. Lindsay, D. Schepers, E. Gillis, G. Mortier, T. Homfray, K. Sauls, R. A. Norris, N. D. Huso, D. Leahy, D. W. Mohr, M. J. Caulfield, A. F. Scott, A. Destree, R. C. Hennekam, P. H. Arn, C. J. Curry, L. Van Laer, A. S. McCallion, B. L. Loeys and H. C. Dietz (2012). "Mutations in the TGF-beta repressor SKI cause Shprintzen-Goldberg syndrome with aortic aneurysm." Nat Genet **44**(11): 1249-1254.
Dugan, S. L., R. T. Temme, R. A. Olson, A. Mikhailov, R. Law, H. Mahmood, A. Noor and J. B. Vincent (2015). "New recessive truncating mutation in LTBP3 in a family with oligodontia, short stature, and mitral valve prolapse." Am J Med Genet A **167**(6): 1396-1399.
Eaton, S. (2003). "Cell biology of planar polarity transmission in the Drosophila wing." Mech Dev **120**(11): 1257-1264.
Eksioglu, Y. Z., I. E. Scheffer, P. Cardenas, J. Knoll, F. DiMario, G. Ramsby, M. Berg, K. Kamuro, S. F. Berkovic, G. M. Duyk, J. Parisi, P. R. Huttenlocher and C. A. Walsh (1996). "Periventricular heterotopia: an X-linked dominant epilepsy locus causing aberrant cerebral cortical development." Neuron **16**(1): 77-87.

Faherty, N., S. P. Curran, H. O'Donovan, F. Martin, C. Godson, D. P. Brazil and J. K. Crean (2012). "CCN2/CTGF increases expression of miR-302 microRNAs, which target the TGFbeta type II receptor with implications for nephropathic cell phenotypes." J Cell Sci **125**(Pt 23): 5621-5629.
Farrar, E. J. and J. T. Butcher (2014). "Heterogeneous susceptibility of valve endothelial cells to mesenchymal transformation in response to TNFalpha." Ann Biomed Eng **42**(1): 149-161.
Feng, Y., M. H. Chen, I. P. Moskowitz, A. M. Mendonza, L. Vidali, F. Nakamura, D. J. Kwiatkowski and C. A. Walsh (2006). "Filamin A (FLNA) is required for cell-cell contact in vascular development and cardiac morphogenesis." Proc Natl Acad Sci U S A **103**(52): 19836-19841.
Fitzgerald, L. W., T. C. Burn, B. S. Brown, J. P. Patterson, M. H. Corjay, P. A. Valentine, J. H. Sun, J. R. Link, I. Abbaszade, J. M. Hollis, B. L. Largent, P. R. Hartig, G. F. Hollis, P. C. Meunier, A. J. Robichaud and D. W. Robertson (2000). "Possible role of valvular serotonin 5-HT(2B) receptors in the cardiopathy associated with fenfluramine." Mol Pharmacol **57**(1): 75-81.
Freed, L. A., J. S. Acierno, Jr., D. Dai, M. Leyne, J. E. Marshall, F. Nesta, R. A. Levine and S. A. Slaugenhaupt (2003). "A locus for autosomal dominant mitral valve prolapse on chromosome 11p15.4." Am J Hum Genet **72**(6): 1551-1559.
Funderburg, F. M. and R. R. Markwald (1986). "Conditioning of native substrates by chondroitin sulfate proteoglycans during cardiac mesenchymal cell migration." J Cell Biol **103**(6 Pt 1): 2475-2487.
Galvin, K. M., M. J. Donovan, C. A. Lynch, R. I. Meyer, R. J. Paul, J. N. Lorenz, V. Fairchild-Huntress, K. L. Dixon, J. H. Dunmore, M. A. Gimbrone, Jr., D. Falb and D. Huszar (2000). "A role for smad6 in development and homeostasis of the cardiovascular system." Nat Genet **24**(2): 171-174.
Garg, V., A. N. Muth, J. F. Ransom, M. K. Schluterman, R. Barnes, I. N. King, P. D. Grossfeld and D. Srivastava (2005). "Mutations in NOTCH1 cause aortic valve disease." Nature **437**(7056): 270-274.
Gawecka, J. E., G. S. Griffiths, B. Ek-Rylander, J. W. Ramos and M. L. Matter (2010). "R-Ras regulates migration through an interaction with filamin A in melanoma cells." PLoS One **5**(6): e11269.
Geirsson, A., M. Singh, R. Ali, H. Abbas, W. Li, J. A. Sanchez, S. Hashim and G. Tellides (2012). "Modulation of transforming growth factor-beta signaling and extracellular matrix production in myxomatous mitral valves by angiotensin II receptor blockers." Circulation **126**(11 Suppl 1): S189-197.
Ghatak, S., S. Misra, R. A. Norris, R. A. Moreno-Rodriguez, S. Hoffman, R. A. Levine, V. C. Hascall and R. R. Markwald (2014). "Periostin induces intracellular cross-talk between kinases and hyaluronan in atrioventricular valvulogenesis." J Biol Chem **289**(12): 8545-8561.
Gittenberger-de Groot, A. C., M. P. Vrancken Peeters, M. M. Mentink, R. G. Gourdie and R. E. Poelmann (1998). "Epicardium-derived cells contribute a novel population to the myocardial wall and the atrioventricular cushions." Circ Res **82**(10): 1043-1052.

Goetsch, S. C., C. M. Martin, L. J. Embree and D. J. Garry (2005). "Myogenic progenitor cells express filamin C in developing and regenerating skeletal muscle." Stem Cells Dev **14**(2): 181-187.
Golzio, C., J. Willer, M. E. Talkowski, E. C. Oh, Y. Taniguchi, S. Jacquemont, A. Reymond, M. Sun, A. Sawa, J. F. Gusella, A. Kamiya, J. S. Beckmann and N. Katsanis (2012). "KCTD13 is a major driver of mirrored neuroanatomical phenotypes of the 16p11.2 copy number variant." Nature **485**(7398): 363-367.
Gonzalez-Morales, N., C. Geminard, G. Lebreton, D. Cerezo, J. B. Coutelis and S. Noselli (2015). "The Atypical Cadherin Dachsous Controls Left-Right Asymmetry in Drosophila." Dev Cell **33**(6): 675-689.
Grego-Bessa, J., J. Diez, L. Timmerman and J. L. de la Pompa (2004). "Notch and epithelial-mesenchyme transition in development and tumor progression: another turn of the screw." Cell Cycle **3**(6): 718-721.
Grewal, J. S., Y. V. Mukhin, M. N. Garnovskaya, J. R. Raymond and E. L. Greene (1999). "Serotonin 5-HT2A receptor induces TGF-beta1 expression in mesangial cells via ERK: proliferative and fibrotic signals." Am J Physiol **276**(6 Pt 2): F922-930.
Griffiths, G. S., M. Grundl, J. S. Allen, 3rd and M. L. Matter (2011). "R-Ras interacts with filamin a to maintain endothelial barrier function." J Cell Physiol **226**(9): 2287-2296.
Groenink, M., A. W. den Hartog, R. Franken, T. Radonic, V. de Waard, J. Timmermans, A. J. Scholte, M. P. van den Berg, A. M. Spijkerboer, H. A. Marquering, A. H. Zwinderman and B. J. Mulder (2013). "Losartan reduces aortic dilatation rate in adults with Marfan syndrome: a randomized controlled trial." Eur Heart J **34**(45): 3491-3500.
Guenette, S., Y. Chang, T. Hiesberger, J. A. Richardson, C. B. Eckman, E. A. Eckman, R. E. Hammer and J. Herz (2006). "Essential roles for the FE65 amyloid precursor protein-interacting proteins in brain development." EMBO J **25**(2): 420-431.
Gupta, V., J. A. Werdenberg, B. D. Lawrence, J. S. Mendez, E. H. Stephens and K. J. Grande-Allen (2008). "Reversible secretion of glycosaminoglycans and proteoglycans by cyclically stretched valvular cells in 3D culture." Ann Biomed Eng **36**(7): 1092-1103.
Gustafsson, B. I., K. Tommeras, I. Nordrum, J. P. Loennechen, A. Brunsvik, E. Solligard, R. Fossmark, I. Bakke, U. Syversen and H. Waldum (2005). "Long-term serotonin administration induces heart valve disease in rats." Circulation **111**(12): 1517-1522.
Habashi, J. P., J. J. Doyle, T. M. Holm, H. Aziz, F. Schoenhoff, D. Bedja, Y. Chen, A. N. Modiri, D. P. Judge and H. C. Dietz (2011). "Angiotensin II type 2 receptor signaling attenuates aortic aneurysm in mice through ERK antagonism." Science **332**(6027): 361-365.
Hagler, M. A., T. M. Hadley, H. Zhang, K. Mehra, C. M. Roos, H. V. Schaff, R. M. Suri and J. D. Miller (2013). "TGF-beta signalling and reactive oxygen species drive fibrosis and matrix remodelling in myxomatous mitral valves." Cardiovasc Res **99**(1): 175-184.

Hajdu, Z., S. J. Romeo, P. A. Fleming, R. R. Markwald, R. P. Visconti and C. J. Drake (2011). "Recruitment of bone marrow-derived valve interstitial cells is a normal homeostatic process." J Mol Cell Cardiol **51**(6): 955-965.
Han, R. I., A. Black, G. J. Culshaw, A. T. French, R. W. Else and B. M. Corcoran (2008). "Distribution of myofibroblasts, smooth muscle-like cells, macrophages, and mast cells in mitral valve leaflets of dogs with myxomatous mitral valve disease." Am J Vet Res **69**(6): 763-769.
Harrelson, Z., R. G. Kelly, S. N. Goldin, J. J. Gibson-Brown, R. J. Bollag, L. M. Silver and V. E. Papaioannou (2004). "Tbx2 is essential for patterning the atrioventricular canal and for morphogenesis of the outflow tract during heart development." Development **131**(20): 5041-5052.
Harris, T. J. and U. Tepass (2010). "Adherens junctions: from molecules to morphogenesis." Nat Rev Mol Cell Biol **11**(7): 502-514.
Hart, A. W., J. E. Morgan, J. Schneider, K. West, L. McKie, S. Bhattacharya, I. J. Jackson and S. H. Cross (2006). "Cardiac malformations and midline skeletal defects in mice lacking filamin A." Hum Mol Genet **15**(16): 2457-2467.
Hiatt, K. K., D. A. Ingram, Y. Zhang, G. Bollag and D. W. Clapp (2001). "Neurofibromin GTPase-activating protein-related domains restore normal growth in Nf1-/- cells." J Biol Chem **276**(10): 7240-7245.
Hinton, R. B., Jr., J. Lincoln, G. H. Deutsch, H. Osinska, P. B. Manning, D. W. Benson and K. E. Yutzey (2006). "Extracellular matrix remodeling and organization in developing and diseased aortic valves." Circ Res **98**(11): 1431-1438.
Holm, T. M., J. P. Habashi, J. J. Doyle, D. Bedja, Y. Chen, C. van Erp, M. E. Lindsay, D. Kim, F. Schoenhoff, R. D. Cohn, B. L. Loeys, C. J. Thomas, S. Patnaik, J. J. Marugan, D. P. Judge and H. C. Dietz (2011). "Noncanonical TGFbeta signaling contributes to aortic aneurysm progression in Marfan syndrome mice." Science **332**(6027): 358-361.
Iwamoto, D. V. and D. A. Calderwood (2015). "Regulation of integrin-mediated adhesions." Curr Opin Cell Biol **36**: 41-47.
Jian, B., J. Xu, J. Connolly, R. C. Savani, N. Narula, B. Liang and R. J. Levy (2002). "Serotonin mechanisms in heart valve disease I: serotonin-induced up-regulation of transforming growth factor-beta1 via G-protein signal transduction in aortic valve interstitial cells." Am J Pathol **161**(6): 2111-2121.
Jiang, H., X. W. Cheng, G. P. Shi, L. Hu, A. Inoue, Y. Yamamura, H. Wu, K. Takeshita, X. Li, Z. Huang, H. Song, M. Asai, C. N. Hao, K. Unno, T. Koike, Y. Oshida, K. Okumura, T. Murohara and M. Kuzuya (2014). "Cathepsin K-mediated Notch1 activation contributes to neovascularization in response to hypoxia." Nat Commun **5**: 3838.
Jiao, K., H. Kulessa, K. Tompkins, Y. Zhou, L. Batts, H. S. Baldwin and B. L. Hogan (2003). "An essential role of Bmp4 in the atrioventricular septation of the mouse heart." Genes Dev **17**(19): 2362-2367.
Kadler, K. (2004). "Matrix loading: assembly of extracellular matrix collagen fibrils during embryogenesis." Birth Defects Res C Embryo Today **72**(1): 1-11.

Kapacee, Z., S. H. Richardson, Y. Lu, T. Starborg, D. F. Holmes, K. Baar and K. E. Kadler (2008). "Tension is required for fibripositor formation." Matrix Biol **27**(4): 371-375.
Karsan, A. (2008). "Notch and integrin affinity: a sticky situation." Sci Signal **1**(2): pe2.
Keller, R. (2002). "Shaping the vertebrate body plan by polarized embryonic cell movements." Science **298**(5600): 1950-1954.
Keshari, R. S., A. Verma, M. K. Barthwal and M. Dikshit (2013). "Reactive oxygen species-induced activation of ERK and p38 MAPK mediates PMA-induced NETs release from human neutrophils." J Cell Biochem **114**(3): 532-540.
Khan, K. M., L. R. Howe and D. J. Falcone (2004). "Extracellular matrix-induced cyclooxygenase-2 regulates macrophage proteinase expression." J Biol Chem **279**(21): 22039-22046.
Khew, S. T., P. P. Panengad, M. Raghunath and Y. W. Tong (2010). "Characterization of amine donor and acceptor sites for tissue type transglutaminase using a sequence from the C-terminus of human fibrillin-1 and the N-terminus of osteonectin." Biomaterials **31**(16): 4600-4608.
Kim, H., A. Sengupta, M. Glogauer and C. A. McCulloch (2008). "Filamin A regulates cell spreading and survival via beta1 integrins." Exp Cell Res **314**(4): 834-846.
Kisanuki, Y. Y., R. E. Hammer, J. Miyazaki, S. C. Williams, J. A. Richardson and M. Yanagisawa (2001). "Tie2-Cre transgenic mice: a new model for endothelial cell-lineage analysis in vivo." Dev Biol **230**(2): 230-242.
Kligfield, P., D. Levy, R. B. Devereux and D. D. Savage (1987). "Arrhythmias and sudden death in mitral valve prolapse." Am Heart J **113**(5): 1298-1307.
Krenz, M., K. E. Yutzey and J. Robbins (2005). "Noonan syndrome mutation Q79R in Shp2 increases proliferation of valve primordia mesenchymal cells via extracellular signal-regulated kinase 1/2 signaling." Circ Res **97**(8): 813-820.
Krug, E. L., M. Rezaee, K. Isokawa, D. K. Turner, L. L. Litke, A. M. Wunsch, J. L. Bain, D. A. Riley, A. A. Capehart and R. R. Markwald (1995). "Transformation of cardiac endothelium into cushion mesenchyme is dependent on ES/130: temporal, spatial, and functional studies in the early chick embryo." Cell Mol Biol Res **41**(4): 263-277.
Krug, E. L., R. B. Runyan and R. R. Markwald (1985). "Protein extracts from early embryonic hearts initiate cardiac endothelial cytodifferentiation." Dev Biol **112**(2): 414-426.
Kuo, L., H. C. Chang, T. H. Leu, M. C. Maa and W. C. Hung (2006). "Src oncogene activates MMP-2 expression via the ERK/Sp1 pathway." J Cell Physiol **207**(3): 729-734.
Kyndt, F., J. P. Gueffet, V. Probst, P. Jaafar, A. Legendre, F. Le Bouffant, C. Toquet, E. Roy, L. McGregor, S. A. Lynch, R. Newbury-Ecob, V. Tran, I. Young, J. N. Trochu, H. Le Marec and J. J. Schott (2007). "Mutations in the gene encoding filamin A as a cause for familial cardiac valvular dystrophy." Circulation **115**(1): 40-49.

Lacerda, C. M., H. B. Maclea, J. D. Kisiday and E. C. Orton (2012). "Static and cyclic tensile strain induce myxomatous effector proteins and serotonin in canine mitral valves." J Vet Cardiol **14**(1): 223-230.
Lange, A. W. and K. E. Yutzey (2006). "NFATc1 expression in the developing heart valves is responsive to the RANKL pathway and is required for endocardial expression of cathepsin K." Dev Biol **292**(2): 407-417.
Lardeux, A., F. Kyndt, S. Lecointe, H. L. Marec, J. Merot, J. J. Schott, T. Le Tourneau and V. Probst (2011). "Filamin-a-related myxomatous mitral valve dystrophy: genetic, echocardiographic and functional aspects." J Cardiovasc Transl Res **4**(6): 748-756.
Launay, J. M., G. Birraux, D. Bondoux, J. Callebert, D. S. Choi, S. Loric and L. Maroteaux (1996). "Ras involvement in signal transduction by the serotonin 5-HT2B receptor." J Biol Chem **271**(6): 3141-3147.
Lawrence, P. A., J. Casal and G. Struhl (2004). "Cell interactions and planar polarity in the abdominal epidermis of Drosophila." Development **131**(19): 4651-4664.
Levine, R. A., A. A. Hagege, D. P. Judge, M. Padala, J. P. Dal-Bianco, E. Aikawa, J. Beaudoin, J. Bischoff, N. Bouatia-Naji, P. Bruneval, J. T. Butcher, A. Carpentier, M. Chaput, A. H. Chester, C. Clusel, F. N. Delling, H. C. Dietz, C. Dina, R. Durst, L. Fernandez-Friera, M. D. Handschumacher, M. O. Jensen, X. P. Jeunemaitre, H. L. Marec, T. L. Tourneau, R. R. Markwald, J. Merot, E. Messas, D. P. Milan, T. Neri, R. A. Norris, D. Peal, M. Perrocheau, V. Probst, M. Puceat, N. Rosenthal, J. Solis, J. J. Schott, E. Schwammenthal, S. A. Slaugenhaupt, J. K. Song, M. H. Yacoub and N. Leducq Mitral Transatlantic (2015). "Mitral valve disease-morphology and mechanisms." Nat Rev Cardiol **12**(12): 689-710.
Levine, R. A., M. D. Handschumacher, A. J. Sanfilippo, A. A. Hagege, P. Harrigan, J. E. Marshall and A. E. Weyman (1989). "Three-dimensional echocardiographic reconstruction of the mitral valve, with implications for the diagnosis of mitral valve prolapse." Circulation **80**(3): 589-598.
Levine, R. A., E. Stathogiannis, J. B. Newell, P. Harrigan and A. E. Weyman (1988). "Reconsideration of echocardiographic standards for mitral valve prolapse: lack of association between leaflet displacement isolated to the apical four chamber view and independent echocardiographic evidence of abnormality." J Am Coll Cardiol **11**(5): 1010-1019.
Levy, D. and D. Savage (1987). "Prevalence and clinical features of mitral valve prolapse." Am Heart J **113**(5): 1281-1290.
Liebner, S., A. Cattelino, R. Gallini, N. Rudini, M. Iurlaro, S. Piccolo and E. Dejana (2004). "Beta-catenin is required for endothelial-mesenchymal transformation during heart cushion development in the mouse." J Cell Biol **166**(3): 359-367.
Lincoln, J., C. M. Alfieri and K. E. Yutzey (2004). "Development of heart valve leaflets and supporting apparatus in chicken and mouse embryos." Dev Dyn **230**(2): 239-250.
Liu, A. C., V. R. Joag and A. I. Gotlieb (2007). "The emerging role of valve interstitial cell phenotypes in regulating heart valve pathobiology." Am J Pathol **171**(5): 1407-1418.

Loeys, B. L., J. Chen, E. R. Neptune, D. P. Judge, M. Podowski, T. Holm, J. Meyers, C. C. Leitch, N. Katsanis, N. Sharifi, F. L. Xu, L. A. Myers, P. J. Spevak, D. E. Cameron, J. De Backer, J. Hellemans, Y. Chen, E. C. Davis, C. L. Webb, W. Kress, P. Coucke, D. B. Rifkin, A. M. De Paepe and H. C. Dietz (2005). "A syndrome of altered cardiovascular, craniofacial, neurocognitive and skeletal development caused by mutations in TGFBR1 or TGFBR2." Nat Genet **37**(3): 275-281.
Lumiaho, A., R. Ikaheimo, R. Miettinen, L. Niemitukia, T. Laitinen, A. Rantala, E. Lampainen, M. Laakso and J. Hartikainen (2001). "Mitral valve prolapse and mitral regurgitation are common in patients with polycystic kidney disease type 1." Am J Kidney Dis **38**(6): 1208-1216.
Lyons, K. M., R. W. Pelton and B. L. Hogan (1990). "Organogenesis and pattern formation in the mouse: RNA distribution patterns suggest a role for bone morphogenetic protein-2A (BMP-2A)." Development **109**(4): 833-844.
Ma, L., M. F. Lu, R. J. Schwartz and J. F. Martin (2005). "Bmp2 is essential for cardiac cushion epithelial-mesenchymal transition and myocardial patterning." Development **132**(24): 5601-5611.
Ma, L. and J. F. Martin (2005). "Generation of a Bmp2 conditional null allele." Genesis **42**(3): 203-206.
Malev, E. G., E. V. Zemtsovskii, M. Omel'chenko and L. V. Vasina (2012). "[The role of transforming growth factor-beta in the pathogenesis of mitral valve prolapse]." Kardiologiia **52**(12): 34-39.
Mansour, S. J., W. T. Matten, A. S. Hermann, J. M. Candia, S. Rong, K. Fukasawa, G. F. Vande Woude and N. G. Ahn (1994). "Transformation of mammalian cells by constitutively active MAP kinase kinase." Science **265**(5174): 966-970.
Mao, Y., J. Mulvaney, S. Zakaria, T. Yu, K. M. Morgan, S. Allen, M. A. Basson, P. Francis-West and K. D. Irvine (2011). "Characterization of a Dchs1 mutant mouse reveals requirements for Dchs1-Fat4 signaling during mammalian development." Development **138**(5): 947-957.
Maria V. de la Cruz, R. R. M. (1998). Embyological Development of the Ventricular Inlets. Septation and Atrioventricular Valve Apparatus. Living Morphogenesis of the Heart, Birkhauser Boston**:** 131-155.
Markwald, R. R., T. P. Fitzharris, D. L. Bolender and D. H. Bernanke (1979). "Sturctural analysis of cell:matrix association during the morphogenesis of atrioventricular cushion tissue." Dev Biol **69**(2): 634-654.
Markwald, R. R., T. P. Fitzharris and F. J. Manasek (1977). "Structural development of endocardial cushions." Am J Anat **148**(1): 85-119.
Markwald, R. R., T. P. Fitzharris and W. N. Smith (1975). "Sturctural analysis of endocardial cytodifferentiation." Dev Biol **42**(1): 160-180.
Markwald, R. R. and W. N. Smith (1972). "Distribution of mucosubstances in the developing rat heart." J Histochem Cytochem **20**(11): 896-907.
Martinez, F. O. and S. Gordon (2014). "The M1 and M2 paradigm of macrophage activation: time for reassessment." F1000Prime Rep **6**: 13.
Matakatsu, H. and S. S. Blair (2006). "Separating the adhesive and signaling functions of the Fat and Dachsous protocadherins." Development **133**(12): 2315-2324.

Matsui, T., H. Ishikawa and Y. Bessho (2015). "Cell collectivity regulation within migrating cell cluster during Kupffer's vesicle formation in zebrafish." Front Cell Dev Biol **3**: 27.
Mekontso-Dessap, A., F. Brouri, O. Pascal, P. Lechat, N. Hanoun, L. Lanfumey, I. Seif, N. Benhaiem-Sigaux, M. Kirsch, M. Hamon, S. Adnot and S. Eddahibi (2006). "Deficiency of the 5-hydroxytryptamine transporter gene leads to cardiac fibrosis and valvulopathy in mice." Circulation **113**(1): 81-89.
Milewicz, D. M. and M. Duvic (1994). "Severe neonatal Marfan syndrome resulting from a de novo 3-bp insertion into the fibrillin gene on chromosome 15." Am J Hum Genet **54**(3): 447-453.
Miquerol, L., M. Gertsenstein, K. Harpal, J. Rossant and A. Nagy (1999). "Multiple developmental roles of VEGF suggested by a LacZ-tagged allele." Dev Biol **212**(2): 307-322.
Miquerol, L., B. L. Langille and A. Nagy (2000). "Embryonic development is disrupted by modest increases in vascular endothelial growth factor gene expression." Development **127**(18): 3941-3946.
Mjaatvedt, C. H., E. L. Krug and R. R. Markwald (1991). "An antiserum (ES1) against a particulate form of extracellular matrix blocks the transition of cardiac endothelium into mesenchyme in culture." Dev Biol **145**(2): 219-230.
Mjaatvedt, C. H. and R. R. Markwald (1989). "Induction of an epithelial-mesenchymal transition by an in vivo adheron-like complex." Dev Biol **136**(1): 118-128.
Nakajima, D., M. Nakayama, R. Kikuno, M. Hirosawa, T. Nagase and O. Ohara (2001). "Identification of three novel non-classical cadherin genes through comprehensive analysis of large cDNAs." Brain Res Mol Brain Res **94**(1-2): 85-95.
Nakajima, Y., T. Yamagishi, S. Hokari and H. Nakamura (2000). "Mechanisms involved in valvuloseptal endocardial cushion formation in early cardiogenesis: roles of transforming growth factor (TGF)-beta and bone morphogenetic protein (BMP)." Anat Rec **258**(2): 119-127.
Nakamura, T., M. C. Colbert and J. Robbins (2006). "Neural crest cells retain multipotential characteristics in the developing valves and label the cardiac conduction system." Circ Res **98**(12): 1547-1554.
Nesta, F., M. Leyne, C. Yosefy, C. Simpson, D. Dai, J. E. Marshall, J. Hung, S. A. Slaugenhaupt and R. A. Levine (2005). "New locus for autosomal dominant mitral valve prolapse on chromosome 13: clinical insights from genetic studies." Circulation **112**(13): 2022-2030.
Ng, C. M., A. Cheng, L. A. Myers, F. Martinez-Murillo, C. Jie, D. Bedja, K. L. Gabrielson, J. M. Hausladen, R. P. Mecham, D. P. Judge and H. C. Dietz (2004). "TGF-beta-dependent pathogenesis of mitral valve prolapse in a mouse model of Marfan syndrome." J Clin Invest **114**(11): 1586-1592.
Nishikawa, T., S. Ishiyama, T. Shimojo, K. Takeda, T. Kasajima and K. Momma (1996). "Hypertrophic cardiomyopathy in Noonan syndrome." Acta Paediatr Jpn **38**(1): 91-98.

Norris, R. A., R. Moreno-Rodriguez, A. Wessels, J. Merot, P. Bruneval, A. H. Chester, M. H. Yacoub, A. Hagege, S. A. Slaugenhaupt, E. Aikawa, J. J. Schott, A. Lardeux, B. S. Harris, L. K. Williams, A. Richards, R. A. Levine and R. R. Markwald (2010). "Expression of the familial cardiac valvular dystrophy gene, filamin-A, during heart morphogenesis." Dev Dyn **239**(7): 2118-2127.
Norris, R. A., R. A. Moreno-Rodriguez, Y. Sugi, S. Hoffman, J. Amos, M. M. Hart, J. D. Potts, R. L. Goodwin and R. R. Markwald (2008). "Periostin regulates atrioventricular valve maturation." Dev Biol **316**(2): 200-213.
Norris, R. A., J. D. Potts, M. J. Yost, L. Junor, T. Brooks, H. Tan, S. Hoffman, M. M. Hart, M. J. Kern, B. Damon, R. R. Markwald and R. L. Goodwin (2009). "Periostin promotes a fibroblastic lineage pathway in atrioventricular valve progenitor cells." Dev Dyn **238**(5): 1052-1063.
Oh, H. and K. D. Irvine (2010). "Yorkie: the final destination of Hippo signaling." Trends Cell Biol **20**(7): 410-417.
Oyama, M. A. and R. J. Levy (2010). "Insights into serotonin signaling mechanisms associated with canine degenerative mitral valve disease." J Vet Intern Med **24**(1): 27-36.
Ozawa, M., M. Ringwald and R. Kemler (1990). "Uvomorulin-catenin complex formation is regulated by a specific domain in the cytoplasmic region of the cell adhesion molecule." Proc Natl Acad Sci U S A **87**(11): 4246-4250.
Paranya, G., S. Vineberg, E. Dvorin, S. Kaushal, S. J. Roth, E. Rabkin, F. J. Schoen and J. Bischoff (2001). "Aortic valve endothelial cells undergo transforming growth factor-beta-mediated and non-transforming growth factor-beta-mediated transdifferentiation in vitro." Am J Pathol **159**(4): 1335-1343.
Paruchuri, S., J. H. Yang, E. Aikawa, J. M. Melero-Martin, Z. A. Khan, S. Loukogeorgakis, F. J. Schoen and J. Bischoff (2006). "Human pulmonary valve progenitor cells exhibit endothelial/mesenchymal plasticity in response to vascular endothelial growth factor-A and transforming growth factor-beta2." Circ Res **99**(8): 861-869.
Pavone, L. M., A. Spina, S. Rea, D. Santoro, V. Mastellone, P. Lombardi and L. Avallone (2009). "Serotonin transporter gene deficiency is associated with sudden death of newborn mice through activation of TGF-beta1 signalling." J Mol Cell Cardiol **47**(5): 691-697.
Peacock, J. D., Y. Lu, M. Koch, K. E. Kadler and J. Lincoln (2008). "Temporal and spatial expression of collagens during murine atrioventricular heart valve development and maintenance." Dev Dyn **237**(10): 3051-3058.
Pellerin, D., S. Brecker and C. Veyrat (2002). "Degenerative mitral valve disease with emphasis on mitral valve prolapse." Heart **88 Suppl 4**: iv20-28.
Perez-Pomares, J. M., A. Phelps, M. Sedmerova, R. Carmona, M. Gonzalez-Iriarte, R. Munoz-Chapuli and A. Wessels (2002). "Experimental studies on the spatiotemporal expression of WT1 and RALDH2 in the embryonic avian heart: a model for the regulation of myocardial and valvuloseptal development by epicardially derived cells (EPDCs)." Dev Biol **247**(2): 307-326.
Perloff, J. K. and J. S. Child (1987). "Clinical and epidemiologic issues in mitral valve prolapse: overview and perspective." Am Heart J **113**(5): 1324-1332.

Person, A. D., S. E. Klewer and R. B. Runyan (2005). "Cell biology of cardiac cushion development." Int Rev Cytol **243**: 287-335.
Pierpont, M. E., C. T. Basson, D. W. Benson, Jr., B. D. Gelb, T. M. Giglia, E. Goldmuntz, G. McGee, C. A. Sable, D. Srivastava, C. L. Webb and C. o. C. D. i. t. Y. American Heart Association Congenital Cardiac Defects Committee (2007). "Genetic basis for congenital heart defects: current knowledge: a scientific statement from the American Heart Association Congenital Cardiac Defects Committee, Council on Cardiovascular Disease in the Young: endorsed by the American Academy of Pediatrics." Circulation **115**(23): 3015-3038.
Ploeger, D. T., N. A. Hosper, M. Schipper, J. A. Koerts, S. de Rond and R. A. Bank (2013). "Cell plasticity in wound healing: paracrine factors of M1/ M2 polarized macrophages influence the phenotypical state of dermal fibroblasts." Cell Commun Signal **11**(1): 29.
Popowicz, G. M., M. Schleicher, A. A. Noegel and T. A. Holak (2006). "Filamins: promiscuous organizers of the cytoskeleton." Trends Biochem Sci **31**(7): 411-419.
Rabkin, E., M. Aikawa, J. R. Stone, Y. Fukumoto, P. Libby and F. J. Schoen (2001). "Activated interstitial myofibroblasts express catabolic enzymes and mediate matrix remodeling in myxomatous heart valves." Circulation **104**(21): 2525-2532.
Rajamannan, N. M., B. Gersh and R. O. Bonow (2003). "Calcific aortic stenosis: from bench to the bedside--emerging clinical and cellular concepts." Heart **89**(7): 801-805.
Ranger, A. M., M. J. Grusby, M. R. Hodge, E. M. Gravallese, F. C. de la Brousse, T. Hoey, C. Mickanin, H. S. Baldwin and L. H. Glimcher (1998). "The transcription factor NF-ATc is essential for cardiac valve formation." Nature **392**(6672): 186-190.
Reddy, K., Z. Zhou, K. Schadler, S. F. Jia and E. S. Kleinerman (2008). "Bone marrow subsets differentiate into endothelial cells and pericytes contributing to Ewing's tumor vessels." Mol Cancer Res **6**(6): 929-936.
Rivera-Feliciano, J. and C. J. Tabin (2006). "Bmp2 instructs cardiac progenitors to form the heart-valve-inducing field." Dev Biol **295**(2): 580-588.
Rock, R., S. Schrauth and M. Gessler (2005). "Expression of mouse dchs1, fjx1, and fat-j suggests conservation of the planar cell polarity pathway identified in Drosophila." Dev Dyn **234**(3): 747-755.
Roger, V. L., A. S. Go, D. M. Lloyd-Jones, E. J. Benjamin, J. D. Berry, W. B. Borden, D. M. Bravata, S. Dai, E. S. Ford, C. S. Fox, H. J. Fullerton, C. Gillespie, S. M. Hailpern, J. A. Heit, V. J. Howard, B. M. Kissela, S. J. Kittner, D. T. Lackland, J. H. Lichtman, L. D. Lisabeth, D. M. Makuc, G. M. Marcus, A. Marelli, D. B. Matchar, C. S. Moy, D. Mozaffarian, M. E. Mussolino, G. Nichol, N. P. Paynter, E. Z. Soliman, P. D. Sorlie, N. Sotoodehnia, T. N. Turan, S. S. Virani, N. D. Wong, D. Woo, M. B. Turner, C. American Heart Association Statistics and S. Stroke Statistics (2012). "Heart disease and stroke statistics--2012 update: a report from the American Heart Association." Circulation **125**(1): e2-e220.

Romano, L. A. and R. B. Runyan (1999). "Slug is a mediator of epithelial-mesenchymal cell transformation in the developing chicken heart." Dev Biol **212**(1): 243-254.
Romano, L. A. and R. B. Runyan (2000). "Slug is an essential target of TGFbeta2 signaling in the developing chicken heart." Dev Biol **223**(1): 91-102.
Roskoski, R., Jr. (2012). "ERK1/2 MAP kinases: structure, function, and regulation." Pharmacol Res **66**(2): 105-143.
Roy, A., N. J. Brand and M. H. Yacoub (2000). "Expression of 5-hydroxytryptamine receptor subtype messenger RNA in interstitial cells from human heart valves." J Heart Valve Dis **9**(2): 256-260; discussion 260-251.
Runyan, R. B. and R. R. Markwald (1983). "Invasion of mesenchyme into three-dimensional collagen gels: a regional and temporal analysis of interaction in embryonic heart tissue." Dev Biol **95**(1): 108-114.
Saburi, S., I. Hester, E. Fischer, M. Pontoglio, V. Eremina, M. Gessler, S. E. Quaggin, R. Harrison, R. Mount and H. McNeill (2008). "Loss of Fat4 disrupts PCP signaling and oriented cell division and leads to cystic kidney disease." Nat Genet **40**(8): 1010-1015.
Sacks, M. S., W. David Merryman and D. E. Schmidt (2009). "On the biomechanics of heart valve function." J Biomech **42**(12): 1804-1824.
Sacks, M. S. and A. P. Yoganathan (2007). "Heart valve function: a biomechanical perspective." Philos Trans R Soc Lond B Biol Sci **362**(1484): 1369-1391.
Sandbo, N. and N. Dulin (2011). "Actin cytoskeleton in myofibroblast differentiation: ultrastructure defining form and driving function." Transl Res **158**(4): 181-196.
Sane, D. C., J. L. Kontos and C. S. Greenberg (2007). "Roles of transglutaminases in cardiac and vascular diseases." Front Biosci **12**: 2530-2545.
Sasaki, A., Y. Masuda, Y. Ohta, K. Ikeda and K. Watanabe (2001). "Filamin associates with Smads and regulates transforming growth factor-beta signaling." J Biol Chem **276**(21): 17871-17877.
Sauls, K., A. de Vlaming, B. S. Harris, K. Williams, A. Wessels, R. A. Levine, S. A. Slaugenhaupt, R. L. Goodwin, L. M. Pavone, J. Merot, J. J. Schott, T. Le Tourneau, T. Dix, S. Jesinkey, Y. Feng, C. Walsh, B. Zhou, S. Baldwin, R. R. Markwald and R. A. Norris (2012). "Developmental basis for filamin-A-associated myxomatous mitral valve disease." Cardiovasc Res **96**(1): 109-119.
Schroeder, J. A., L. F. Jackson, D. C. Lee and T. D. Camenisch (2003). "Form and function of developing heart valves: coordination by extracellular matrix and growth factor signaling." J Mol Med (Berl) **81**(7): 392-403.
Schwarz, J. M., C. Rodelsperger, M. Schuelke and D. Seelow (2010). "MutationTaster evaluates disease-causing potential of sequence alterations." Nat Methods **7**(8): 575-576.
Scordo, K. A. (1998). "Mitral valve prolapse syndrome: interventions for symptom control." Dimens Crit Care Nurs **17**(4): 177-186.
Sergeeva, I. A. and V. M. Christoffels (2013). "Regulation of expression of atrial and brain natriuretic peptide, biomarkers for heart development and disease." Biochim Biophys Acta **1832**(12): 2403-2413.

Shapero, K., J. Wylie-Sears, R. A. Levine, J. E. Mayer, Jr. and J. Bischoff (2015). "Reciprocal interactions between mitral valve endothelial and interstitial cells reduce endothelial-to-mesenchymal transition and myofibroblastic activation." J Mol Cell Cardiol **80**: 175-185.
Shaul, Y. D. and R. Seger (2007). "The MEK/ERK cascade: from signaling specificity to diverse functions." Biochim Biophys Acta **1773**(8): 1213-1226.
Sheen, V. L., Y. Feng, D. Graham, T. Takafuta, S. S. Shapiro and C. A. Walsh (2002). "Filamin A and Filamin B are co-expressed within neurons during periods of neuronal migration and can physically interact." Hum Mol Genet **11**(23): 2845-2854.
Shelton, E. L. and K. E. Yutzey (2007). "Tbx20 regulation of endocardial cushion cell proliferation and extracellular matrix gene expression." Dev Biol **302**(2): 376-388.
Shelton, E. L. and K. E. Yutzey (2008). "Twist1 function in endocardial cushion cell proliferation, migration, and differentiation during heart valve development." Dev Biol **317**(1): 282-295.
Shively, B. K., C. A. Roldan, E. A. Gill, T. Najarian and S. B. Loar (1999). "Prevalence and determinants of valvulopathy in patients treated with dexfenfluramine." Circulation **100**(21): 2161-2167.
Shizuta, Y., H. Shizuta, M. Gallo, P. Davies and I. Pastan (1976). "Purification and properties of filamin, and actin binding protein from chicken gizzard." J Biol Chem **251**(21): 6562-6567.
Simon, M. A. (2004). "Planar cell polarity in the Drosophila eye is directed by graded Four-jointed and Dachsous expression." Development **131**(24): 6175-6184.
Stamenkovic, I. (2003). "Extracellular matrix remodelling: the role of matrix metalloproteinases." J Pathol **200**(4): 448-464.
Stegemann, J. P. and R. M. Nerem (2003). "Altered response of vascular smooth muscle cells to exogenous biochemical stimulation in two- and three-dimensional culture." Exp Cell Res **283**(2): 146-155.
Strahan, N. V., E. A. Murphy, N. J. Fortuin, P. C. Come and J. O. Humphries (1983). "Inheritance of the mitral valve prolapse syndrome. Discussion of a three-dimensional penetrance model." Am J Med **74**(6): 967-972.
Sugi, Y., N. Ito, G. Szebenyi, K. Myers, J. F. Fallon, T. Mikawa and R. R. Markwald (2003). "Fibroblast growth factor (FGF)-4 can induce proliferation of cardiac cushion mesenchymal cells during early valve leaflet formation." Dev Biol **258**(2): 252-263.
Surachetpong, S., T. Jiranantasak, A. Rungsipipat and E. C. Orton (2013). "Apoptosis and abundance of Bcl-2 family and transforming growth factor beta1 signaling proteins in canine myxomatous mitral valves." J Vet Cardiol **15**(3): 171-180.
Tamura, K., Y. Fukuda, M. Ishizaki, Y. Masuda, N. Yamanaka and V. J. Ferrans (1995). "Abnormalities in elastic fibers and other connective-tissue components of floppy mitral valve." Am Heart J **129**(6): 1149-1158.

Tan, H., L. Junor, R. L. Price, R. A. Norris, J. D. Potts and R. L. Goodwin (2011). "Expression and deposition of fibrous extracellular matrix proteins in cardiac valves during chick development." Microsc Microanal **17**(1): 91-100.
Tanoue, T. and M. Takeichi (2005). "New insights into Fat cadherins." J Cell Sci **118**(Pt 11): 2347-2353.
Timmerman, L. A., J. Grego-Bessa, A. Raya, E. Bertran, J. M. Perez-Pomares, J. Diez, S. Aranda, S. Palomo, F. McCormick, J. C. Izpisua-Belmonte and J. L. de la Pompa (2004). "Notch promotes epithelial-mesenchymal transition during cardiac development and oncogenic transformation." Genes Dev **18**(1): 99-115.
Togashi, M., K. Tamura, T. Nitta, M. Ishizaki, Y. Sugisaki and Y. Fukuda (2007). "Role of matrix metalloproteinases and their tissue inhibitor of metalloproteinases in myxomatous change of cardiac floppy valves." Pathol Int **57**(5): 251-259.
Torii, S., K. Nakayama, T. Yamamoto and E. Nishida (2004). "Regulatory mechanisms and function of ERK MAP kinases." J Biochem **136**(5): 557-561.
Tornavaca, O., M. Chia, N. Dufton, L. O. Almagro, D. E. Conway, A. M. Randi, M. A. Schwartz, K. Matter and M. S. Balda (2015). "ZO-1 controls endothelial adherens junctions, cell-cell tension, angiogenesis, and barrier formation." J Cell Biol **208**(6): 821-838.
Visconti, R. P., Y. Ebihara, A. C. LaRue, P. A. Fleming, T. C. McQuinn, M. Masuya, H. Minamiguchi, R. R. Markwald, M. Ogawa and C. J. Drake (2006). "An in vivo analysis of hematopoietic stem cell potential: hematopoietic origin of cardiac valve interstitial cells." Circ Res **98**(5): 690-696.
Walker, G. A., K. S. Masters, D. N. Shah, K. S. Anseth and L. A. Leinwand (2004). "Valvular myofibroblast activation by transforming growth factor-beta: implications for pathological extracellular matrix remodeling in heart valve disease." Circ Res **95**(3): 253-260.
Walther, D. J., S. Stahlberg and J. Vowinckel (2011). "Novel roles for biogenic monoamines: from monoamines in transglutaminase-mediated post-translational protein modification to monoaminylation deregulation diseases." FEBS J **278**(24): 4740-4755.
Wang, J., N. S. Hamblet, S. Mark, M. E. Dickinson, B. C. Brinkman, N. Segil, S. E. Fraser, P. Chen, J. B. Wallingford and A. Wynshaw-Boris (2006). "Dishevelled genes mediate a conserved mammalian PCP pathway to regulate convergent extension during neurulation." Development **133**(9): 1767-1778.
Watanabe, Y., S. Zaffran, A. Kuroiwa, H. Higuchi, T. Ogura, R. P. Harvey, R. G. Kelly and M. Buckingham (2012). "Fibroblast growth factor 10 gene regulation in the second heart field by Tbx1, Nkx2-5, and Islet1 reveals a genetic switch for down-regulation in the myocardium." Proc Natl Acad Sci U S A **109**(45): 18273-18280.
Watts, S. W., J. R. Priestley and J. M. Thompson (2009). "Serotonylation of vascular proteins important to contraction." PLoS One **4**(5): e5682.
Weiss, A. N., J. W. Mimbs, P. A. Ludbrook and B. E. Sobel (1975). "Echocardiographic detection of mitral valve prolapse. Exclusion of false positive diagnosis and determination of inheritance." Circulation **52**(6): 1091-1096.

Wessels, A. and D. Sedmera (2003). "Developmental anatomy of the heart: a tale of mice and man." Physiol Genomics **15**(3): 165-176.
Wessels, A., M. J. van den Hoff, R. F. Adamo, A. L. Phelps, M. M. Lockhart, K. Sauls, L. E. Briggs, R. A. Norris, B. van Wijk, J. M. Perez-Pomares, R. W. Dettman and J. B. Burch (2012). "Epicardially derived fibroblasts preferentially contribute to the parietal leaflets of the atrioventricular valves in the murine heart." Dev Biol **366**(2): 111-124.
Wilcken, D. E. and A. J. Hickey (1988). "Lifetime risk for patients with mitral valve prolapse of developing severe valve regurgitation requiring surgery." Circulation **78**(1): 10-14.
Wong, L. L. and P. N. Adler (1993). "Tissue polarity genes of Drosophila regulate the subcellular location for prehair initiation in pupal wing cells." J Cell Biol **123**(1): 209-221.
Wu, B., Y. Wang, W. Lui, M. Langworthy, K. L. Tompkins, A. K. Hatzopoulos, H. S. Baldwin and B. Zhou (2011). "Nfatc1 coordinates valve endocardial cell lineage development required for heart valve formation." Circ Res **109**(2): 183-192.
Wylie-Sears, J., R. A. Levine and J. Bischoff (2014). "Losartan inhibits endothelial-to-mesenchymal transformation in mitral valve endothelial cells by blocking transforming growth factor-beta-induced phosphorylation of ERK." Biochem Biophys Res Commun **446**(4): 870-875.
Xu, J., B. Jian, R. Chu, Z. Lu, Q. Li, J. Dunlop, S. Rosenzweig-Lipson, P. McGonigle, R. J. Levy and B. Liang (2002). "Serotonin mechanisms in heart valve disease II: the 5-HT2 receptor and its signaling pathway in aortic valve interstitial cells." Am J Pathol **161**(6): 2209-2218.
Xu, J. and T. Kisseleva (2015). "Bone marrow-derived fibrocytes contribute to liver fibrosis." Exp Biol Med (Maywood) **240**(6): 691-700.
Yalcin, H. C., A. Shekhar, T. C. McQuinn and J. T. Butcher (2011). "Hemodynamic patterning of the avian atrioventricular valve." Dev Dyn **240**(1): 23-35.
Yang, C. H., J. D. Axelrod and M. A. Simon (2002). "Regulation of Frizzled by fat-like cadherins during planar polarity signaling in the Drosophila compound eye." Cell **108**(5): 675-688.
Yang, J., D. Hills, E. Taylor, K. Pfeffer, J. Ure and A. Medvinsky (2008). "Transgenic tools for analysis of the haematopoietic system: knock-in CD45 reporter and deletor mice." J Immunol Methods **337**(2): 81-87.
Ybot-Gonzalez, P., D. Savery, D. Gerrelli, M. Signore, C. E. Mitchell, C. H. Faux, N. D. Greene and A. J. Copp (2007). "Convergent extension, planar-cell-polarity signalling and initiation of mouse neural tube closure." Development **134**(4): 789-799.
Yue, J., S. Huhn and Z. Shen (2013). "Complex roles of filamin-A mediated cytoskeleton network in cancer progression." Cell Biosci **3**(1): 7.
Zeidler, M. P., N. Perrimon and D. I. Strutt (1999). "The four-jointed gene is required in the Drosophila eye for ommatidial polarity specification." Curr Biol **9**(23): 1363-1372.

Zhao, X., C. H. Yang and M. A. Simon (2013). "The Drosophila Cadherin Fat regulates tissue size and planar cell polarity through different domains." PLoS One **8**(5): e62998.
Zhou, A. X., J. H. Hartwig and L. M. Akyurek (2010). "Filamins in cell signaling, transcription and organ development." Trends Cell Biol **20**(2): 113-123.
Zois, N. E., S. G. Moesgaard, M. Kjelgaard-Hansen, C. E. Rasmussen, T. Falk, C. Fossing, J. Haggstrom, H. D. Pedersen and L. H. Olsen (2012). "Circulating cytokine concentrations in dogs with different degrees of myxomatous mitral valve disease." Vet J **192**(1): 106-111.